

**Effects of Glycosylation on the Structure and Fibrillization of Prion Protein  
Fragments**

by

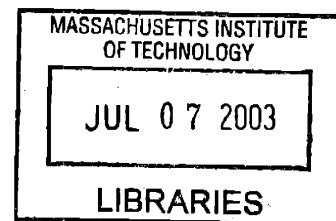
Carlos J. Bosques

B. S. Chemistry  
University of Puerto Rico, Río Piedras, 1997

SUBMITTED TO THE DEPARTMENT OF CHEMISTRY IN PARTIAL  
FULFILLMENT OF THE REQUIREMENTS FOR THE DEGREE OF  
DOCTOR OF PHILOSOPHY FROM THE DEPARTMENT OF CHEMISTRY  
AT THE  
MASSACHUSETTS INSTITUTE OF TECHNOLOGY

June 2003

© 2003 Massachusetts Institute of Technology. All rights reserved.



Signature of Author: \_\_\_\_\_

Department of Chemistry  
April 4, 2003

Certified by: \_\_\_\_\_

Barbara Imperiali  
Ellen Swallow Richards Professor of Chemistry and Biology  
Thesis Supervisor

Accepted by: \_\_\_\_\_

Robert W. Field  
Chair, Departmental Committee on Graduate Students

ARCHIVES

This thesis has been examined by a committee of the Department of Chemistry and the Division of Biological Engineering as follows:

Peter Seeberger

Chair

Barbara Imperiali

Thesis Supervisor

Ram Sasisekharan

# EFFECTS OF GLYCOSYLATION ON THE STRUCTURE AND FIBRILLIZATION OF PRION PROTEIN FRAGMENTS

by  
Carlos J. Bosques

Submitted to the Department of Chemistry  
on April 4, 2003 in Partial Fulfillment of the Requirements for the  
Degree of Doctor of Philosophy

## ABSTRACT

It is now accepted that the structural transition from PrP<sup>C</sup> to PrP<sup>Sc</sup> is the major event leading to transmissible spongiform encephalopathies. Although the mechanism of this transition remains elusive, glycosylation has been proposed to impede the PrP<sup>C</sup> to PrP<sup>Sc</sup> conversion. Structural studies on glycoprotein fragments in the Imperiali group has previously shown that *N*-linked glycosylation can play a major role modulating polypeptide conformation. It has also been shown that glycosylation can alter the thermodynamics of disulfide bond formation, favoring oxidation. To address the role of glycosylation on PrP, we have prepared glycosylated and unglycosylated peptides derived from the 175-195 fragment of the human prion protein. The synthesis of a Fmoc-Asn[chitobiose(TBDMS)<sub>5</sub>-OH amino acid precursor allowed the preparation of the glycopeptide in high yields. Comparison of the structure, aggregation kinetics, fibril formation capabilities and redox susceptibility of Cys 179 has shown that the *N*-linked glycan (at Asn 181) significantly reduces the rate of fibrillization by promoting intermolecular disulfide formation *via* Cys 179. Furthermore, the aggressive fibrillization of a C179S mutant of this fragment highlights the significant role of disulfide stability in retarding the rate of fibril formation. Additionally, a novel method for the temporal control of fibrillization of this peptide was developed using a synthetic photolabile linker and a "fibril inhibitory unit" positioned at the N-terminus of the peptide. This stabilized the fragment as a soluble monomeric species until photoactivation, which triggered the peptide self-assembly.

Thesis Supervisor: Barbara Imperiali

Title: Ellen Swallow Richards Professor of Chemistry and Biology

## Acknowledgements

As feelings of gratitude and appreciation experienced throughout graduate school are usually unexpressed, these few pages become the only opportunity to share them. For this reason, I want to use these lines to compensate for all the times I simply did not say...thanks.

The last five and a half years have been a unique and life-changing experience both professionally and personally. I went to Caltech as one type of individual and today I leave MIT as a different one. I can now look back and realize that, in every way, shape and form, this life-molding experience has been a positive one and I take with me many lessons as new tools for my future. I owe to many people the numerous great moments and lessons that I have acquired throughout this journey both inside and outside the laboratory.

First, I would like to thank my thesis advisor, Professor Barbara Imperiali for not only introducing me to interesting the field of protein glycosylation, but also to the wide variety of scientific questions addressed daily in her laboratory. I also like to thank her for giving me the tools to be a better scientist and for never settling for less than excellence. Now I realize how important this is.

I also thank the members of my thesis committee, Professor Peter Seeberger and Professor Ram Sasisekharan for their support and interest in my scientific career.

To the various members of the Imperiali group: it has been an enormous pleasure to learn from all of you. I really appreciate the many friendships that originated here. Thanks to Professor Sarah O'Connor for all her patience while teaching me about NMR and protein glycosylation. Best of luck in your new career as professor: I have no doubt it will be a success! I also thank my late-night laboratory companion Dr. Jennifer Ottesen (the Cucu-girl) for all the help with NMR and protein structure and for answering all my SGI-related questions. One of the most important persons in my career as a graduate student is "the Sen Sei" Dr. Vincent Tai. I have never had such an intense training, as the one I had in your personal "synthesis boot camp". Thanks for being tough, but at the same time caring so much about my well being in your own "Vince-way". I will always be your apprentice. Thanks to "the man of ideas", Dr. Kevin McDonnell. Thanks for your help on peptide synthesis, your continuous support, encouragement and friendship throughout these years. I also thank my good friend Dr. Stephane Peluso for all the techniques in peptide synthesis and overall scientific suggestions. Friendships are built upon simple things of great meaning. Thanks to Dr. Adam Mezo for his assistance with peptide synthesis and AUC and great scientific advice. Thanks for the good snowboarding moments. Thanks to my baymate Dr. Dierdre Pierce for reviewing my

writings and talks. I also thank Dr. Michael Shrogen-Knaack, Harm-Brummerhop, and Dr. Jens Pohlman for great scientific discussions.

I appreciate all the assistance from present members of the Imperiali group. Thanks to Professor Katherine Franz, Dr. Mark Nitz, Dr. Eugenio Vazquez and Dr. Jebrell Glover for sharing their wide scientific knowledge. Kathy, thanks for taking so much of your time to review my papers and thesis chapters. Specially, I want to thank you for all positive comments and words of encouragement; they can really make you go the extra mile. Good luck in your new exciting career! Dr. J., thanks for assistance with NMR, the great suggestions and for all the scientific and philosophical discussions. It's been great sharing a bench with the "Regulator". I would also like to thank Mary, Debbie and Eranthie ("the heterotrimer mini-motif"), Melissa and Seungjib for all their helpful discussions. It's been a lot of fun working with all of you. Thanks for the incentives for good OT assays. Thanks to Soonsil for advice about photolinkers. I also want to thank a very important labmate, Maria Ufret. Thanks for advice in peptide and solution-phase synthesis, enzymatic assays and many others. I really appreciate your help through candidacy and all the great Puerto Rican food. You are a true friend. Thanks to Mayssam and Beth for reviewing papers and thesis chapters. Good luck to Rob in his defense and to Elvidin in graduate school.

Thanks to Nicky Watson for assistance with electron microscopy, Chris Cheatum for assistance with FTIR and Jeff Spencer and Mark Wall for assistance with NMR spectroscopy.

I will also like to acknowledge financial support from the James Irving Fellowship Foundation, MIT Graduate Student Office, NIH Biotechnology Training Grant.

I dedicate this thesis to the most important people in my life: my family. Without your unconditional support, encouragement and care none of this would be possible. All I am, is because of you and your examples. To my brother Ruben and sister Marisol for being a true representation of what strength and perseverance really means. I thank God for having you as my "older" siblings. I specially thank my parents Myrta and Ruben for giving more than what is possible to facilitate my search for new horizons. Thanks for giving me so much!

Finally, I will like to thank my new family: my wife, Dr. Karen G. Carrasquillo. In addition to scientific advice, you have provided a great example of what hard work and excellence really means. Thanks for the unconditional support and for lifting my spirit through all these years. You have been part of this since we started visiting career fairs in high school. At that time, I never imagine this moment will be a part of my life, but more importantly, that I'll be blessed to share it with you. I love you. To you, I dedicate this thesis.

## Table of Contents

<b>List of Figures</b> .....	8
<b>List of Schemes</b> .....	10
<b>List of Tables</b> .....	12
<b>List of Abbreviations</b> .....	13
<b>Chapter 1. Introduction</b> .....	15
References.....	36
<b>Chapter 2. Synthesis of amyloidogenic glycopeptides</b> .....	48
Introduction.....	49
Results.....	53
Discussion.....	72
Acknowledgements.....	73
Materials and Methods.....	74
References.....	86
<b>Chapter 3. Effects of carbohydrate stereochemistry on glycopeptide structure</b> .....	91
Introduction.....	92
Results.....	97
Discussion.....	111
Acknowledgements.....	112
Materials and Methods.....	113
References.....	122
<b>Chapter 4. The interplay of glycosylation and disulfide formation influences fibrillization in a prion protein fragment</b> .....	128
Introduction.....	129
Results.....	133
Discussion.....	149
Acknowledgements.....	154
Materials and Methods.....	155
References.....	164

<b>Chapter 5. Photolytic control of peptide self-assembly</b> .....	170
Introduction.....	171
Results.....	174
Discussion.....	191
Acknowledgements.....	192
Appendix 1.....	193
Discussion.....	198
Materials and Methods.....	199
References.....	208
<b>Curriculum Vitae</b> .....	213

## List of Figures

### Chapter 1

- 1.1 Schematic representation of the early steps in *N*-linked glycoprotein biosynthesis. Mechanism of *N*-linked protein glycosylation catalyzed by oligosaccharyl transferase (OT).....17
- 1.2 Three main classes of *N*-linked oligosaccharides found in mature glycoproteins.....20
- 1.3 Schematic representation of possible effects of the *N*-linked carbohydrate during protein folding. Illustration of the large surface area occupied by the glycan chain in the CD2 structure.....22
- 1.4 Glycosylation effects on the secondary structure of a hemagglutinin peptide...23
- 1.5 Proposed mechanism for the generation and replication cycle of PrP<sup>Sc</sup>.....28
- 1.6 Schematic representation of the large surface occupied by the *N*-linked glycans on moPrP 124-226.....30
- 1.7 Ribbon diagram of moPrP 124-226 generated from its NMR structure and mutations associated with inherited prion disease. ....33

### Chapter 2

- 2.1 Schematic representation of the experimental approach for monitoring the chemoenzymatic generation of **PrPGP**. Determination of  $K_m$  and  $V_{max}$  for the conversion of **PrPUP** to **PrPGP**.....55
- 2.2 Large scale enzymatic conversion of **PrPUP** into **PrPGP**.....57
- 2.3 Electron microscopy of **PrPUP** samples after incubation at different pH.....64
- 2.4 Comparison of the purity of the crude glycopetides using the acetylated and the silylated building blocks.....72

### Chapter 3

- 3.1 Crystal structure of the hemagglutinin protein and the heavily glycosylated subunit A from the hemagglutinin trimer.....94
- 3.2 CD spectra of glycopeptide **1- $\alpha$**  and alpha proton deviation from random coil values for glycopeptide **1- $\alpha$** .....100
- 3.3 Complete list of variable temperature coefficients of amide protons for glycopeptide **1- $\alpha$** .....104



3.4	Structures derived from a simulated annealing protocol for glycopeptide 1- $\alpha$ .....	109
3.5	Comparison of the solution state structure among peptide 1 and glycopeptides 1- $\beta$ and 1- $\alpha$ .....	110

#### Chapter 4

4.1	CD and FTIR spectra of <b>PrPUP</b> and <b>PrPGP</b> .....	134
4.2	Comparison of aggregation kinetics for <b>PrPUP</b> and <b>PrPGP</b> at different DTT concentrations.....	137
4.3	Congo red binding assay for <b>PrPUP</b> and <b>PrPGP</b> .....	139
4.4	EM pictures for <b>PrPUP</b> and <b>PrPGP</b> .....	141
4.5	Effect of C179S mutation on the fibril formation of the PrP175-195 fragment.....	143
4.6	Electron microscopy of <b>C179S</b> compared to wild type <b>PrPUP</b> .....	143
4.7	ESMS spectra of <b>PrPUP</b> and <b>PrPGP</b> after incubation with and without DTT.....	146
4.8	Differences in $^3J_{\text{HN}\alpha}$ (Hz) values between <b>PrPGP</b> and <b>PrPUP</b> .....	149
4.9	Deviations of $\text{H}\alpha$ chemical shift from random coil values.....	163

#### Chapter 5

5.1	Effect of the electrostatic environment near the N-terminus of the PrP 175-195 peptide fragment.....	173
5.2	Reactivity of Cys 179 during photolysis as assessed by Ellman's test.....	179
5.3	HPLC traces and a possible mechanism for the formation of the unexpected photoproducts from the photolysis of peptide 1-Cys.....	181
5.4	HPLC traces for the photolysis of peptide 1 to release peptide 2.....	185
5.5	Aggregation kinetics for photolyzed and unphotolyzed peptide 1 and peptide 2.....	187
5.6	Time dependent-electron microscopy analysis of peptides.....	189
5.7	Effect of pH on the aggregation kinetics for peptide 1.....	190
5.8	Photolysis of peptide 3 in water monitored by HPLC.....	196
5.9	HPLC traces for the recovery of the His-Tag fragment after photolysis of peptide 3.....	197

## List of Schemes

### Chapter 2

- 2.1 Schematic representation of the different synthetic approaches for the preparation of *N*-linked glycopeptides.....51
- 2.2 Structure of **PrPGP** and the Fmoc-L-Asn[ $\beta$ -chitobiose(TBDMS)<sub>5</sub>]-OH building block used for the preparation of the peptide.....53
- 2.3 Proposed mechanism for aspartimide formation during glycopeptide synthesis using the convergent approach.....59
- 2.4 Synthetic scheme for the synthesis of Fmoc-L-Asn[ $\beta$ -chitobiose(acetyl)<sub>5</sub>]-OH...61
- 2.5 Acetyl-protected building block incorporation and final glycopeptide deprotection.....63
- 2.6 Synthetic scheme for the preparation of Fmoc-L-Asn[ $\alpha$ -chitobiose(TBDMS)<sub>5</sub>]-OH and Fmoc-L-Asn[ $\beta$ -chitobiose(TBDMS)<sub>5</sub>]-OH.....67
- 2.7 Anomerization of the TBDMS-protected carbohydrate during the reduction and coupling conditions.....68
- 2.8 Synthetic scheme for the stereoselective preparation of Fmoc-L-Asn[ $\beta$ -chitobiose(TBDMS)<sub>5</sub>]-OH and the incorporation into **PrPGP**.....70

### Chapter 3

- 3.1 Chemical structures of peptide **1** and glycopeptide **1- $\beta$**  and **1- $\alpha$** .....96
- 3.2 Anomerization of TBDMS-protected carbohydrate during the reduction of azidochitobiose and subsequent coupling of the aminochitobiose to the activated aspartic acid.....97
- 3.3 Structures of Asx and Type I  $\beta$ -turn and their NOE patterns.....101

### Chapter 4

- 4.1 Ribbon diagram generated from the human PrP 121-230 NMR structure. Synthetic unglycosylated (**PrPUP**) and glycosylated (**PrPGP**) peptides derived from the PrP 175-195 fragment.....132
- 4.2 Disulfide stabilization by *N*-linked glycans in the PrP 175-195 fragment and in the context of the protein .....152

### Chapter 5

- 5.1 General representation of the photolysis-dependent fibrillization of the amyloidogenic peptide.....174
- 5.2 Attachment of photo-adduct to the N-terminus of a peptide using the commercially available ANP linker. Sequence and structure of peptide **1** and the resulting peptide **2** from the photolysis.....175

5.3	Synthetic scheme for the preparation of the amino-ANP-ethylenediamine-Fmoc photolinker.....	176
5.4	Synthetic scheme for the preparation of the asparagine-DMDA amino acid.....	177
5.5	Sequence and structure of peptide <b>1-Cys</b> .....	178
5.6	Synthetic scheme for the preparation of peptide <b>1</b> .....	184
5.7	Use of His-Tag linked through a photolinker for the purification of PrP peptides.....	194

## List of Tables

### Chapter 2

2.1	Survey of experimental conditions for the synthesis of the TBDMS-protected, $\beta$ -linked chitobiose building block.....	69
-----	--	----

### Chapter 3

3.1	Comparison of the relative intensities of the diagnostic ROESY crosspeaks in the turn region of peptides <b>1</b> , <b>1-<math>\beta</math></b> , and <b>1-<math>\alpha</math></b> .....	103
3.2	Comparison of the amide proton variable temperature coefficients ( $-\Delta\delta/\Delta T$ , ppb/K) for peptides <b>1</b> , <b>1-<math>\beta</math></b> and <b>1-<math>\alpha</math></b> .....	105
3.3	Comparison of the $^3J_{HN\alpha}$ (Hz) of Asn <sub>5</sub> for different glycopeptides.....	107
3.4	$^1H$ assignment for glycopeptide <b>1-<math>\alpha</math></b> .....	115
3.5	$^3J_{HN\alpha}$ coupling constants for all residues in glycopeptide <b>1-<math>\alpha</math></b> .....	116
3.6	Simulated Annealing Schedule.....	117
3.7	Distance restraints for glycopeptide <b>1-<math>\alpha</math></b> .....	118

### Chapter 4

4.1	Summary of aggregation lag times for <b>PrPUP</b> and <b>PrPGP</b> under different reducing conditions.....	137
4.2	Comparison of the $^3J_{HN\alpha}$ (Hz) values for <b>PrPGP</b> and <b>PrPUP</b> .....	148
4.3	$^1H$ assignment for <b>PrPUP</b> .....	161
4.4	$^1H$ assignment for <b>PrPGP</b> .....	162

## Abbreviations

Standard one and three letter codes are used for the naturally occurring amino acids.

PyAOP:	7-Azabenzotriazol-1-yloxytris (pyrrolidino) phosphonium-hexafluorophosphate
PrP <sup>C</sup> :	Cellular prion protein
PrP <sup>Sc</sup> :	Proteinase K resistant prion protein scrapie
GSH:	Reduced glutathione
CAM:	Ceric ammonium molybdate
PMA:	Phosphomolybdic acid
TBDMS:	<i>tert</i> -butyldimethylsilyl
EM:	Electron Microscopy
Boc:	<i>tert</i> -butoxycarbonyl
BOP:	Benzotriazole-1-yl-oxy-tris-(dimethylamino)-phosphoniumhexafluorophosphate
CD:	Circular dichroism
CHCl <sub>3</sub> :	Chloroform
CH <sub>2</sub> Cl <sub>2</sub> :	Methylene chloride
DCC:	Dicyclohexylcarbodiimide
Dhbt:	3,4-dihydro-4-oxo-1,2,3-benzotriazin-3-yl
DIPCDI:	Diisopropylcarbodiimide
DIPEA:	Diisopropylethylamine
DMF:	Dimethylformamide
DMSO:	Dimethylsulfoxide
Dol:	Dolichol
dpm:	Disintegrations per minute
DQF-COSY:	Double quantum filtered correlated overhauser spectroscopy
DTT:	Dithiothreitol
ER:	Endoplasmic reticulum
ESMS:	Electrospray mass spectrometry
Fmoc:	9-fluorenylmethoxycarbonyl
GlcNAc:	<i>N</i> -acetylglucosamine
GPI:	Glycosylphosphatidyl inositol
HATU:	O-1-hydroxy-7-azabenzotriazolyl tetramethyluronium hexafluorophosphate
HBTU:	Hydroxybenzotriazolyl tetramethyluronium hexafluorophosphate
HOAT:	1-hydroxy-7-azabenzotriazole
HOBt:	Hydroxybenzotriazole

HPLC:	High-performance liquid chromatography
Hz:	Hertz
K:	Kelvin
MeCN:	Acetonitrile
MeOH:	Methanol
NMR:	Nuclear magnetic resonance
NOE:	Nuclear Overhauser effect
NOESY:	Nuclear overhauser effect spectroscopy
OPfp:	Pentafluorophenyl ester
OT:	Oligosaccharyl transferase
ppb:	Parts per billion
ROESY:	Rotating frame overhauser effect spectroscopy
TFA:	Trifluoroacetic acid
TLC:	Thin layer chromatography
TOCSY:	Total correlation spectroscopy
$t_R$ :	Retention time
VT:	Variable temperature

## **Chapter 1**

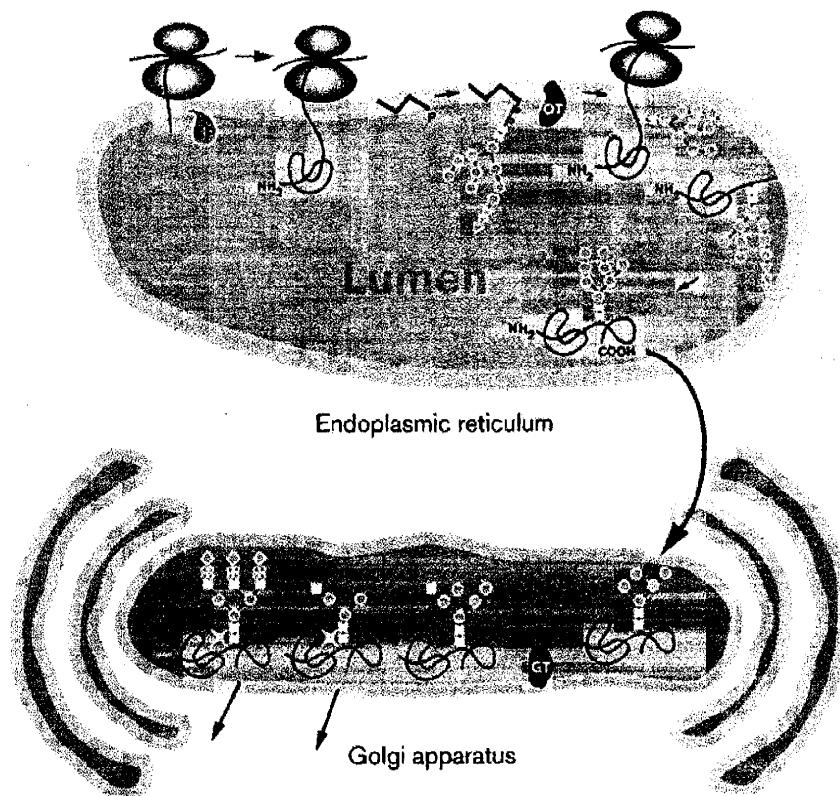
### **Introduction**

## **Protein Glycosylation**

Protein glycosylation, the covalent attachment of carbohydrates to protein, is one of the most common co- and post-translational modifications performed in eukaryotic cells. The generation of a great diversity of glycoproteins by carbohydrate modification expands the structural and functional roles of otherwise relatively simple proteins.<sup>1</sup> Critical roles have been attributed to the carbohydrate moiety of glycoproteins in a variety of biological processes, including cellular recognition, immune response, and protein folding, stability and solubility.<sup>1,2</sup> The large number of possible permutations of glycan structures, resulting from multiple linkages, stereochemistry and flexibility (compared to DNA and proteins), provides carbohydrates with a large capacity for the storage of information. At the same time, this complexity has hampered the elucidation of the specific mode of action of carbohydrates for many years. However, recent technological advances in glycopeptide synthesis,<sup>3</sup> mass spectrometry,<sup>4</sup> and nuclear magnetic resonance<sup>5</sup> have facilitated the study of the direct relation between the structure and function of glycans. This has promoted an increasing interest in protein glycosylation.



A



B

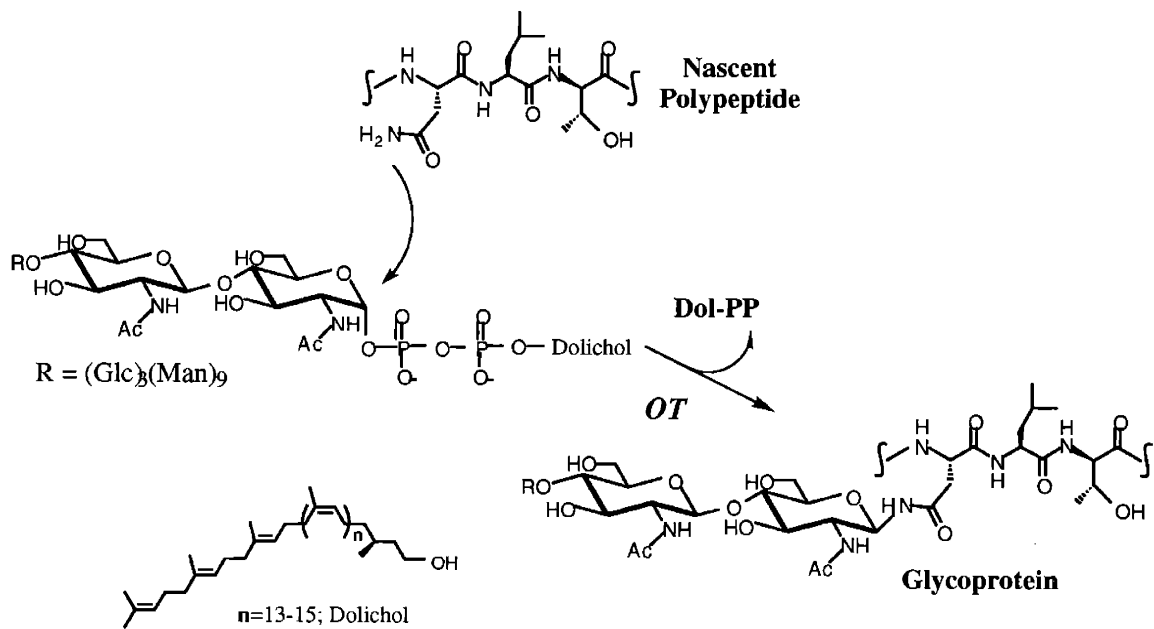


**Figure 1.1.** A. Schematic representation of the early steps in *N*-linked glycoprotein biosynthesis. As the protein is translated in the ribosome, the polypeptide is translocated into the lumen of the ER. Here, oligosaccharyl transferase (OT) catalyzes the transfer of the carbohydrate from the Glc<sub>3</sub>Man<sub>9</sub>GlcNAc<sub>2</sub>-PP-dolichol donor to the Asn side chain of the nascent protein. The glycan chain is further modified in the ER and then in the Golgi. Figure taken from.<sup>18</sup> B. Mechanism of *N*-linked protein glycosylation catalyzed by oligosaccharyl transferase (OT).

## **Carbohydrate attachment to proteins and glycan processing**

Carbohydrate modifications of glycoproteins fall into three categories: *N*-linked modification of the asparagine (Asn) side chain,<sup>6</sup> *O*-linked modification of serine (Ser) or threonine (Thr)<sup>7,8</sup> and the modification of the protein *C*-carboxyl terminus by glycosylphosphatidylinositol (GPI) derivatization.<sup>9</sup> While *O*-linked glycosylation and GPI anchor derivatization are post-translational modifications and take place in the Golgi apparatus, *N*-linked glycosylation occurs co-translationally and takes place in the lumen of the endoplasmic reticulum (ER) (Figure 1.1A). Proteins destined to be secreted from the cell or to be integrated into the cell membrane are synthesized with an *N*-terminal signal sequence that is recognized by the signal recognition particle (SRP) in the ER membrane. This signal sequence is cleaved as the nascent peptide is translocated across the ER membrane.<sup>10</sup> At this point, oligosaccharyl transferase (OT), a heteromeric-multisubunit enzyme embedded within the membrane of the endoplasmic reticulum, catalyzes the transfer of the glycan chain from a lipid-linked carbohydrate to the asparagine of the nascent polypeptide (Figure 1.1B).<sup>11</sup> Specifically, a triantennary tetradecasaccharide carbohydrate is transferred from the Glc<sub>3</sub>Man<sub>9</sub>GlcNAc<sub>2</sub>-PP-dolichol donor to the carboxamide side chain of the asparagine in the Asn-Xaa-Thr/Ser consensus sequence (Figure 1.1B).<sup>12</sup> In this consensus sequence, Xaa could be any of the 20 naturally occurring amino acids except proline.<sup>13</sup> The OT-orchestrated transfer is very

specific generating the beta linkage between the anomeric carbon of the carbohydrate and the nitrogen of the asparagine carboxamide.<sup>14</sup> After this first stage in the *N*-linked glycosylation pathway is complete, processing of the glycans begins within the ER by the removal of the three terminal glucose residues and one mannose. This step is important to ensure the interaction of the glycoprotein with specific chaperones that facilitate the protein folding of the new polypeptide.<sup>15</sup> Further processing of the glycan chains takes place after the glycoprotein is transferred to the Golgi. Here, mannosidases and *N*-acetylglucosamine transferases act on the carbohydrate to generate the pentameric core present in all *N*-linked saccharides.<sup>16</sup> The glycoprotein is further decorated resulting high-mannose, complex or hybrid type glycan structures (Figure 1.2). The type of glycan structures in the mature glycoprotein depends on the organism, the nature of the cell, the type of tissue, and the final destination of the protein.

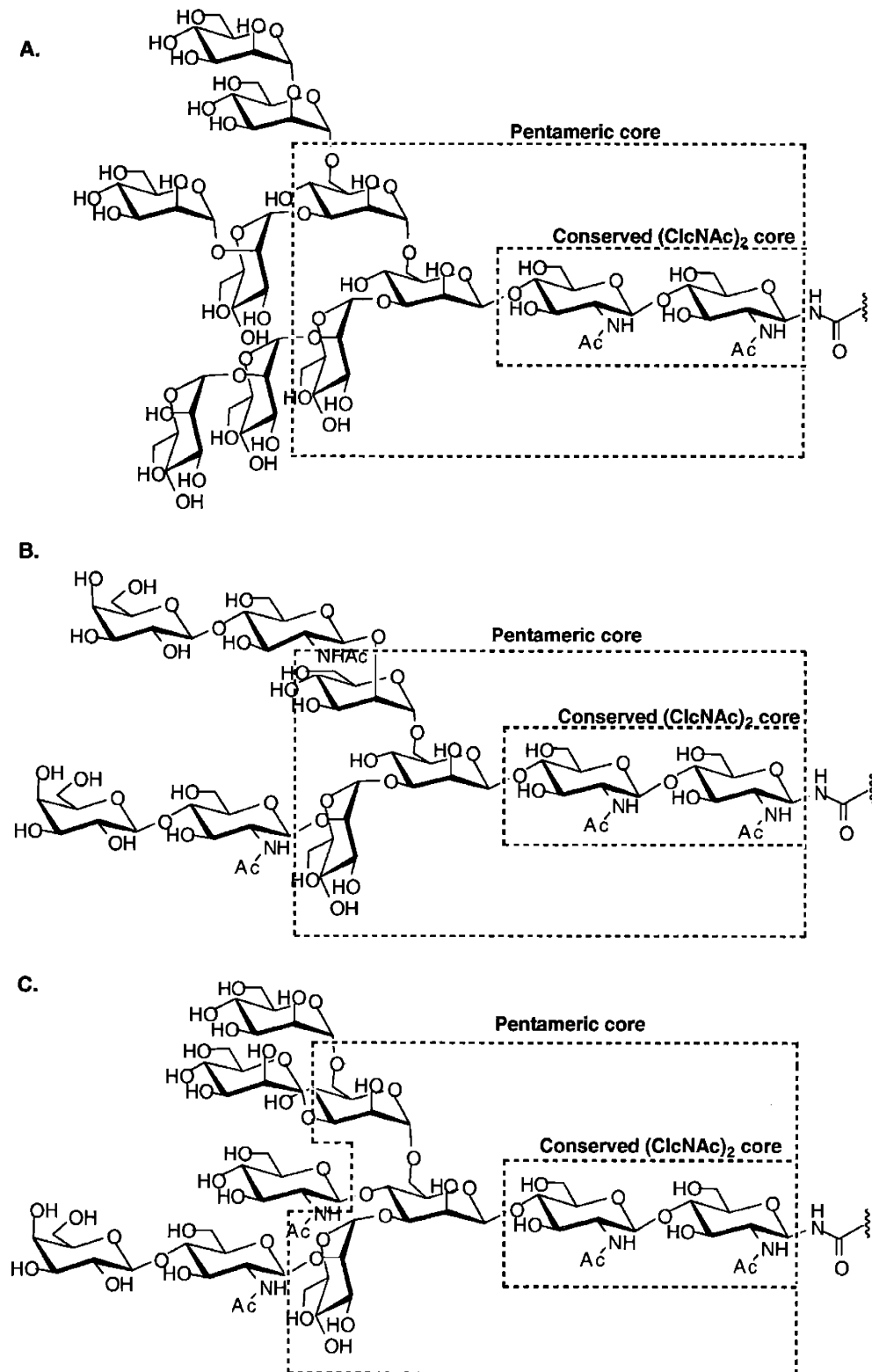


**Figure 1.2.** Three main classes of *N*-linked oligosaccharides found in mature glycoproteins. **A.** High-mannose, **B.** complex and **C.** hybrid type. The conserved chitobiose (GlcNAc)<sub>2</sub> and pentameric cores are displayed within boxes.

## **Conformational effects of protein glycosylation and their role in protein folding**

*N*-linked glycosylation can affect the protein folding process during protein biosynthesis, as this derivatization occurs co-translationally.<sup>17</sup> For example, site-directed mutagenesis affecting protein glycosylation sites has induced incorrect folding, aggregation, and secretion inhibition of numerous glycoproteins.<sup>18</sup> In contrast to other types of post-translational modifications such as phosphorylation and prenylation, *N*-linked glycosylation involves the attachment of a large, hydrophilic structure onto the protein. With molecular weights ranging from 1880 to 2851 Da, the carbohydrate chain can occupy a significant surface area of the glycoprotein. Therefore, this modification can limit the possible degrees of freedom of the nascent polypeptide, narrowing its accessible conformations (Figure 1.3). While the phosphorylation occupies a small volume of approximately 84 Å<sup>3</sup>, the carbohydrate chains can occupy volumes ranging from 1840 Å<sup>3</sup> to 2542 Å<sup>3</sup>, depending on the class of oligosaccharide chain (Figure 1.3B).<sup>19</sup> Also, chaperones involved in protein folding, such as calnexin and calreticulin, require the specific carbohydrate processing of the new glycoprotein in order to generate the correctly folded protein and liberate it from the endoplasmic reticulum.<sup>15,20</sup>

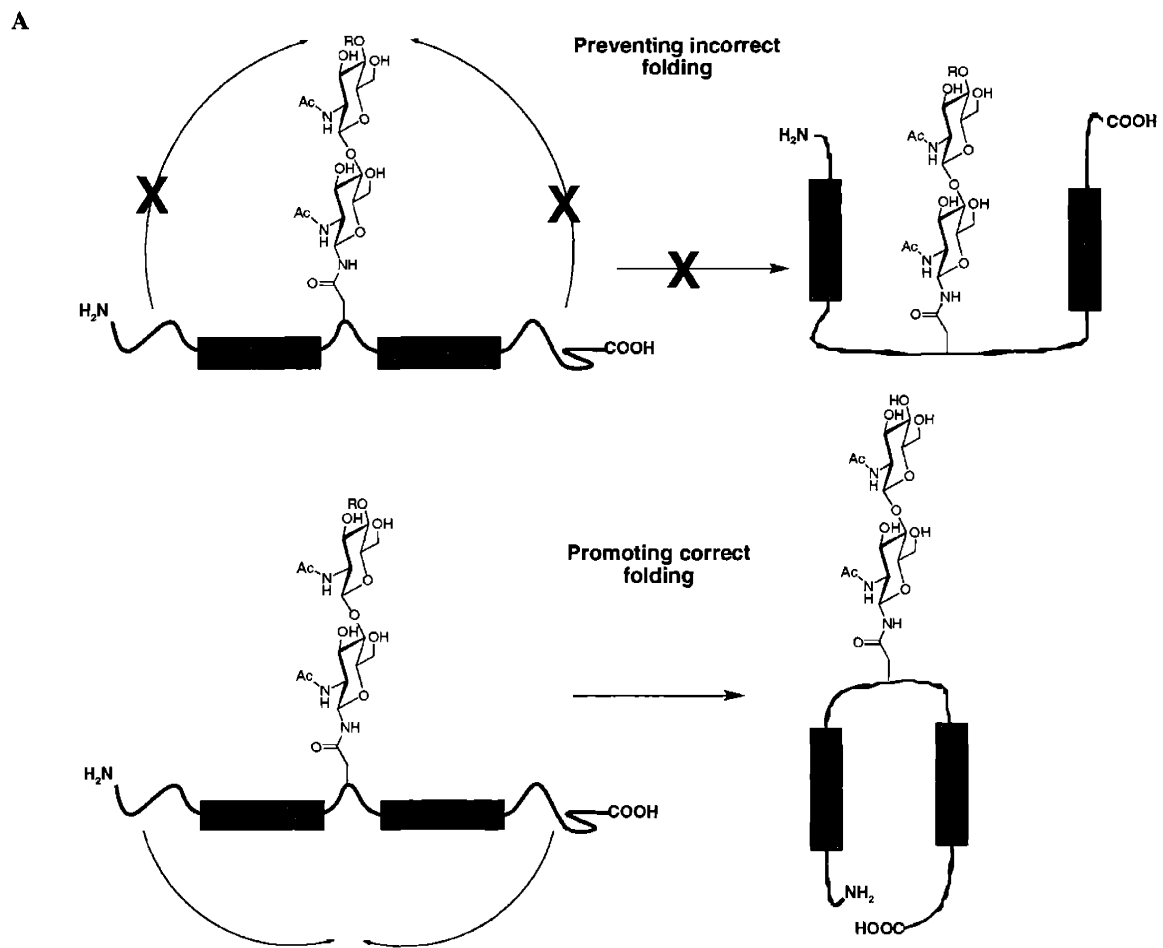


**Figure 1.3 A.** Schematic representation of possible effects of the *N*-linked carbohydrate during protein folding. The large glycan can narrow the possible trajectories of the protein backbone during the folding process facilitating the formation of the native fold. **B.** Illustration of the large surface area occupied by the glycan chain in the CD2 structure (PDB identification number 1GYA). The protein is shown in purple and the carbohydrate portion in white.

Furthermore, glycan modification of short glycopeptides that mimic flexible, nascent proteins, triggers a switch from an extended to a compact conformation (Figure 1.4).<sup>21-23</sup> It is not yet entirely clear how the carbohydrate moiety triggers a change in peptide conformation. In a few isolated cases, specific, stabilizing contacts between the carbohydrate moiety and the protein have been observed.<sup>22,24</sup> Also, it has been proposed that the sugar moiety may influence the local structure of the glycosylation site by affecting the solvation characteristics of the peptide or by making hydrogen-bonding interactions with the polypeptide.<sup>2</sup> In aqueous media, the conformational effects of the carbohydrate appear to be steric in nature, limiting the thermodynamical conformations accessible to the polypeptide.<sup>21,25</sup>

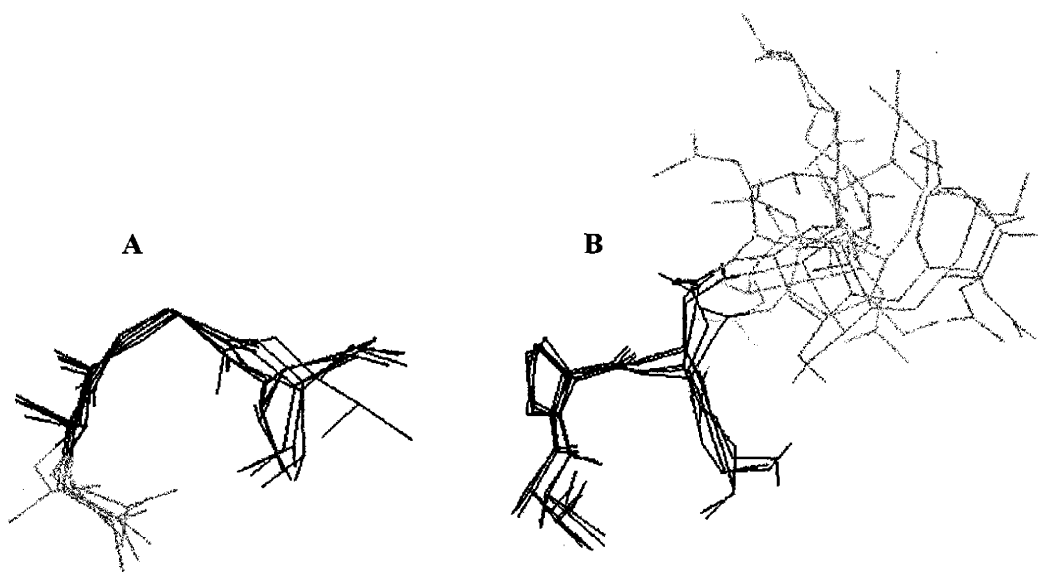


**Figure 1.4.** Glycosylation effects on the secondary structure of a hemagglutinin peptide. Backbone superimposition of NMR structures for: **A**, residues Asn<sup>5</sup> to Thr<sup>7</sup> of the unglycosylated peptide and **B**, residues Thr<sup>3</sup> to Thr<sup>7</sup> of the respective peptide modified with chitobiose at Asn<sup>5</sup>. Peptide backbone is shown in black, Asn<sup>5</sup> side chain and carbohydrates are shown in gray. Adapted from O'Connor, et. al.<sup>21</sup>

Key elements of the carbohydrates have been proven to play a critical role in the conformation of glycopeptides, as shown by NMR studies. In comparison to other similarly studied carbohydrates, chitobiose (D-GlcNAc-[ $\beta$ (1-4)] $\beta$ -D-GlcNAc) has been shown to play a unique role in determining the glycopeptide conformation. By disrupting the Asx-turn present in peptide substrates recognized by OT, chitobiose converts this turn into an energetically similar type I  $\beta$ -turn.<sup>21</sup> This switch in turn types is consistent with the fact that glycosylation sites are often found in  $\beta$ -turns in glycoproteins. Specifically, the *N*-acetyl groups on chitobiose seem to be responsible for the induction of the  $\beta$ -turn and for rigidifying the sugar moiety and peptidyl fragment of the glycopeptides.<sup>25</sup> In summary, co-translational, *N*-linked carbohydrate modifications can induce specific, regional conformational effects on nascent glycopeptides that may have a direct influence on their subsequent folding and final structure.

### **Disorders of protein glycosylation and activity of protein glycoforms**

Inhibition of protein glycosylation can have devastating effects, such as embryonic lethality.<sup>26</sup> Presently, six congenital disorders of glycosylation (CDGs) are known. These are divided into two categories. Type one, or CDG1, arises from the dysfunction of enzymes involved in the assembly of the Glc<sub>3</sub>Man<sub>9</sub>GlcNAc<sub>2</sub>-PP-dolichol donor. Type II, or CDG2, is a result of mutations affecting the enzymes responsible for



the *N*-linked processing. Infants with these defects share clinical features, including developmental delay, multiple organ abnormalities, coagulation disorders, and severe neurologic dysfunction.<sup>27-29</sup>

The complex glycosylation machinery can generate a wide variety of protein glycoforms. This is a result of a natural mechanism to ensure diversity, but can also be due to defects of enzymes that are involved in the modification of the carbohydrate antennae structures. What seem to be minor variations of the glycan chain can result in significant alterations in protein activity. In fact, the potency of a glycoprotein is considered to be the weighted average of the specific activities of the glycoform population.<sup>30</sup> For example, peptide hormones lutropin and erythropoietin are expressed with structurally diverse glycans, and the discrete glycoforms have different affinities for hepatic lectins, thereby determining serum half-lives and potency *in vivo*.<sup>30-32</sup> Studies of individual glycoforms of RNase B showed significant differences in dynamic fluctuations and exhibited a range of activity toward double-stranded RNA.<sup>33</sup> A similar case results in the development of rheumatoid arthritis. This disease is associated with an increase in IgG glycoforms that lack galactose in the Fc region of the molecule. These glycoforms result in the loss of interaction with the C<sub>H</sub>2 domain surface and, ultimately, activation of the complement pathway.<sup>34,35</sup> These examples indicate that glycosylation and the processing of the glycans represent a major regulatory mechanism for cell- and tissue-

specific control of protein function, and that alteration of this biosynthetic pathway can result in fatal disorders.<sup>1,35</sup>

### **Transmissible Spongiform Encephalopathies and the Prion protein**

Transmissible spongiform encephalopathies (TSEs) are a group of fatal neurodegenerative diseases that can affect both animals and humans.<sup>36,37</sup> TSEs include Creutzfeldt-Jakob disease, fatal familial insomnia, Grestmann-Sträussler-Scheinker syndrome, and Kuru in humans, bovine spongiform encephalopathies in cattle and Scrapie in sheep.<sup>36,38,39</sup> These fatal neurodegenerative diseases can be manifested as genetic, sporadic, and, in some cases, infectious disorders.<sup>37,39-41</sup> TSEs have become a major concern for public health, especially since the bovine spongiform encephalopathy (BSE) epidemic in the United Kingdom and the report of a new variant of Creutzfeldt-Jakob disease.<sup>42-44</sup> A major effort has been devoted to the study of the molecular nature of the infectious agents responsible for these diseases, since no virus particle has yet been isolated from infected species, and since nucleic acids are not associated with the disease. These observations have led to the formulation of the protein-only hypothesis, which argues that the molecular basis of TSEs is caused exclusively by the conformational polymorphism of the membrane-associated sialoglycoprotein, cellular prion protein (PrP<sup>C</sup>).<sup>37,45,46</sup> Specifically, this hypothesis claims that the disease is caused by the

formation of amyloid plaques, primarily in the central nervous system, when PrP<sup>C</sup> undergoes a structural transformation to its infectious scrapie isoform PrP<sup>Sc</sup>.<sup>37</sup> One of the most distinguishing properties of the prion protein is that it can be independently infectious and self-replicating.<sup>47</sup> A compilation of evidence has led to the acceptance of the protein-only hypothesis as the explanation for the nature of these disorders. In fact, the name prion (for proteinacious infectious particle) is presently used as a synonym for TSE-type infectious agents.

### **Differences between PrP<sup>C</sup> and PrP<sup>Sc</sup>**

PrP<sup>C</sup> is an *N*-linked glycoprotein of yet unknown function. Both PrP<sup>C</sup> and the pathogenic PrP<sup>Sc</sup> contain the same amino acid sequence and similar covalent modifications, including two *N*-linked carbohydrate moieties<sup>48,49</sup> and a C-terminal glycosylphosphatidylinositol (GPI) anchor.<sup>50,51</sup> However, PrP<sup>C</sup> is detergent soluble and sensitive to digestion with proteinase K, while PrP<sup>Sc</sup> is highly aggregated, detergent insoluble and resistant to proteinase K digestion.<sup>52</sup> Additionally, PrP<sup>C</sup> is usually found on the cell surface, while PrP<sup>Sc</sup> is found primarily in the cytoplasm.<sup>53</sup> Although the mechanism by which PrP<sup>C</sup> is transformed into PrP<sup>Sc</sup> is unknown, it may involve the conversion of critical domains of the protein from  $\alpha$ -helix to  $\beta$ -sheet. Spectroscopic

studies have shown that PrP<sup>C</sup> is 42%  $\alpha$ -helix and 3%  $\beta$ -sheet, while PrP<sup>Sc</sup> has  $\alpha$ -helical and  $\beta$ -sheet contents of 30% and 43% respectively.<sup>54</sup>

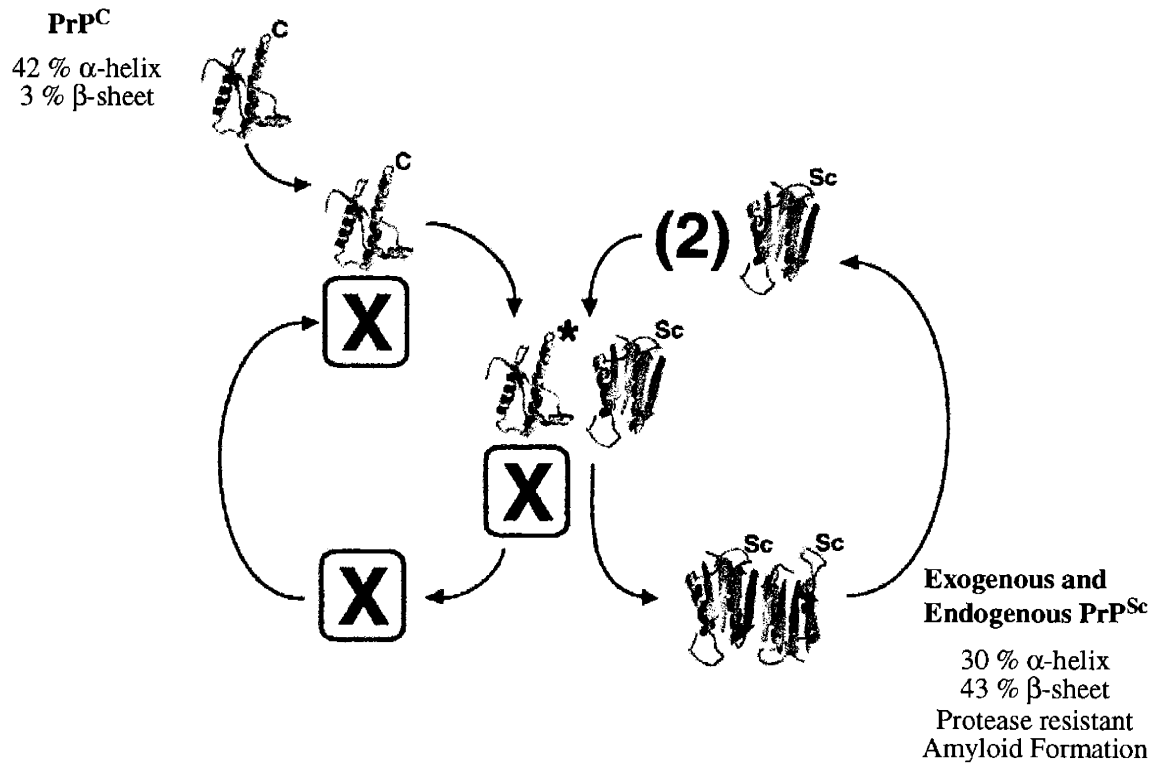


**Figure 1.5.** Proposed mechanism for the generation and replication cycle of PrP<sup>Sc</sup>. “Protein X” facilitates the conversion of PrP<sup>C</sup> into the transition intermediate PrP<sup>\*</sup>, which can interact with exogenous PrP<sup>Sc</sup> to form homomultimeric PrP<sup>Sc</sup>. PrP<sup>Sc</sup> then serves as a template to continue the replication cycle (2) to form additional PrP<sup>Sc</sup>. Figure adapted from Cohen, F. E. and Prusiner, S. B.<sup>55</sup>

## **PrP<sup>C</sup> to PrP<sup>Sc</sup> transition**

Despite the significant efforts to determine the mechanism of the PrP<sup>C</sup> to PrP<sup>Sc</sup> transition, this key event in TSE propagation remains elusive. In contrast to other amyloidogenic proteins in which a specific region of the protein has been identified as the sole amyloid unit, no specific sequence in the prion protein has been conclusively identified as the unique determinant for fibrillization. In fact, several small PrP fragments (109-122, 113-127, 113-120, 178-191 and 202-218) have been shown to form amyloids *in vitro* when synthesized as peptides.<sup>56</sup> In general, it is believed that PrP<sup>C</sup> can exist in equilibrium with a transient intermediate state (PrP\*) that in turn may interact with exogenous PrP<sup>Sc</sup>. The resulting heteromultimer PrP\*/PrP<sup>Sc</sup>, can finally be converted into the homomultimer PrP<sup>Sc</sup> (Figure 1.5).<sup>55</sup> It has been proposed that the PrP<sup>C</sup> to PrP\* transition is facilitated by a species of unknown origin, called protein X.<sup>57,58</sup> Upon the conversion of the PrP\* to PrP<sup>Sc</sup>, protein X is liberated and can interact again with PrP<sup>C</sup> to continue the cycle.<sup>55</sup> The newly formed PrP<sup>Sc</sup> can then serve as a template to continue the generation of more pathogenic PrP (Figure 1.5). This recycling mechanism could explain the exponential increase in PrP<sup>Sc</sup> concentrations.<sup>55</sup> In the inherited form of TSEs, the mutations in PrP can cause the destabilization of PrP<sup>C</sup>, shifting the equilibrium towards PrP\*, and therefore facilitating the formation of PrP\*/PrP<sup>Sc</sup>.<sup>55,59</sup> For sporadic cases of

prion diseases, the initiation of the PrP<sup>C</sup> destabilization is believed to be triggered by other endogenous conditions.

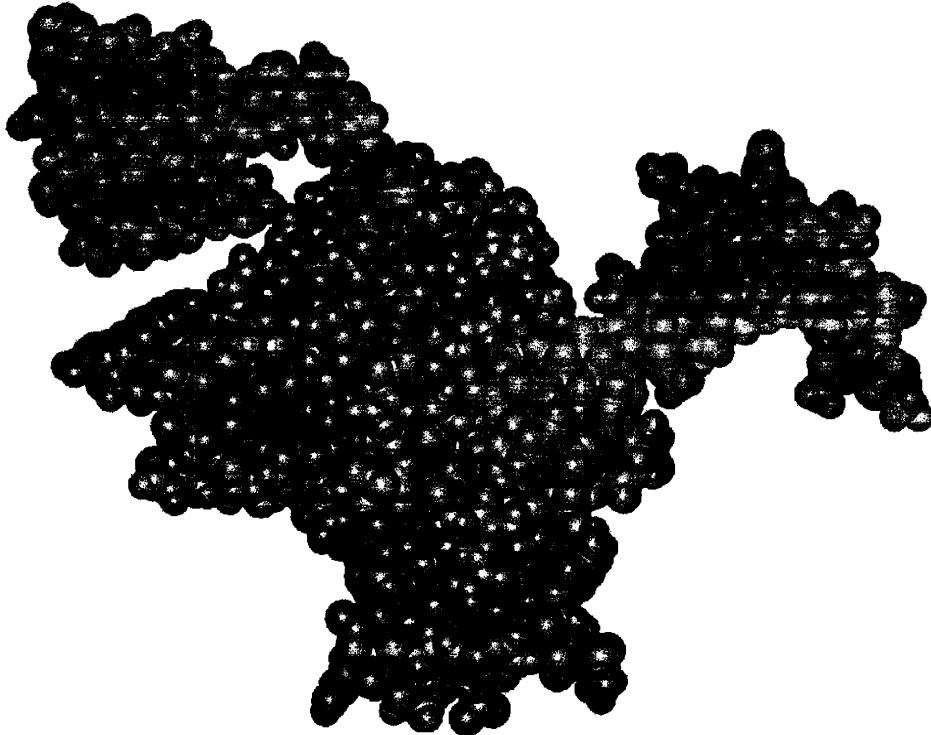


**Figure 1.6.** Schematic representation of the large surface occupied by the *N*-linked glycans on moPrP 124-226. Structure was generated from the unglycosylated moPrP NMR structure from Riek, et. al.<sup>73</sup> and complex *N*-linked glycans were attached to Asn 181 and 197 using Insight II.

### **Factors promoting or stabilizing the PrP<sup>C</sup> to PrP<sup>Sc</sup> transition and PrP glycosylation**

Factors such as GPI anchor stability,<sup>60</sup> pH,<sup>61</sup> fluctuations in metal ion concentrations,<sup>62,63</sup> redox environment,<sup>64-66</sup> extracellular molecules as

glycosaminoglycans,<sup>67,68</sup> and *N*-linked glycosylation,<sup>69,70</sup> have all been associated with the conversion of PrP<sup>C</sup> to PrP<sup>Sc</sup>. Among these factors, *N*-linked glycosylation has been given much attention due to its role in other diseases, its relation to protein structure and function, and because the large size of the oligosaccharides could interfere with protein-protein interactions, leading to aggregation. In PrP, the *N*-linked carbohydrate moieties can occupy a significant surface area of the protein (Figure 1.6). It has also been proposed that protein X binding involves residues close to the glycosylation sites of PrP.<sup>58</sup> Therefore, it is expected that the large oligosaccharide chains interfere with this interaction. The characterization of the specific *N*-linked carbohydrates attached to PrP<sup>C</sup> and PrP<sup>Sc</sup> has been complicated by the presence of an ensemble of different PrP glycoforms that have highly heterogeneous *N*-linked glycans. PrP<sup>C</sup> and PrP<sup>Sc</sup> from Syrian hamsters cells contain the same set of at least 52 bi-, tri-, and tetraantennary *N*-linked oligosaccharides, but the relative proportions of individual glycans is different.<sup>71</sup> The differences in the ratio of glycoforms between PrP<sup>C</sup> and PrP<sup>Sc</sup> has suggested that glycosylation can modulate the PrP<sup>C</sup> to PrP<sup>Sc</sup> conversion.<sup>65,72</sup>

Numerous studies indicate that glycan chains may reduce the efficacy by which PrP<sup>Sc</sup> is generated. It has been shown that blockading glycosylation, either by mutation or by inhibition with tunicamycin, promotes PrP<sup>Sc</sup> accumulation in cultured cells.<sup>70,74</sup> Also, PrP<sup>Sc</sup> synthesized in scrapie-infected cells displays a preponderance of lower molecular

weight glycoforms, suggesting that molecules with less glycosylation may be preferred substrates in the PrP<sup>Sc</sup> generation.<sup>75</sup> An inherited form of spongiform encephalopathy with a characteristic T183A mutation (that eliminates the first glycosylation site) has been observed in a Brazilian family.<sup>76</sup> Further studies on the corresponding mouse mutant have shown that elimination of the glycosylation site N181 by a T183A mutation results in increased PrP<sup>Sc</sup> characteristics and a failure to reach the cell membrane. In fact, a large fraction of the mutations associated with inherited prion diseases occur in close proximity to the glycosylation site (Figure 1.7B). Also, glycosylation may be interrelated to other properties of PrP, such as disulfide stability, which has been related to PrP<sup>Sc</sup> formation.<sup>64</sup> For example, the reduction of the single disulfide bond in the protein changes the distribution of PrP glycoforms. The result is exclusive expression of the diglycosylated form.<sup>65</sup> The pattern of PrP glycosylation also appears to be an important marker of prion species variation. For example, when the disease is passed from an infected animal to a new host, the glycosylation site occupancy of the newly diseased PrP<sup>Sc</sup> reflects that of the prion from the original infected animal and not that of the recipient.<sup>69</sup> This is the case for the nvCJD in humans, which reflects glycosylation patterns similar to that of BSE in cattle.<sup>69</sup>



A



B

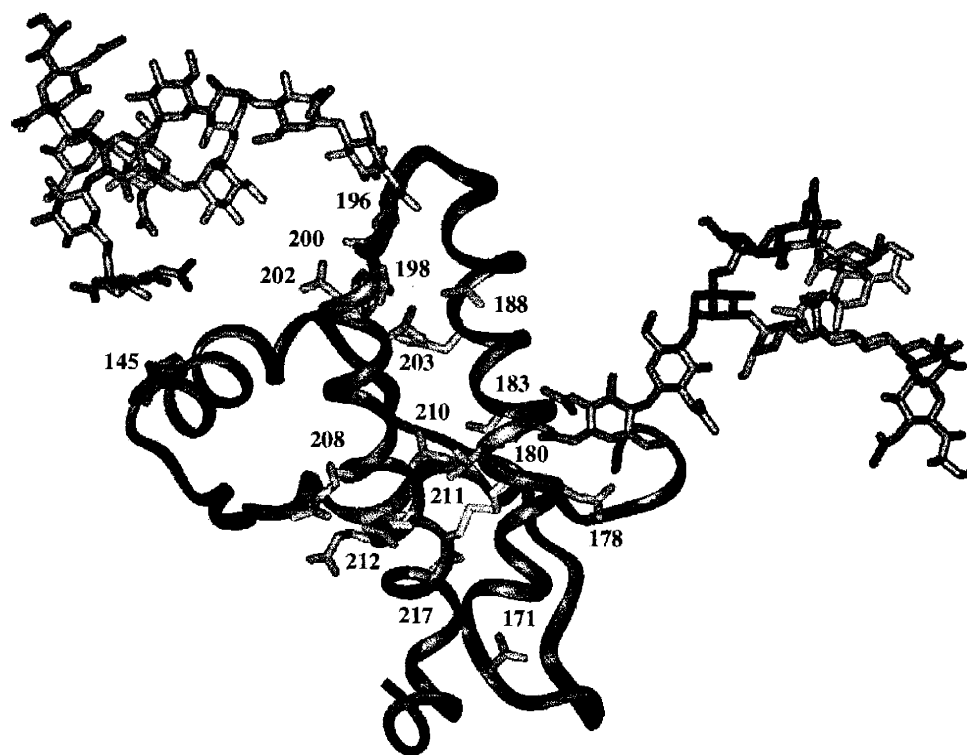


**Figure 1.7** A. Ribbon diagram of moPrP 124-226 generated from its NMR structure.<sup>73</sup> The C-terminal helix-loop-helix region of the protein is shown in red, glycosylation sites (Asn 181 and 197) are colored by atom, and the disulfide bridge between Cys 179 and 214 is shown in yellow. B. Mutations associated with inherited prion disease. Mutations within the C-terminal helix-loop-helix (near the glycosylation site) are shown in green. The mutant outside this region (position 145) is shown in purple. Complex *N*-linked carbohydrates (red) were attached using Insight II.

## PrP structure

NMR structures of the prion protein from different species and from different PrP fragments have been solved.<sup>73,77</sup> These structures have made a significant contribution to the understanding of specific structural features of PrP<sup>C</sup>, such as the direct residue interactions that lead to the formation of disulfide bonds, and the presence of exposed glycosylation sites. The *N*-linked glycosylation sites (at Asn 181 and 197) are located at the C-terminus helix-loop-helix region of the protein, which is the segment with best defined secondary structure (Figure 1.7A).<sup>73</sup> This helix-loop-helix region is strongly stabilized by the disulfide bridge (Cys 179-Cys 214) between the two helices. In fact, reduction of this disulfide bond causes a major destabilization of the native structure of PrP<sup>C</sup> and increases the  $\beta$ -sheet content of the protein.<sup>78</sup> Unfortunately, the proteins used for the generation of the NMR structures were unglycosylated and thus do not provide any information about the effects that the carbohydrate moiety could have on the real PrP structure. Presently, no detailed information about the mode of action of the *N*-linked glycans in the PrP conversion is available. Recently, the crystal structure of an unglycosylated prion dimer has been solved, providing possible insights for the mechanism of the PrP<sup>Sc</sup> formation,<sup>79</sup> This structure reveals a three-dimensional swapping of the C-terminal helix 3 and rearrangement of the disulfide bond. Solving this interesting structure enabled the suggestion that the surface occupancy of the *N*-linked glycans at

this region could prevent this mechanism.<sup>79</sup> Considering all of the evidence above and the well documented effects of *N*-linked glycosylation in folding and maturation of nascent proteins, a possible interrelationship is suggested to exist between the carbohydrate modification and the conformational transition from PrP<sup>C</sup> to PrP<sup>Sc</sup>.

## References

- 1)Varki, A. "Biological Roles of Oligosaccharides: all of the Theories are Correct" *Glycobiology* **1993**, *3*, 97-130.
- 2)Dwek, R. A. "Glycobiology: Toward Understanding the Function of Sugars" *Chem. Rev.* **1996**, *96*, 683-720.
- 3)Meldal, M.; St. Hilaire, P. M. "Synthetic Methods of Glycopeptide Assembly, and Biological Analysis of Glycopeptide Products" *Curr. Opin. Chem. Biol.* **1997**, *1*, 552-563.
- 4)Hooker, A. D.; James, D. C. "Analysis of Glycoprotein Heterogeneity by Capillary Electrophoresis and Mass Spectrometry" *Mol. Biotech.* **2000**, *14*, 241-249.
- 5)Poveda, A.; Jimenez-Barbero, J. "NMR Studies of Carbohydrate-Protein Interactions in Solution" *Chem. Soc. Rev.* **1998**, *27*, 133-143.
- 6)Reuter, G.; Gabius, H. J. "Eukaryotic Glycosylation: Whim of Nature or Multipurpose Tool?" *Cel. Mol. Life Sci.* **1999**, *55*, 368-422.
- 7)Van den Steen, P.; Rudd, P. M.; Dwek, R. A.; Opdenakker, G. "Concepts and Principles of O-Linked Glycosylation" *Crit. Rev. Biochem. Mol. Biol.* **1998**, *33*, 151-208.

- 8)Van den Steen, P. E.; Rudd, P. M.; Wormald, M. R.; Dwek, R. A.; Opdenakker, G. "O-Linked Glycosylation in Focus" *Trends Glycos. Glycotech.* **2000**, *12*, 35-49.
- 9)Gerold, P.; Eckert, V.; Schwarz, R. T. "GPI-Anchors: An Overview" *Trends Glycos. Glycotech.* **1996**, *8*, 265-277.
- 10)Young, B.; Craven, R.; Reid, P.; Willer, M.; Stirling, C. "Sec63p and Far2p are Required for Translocation of SRP-Dependent Precursors Into the Yeast Endoplasmic Reticulum *in Vivo*" *EMBO J.* **2001**, *20*, 262-271.
- 11)Hirschberg, C. B.; Snider, M. D. "Topography of Glycosylation in the Rough Endoplasmic Reticulum and Golgi Apparatus" *Annu. Rev. Biochem.* **1987**, *56*, 63-87.
- 12)Silberstein, S.; Gilmore, R. "Biochemistry, Molecular Biology, and Genetics of the Oligosaccharyl Transferase" *FASEB J.* **1996**, 849-858.
- 13)Marshall, R. D. "Glycoproteins" *Annu. Rev. Biochem.* **1972**, *41*, 673-702.
- 14)Imperiali, B. "Protein Glycosylation: The Clash of the Titans" *Acc. Chem. Res.* **1997**, *30*, 452-459.
- 15)Helenius, A.; Aebi, M. "Intracellular Function of N-linked Glycans" *Science* **2001**, *291*, 2364-2369.

16)Sears, P.; Wong, C.-H. "Enzymatic Action in Glycoprotein Synthesis" *Cell. Mol. Life Sci.* **1998**, *54*, 223-252.

17)Nilsson, I.; von Hiejne, G. "Determination of the Distance between the Oligosaccharyltransferase Active Site and the Endoplasmic Reticulum Membrane" *J. Biol. Chem.* **1993**, *268*, 5798-5801.

18)O'Connor, S. E.; Imperiali, B. "Modulation of Protein Structure and Function by Asparagine-Linked Glycosylation" *Chem. Biol.* **1996**, *3*, 803-812.

19)O'Connor, S. E. *Conformational Effects of Asparagine-Linked Glycosylation*; Massachusetts Institute of Technology: Cambridge, 2000, pp 28.

20)Parodi, A. J. "Protein Glucosylation and its Role in Protein Folding" *Annu. Rev. Biochem.* **2000**, *69*, 69-93.

21)O'Connor, S. E.; Imperiali, B. "Conformational Switching by Asparagine-linked Glycosylation" *J. Am. Chem. Soc.* **1997**, *119*, 2295-2296.

22)Live, D. H.; Kumar, R. A.; Beebe, X.; Danishefsky, S. J. "Conformational Influences of Glycosylation of a Peptide: A Possible Model for the Effect of Glycosylation on the Rate of Protein Folding" *Proc. Natl. Acad. Sci. USA* **1996**, *93*, 12759-12761.

- 23)DeKoster, G. T.; Robertson, A. D. "Thermodynamics of Unfolding for Kazal-Type Serine Protease Inhibitors: Entropic Stabilization of Ovomuroid First Domain by Glycosylation" *Biochemistry* **1997**, *36*, 2323-2331.
- 24)Dwek, R. A.; Lellouch, A. C.; Wormald, M. R. "Glycobiology- The Function of Sugar in the IgG Molecule" *J. Anatomy* **1995**, *187*, 279-292.
- 25)O'Connor, S. E.; Imperiali, B. "A Molecular Basis for Glycosylation Induced Conformational Switching" *Chem. Biol.* **1998**, *5*, 427-437.
- 26)Marek, K.; Vijay, I.; Marth, J. "A Recessive Deletion in the GlcNAc-1-Phosphotransferase Gene Results in Periimplantation Embryonic Lethality" *Glycobiology* **1999**, *9*, 1263-1271.
- 27)Matthijs, G.; Jaeken, J. "Congenital Disorders of Glycosylation" *Annu. Rev. Genom. Hum. Genet.* **2001**, *2*, 129-151.
- 28)Carchon, H.; Van Schaftingen, E.; Matthijs, G.; Jaeken, J. "Carbohydrate-Deficient Glycoprotein Syndrome Type IA (Phosphomannomutase-Deficiency)" *Biochim Biophys Acta* **1999**, *1455*, 155-165.
- 29)Freeze, H. H.; Aebi, M. "Molecular Basis of Carbohydrate-Deficient Glycoprotein Syndromes Type I With Normal Phosphomannomutase Activity" *Biochim. Biophys. Acta* **1999**, *1455*, 167-178.

- 30)Dennis, J. W.; Warren, C. E.; Granovsky, M.; Demetriou, M. "Genetic Defects in N-Glycosylation and Cellular Diversity in Mammals" *Curr. Opin. Struc. Biol.* **2001**, *11*, 601-607.
- 31)Fiete, D.; Srivastava, V.; Hindsgaul, O.; Baenziger, J. U. "A Hepatic Reticuloendothelial Cell Receptor Specific for SO<sub>4</sub>-4GalNAcβ1,4GlcNAcβ1, Manα that Mediates Rapid Clearance of Lutropin" *Cell* **1991**, *67*, 1103-1110.
- 32)Takeuchi, M.; Kobata, A. "Structures and Functional Roles of the Sugar Chains of Human Erythropoietins" *Glycobiology* **1991**, *1*, 337-346.
- 33)Rudd, P. M.; Joao, H. C.; Coghill, E.; Fiten, P.; Saunders, M. R.; Opdenakker, G.; Dwek, R. A. "Glycoforms Modify the Dynamic Stability and Functional Activity of an Enzyme" *Biochemistry* **1994**, *33*, 17-22.
- 34)Malhotra, R.; Wormald, M. R.; Rudd, P. M.; Fischer, P. B.; Dwek, R. A.; Sim, R. B. "Glycosylation Changes of IgG Associated with Rheumatoid Arthritis can Activate Complement Via the Mannose-Binding Protein" *Nat. Med.* **1995**, *1*, 237-243.
- 35)Wyss, D. F.; Wagner, G. "The Structural Role of Sugars in Glycoproteins" *Curr. Opin. Biotech.* **1996**, *7*, 409-416.
- 36)Prusiner, S. B. "Prion Encephalopathies of Animals and Humans" *Dev. Biol. Stand.* **1993**, *80*, 31-44.



- 37) Prusiner, S. B. "Prions" *Proc. Natl. Acad. Sci. USA* **1998**, 95, 13363-13383.
- 38) Horwich, A. L.; Weissman, J. S. "Deadly Conformations-Protein Misfolding in Prion Disease" *Cell* **1997**, 89, 499-510.
- 39) Caughey, B.; Chesebro, B. "Prion Protein and the Transmissible Spongiform Encephalopathies" *Trends Cell Biol.* **1997**, 7, 56-62.
- 40) Prusiner, S. B. "Molecular Biology of Prion Diseases" *Science* **1991**, 252, 1515-1522.
- 41) Weissmann, C. "Molecular Biology of Prion Disease" *Trends Cell Biol.* **1994**, 4, 10.
- 42) Schonberger, L. B. "New Variant Creutzfeldt-Jakob Disease and Bovine Spongiform Encephalopathy" *Infect. Dis. Clin. North Am.* **1998**, 12, 111-121.
- 43) Patterson, W. J.; Painter, M. J. "Bovine Spongiform Encephalopathy and New Variant Creutzfeldt-Jakob Disease: an Overview" *Commun. Dis. Public Health* **1999**, 2, 5-13.
- 44) Wells, G. A. H.; Wilesmith, J. W. "The Neuropathology and Epidemiology of Bovine Spongiform Encephalopathy" *Brain Pathol.* **1995**, 5, 91-103.
- 45) Bolton, D. C.; McKinley, M. P.; Prusiner, S. B. "Identification of a Protein that Purifies with the Scrapie Prion" *Science* **1982**, 218, 1309-1311.

- 46)McKinley, M. P.; Bolton, D. C.; Prusiner, S. B. "A Protease-Resistant Protein is a Structural Component of the Scrapie Prion" *Cell* **1983**, *35*, 57-62.
- 47)Kaneko, K.; Ball, H. L.; Wille, H.; Zhang, H.; Groth, D.; Torchia, M.; Tremblay, P.; Safar, J.; Prusiner, S. B.; DeArmond, S. J.; Baldwin, M. A.; Cohen, F. E. "A Synthetic Peptide Initiates Gerstmann-Sträussler-Scheinker (GSS) Disease in Transgenic Mice" *J. Mol. Biol.* **2000**, *295*, 997-1007.
- 48)Endo, T.; Groth, D.; Prusiner, S. B.; Kobata, A. "Diversity of Oligosaccharide Structures Linked to Asparagines of the Scrapie Prion Protein" *Biochemistry* **1989**, *28*.
- 49)Haraguchi, T.; Fisher, S.; Olofsson, S.; Endo, T.; Groth, D.; Tarentino, A.; Borchelt, D. R.; Teplow, D.; Hood, L.; Burlingame, A.; Lycke, E.; kobata, A.; Prusiner, S. B. "Asparagine-Linked Glycosylation of the Scrapie and Cellular Prion Proteins" *Arch. Biochem. Biophys.* **1989**, *274*, 1-13.
- 50)Stahl, N.; Borchelt, D. R.; Hsiao, K.; Prusiner, S. B. "Scrapie Prion Protein Contains a Phosphatidylinositol Glycolipid" *Cell* **1987**, *51*, 229-240.
- 51)Stahl, N.; Baldwin, M. A.; Hecker, R.; Pan, K. M.; Burligame, A. L.; Prusiner, S. B. "Glycosylinositol Phospholipid Anchors of the Scrapie and Cellular Prion Proteins Contain Sialic-Acid" *Biochemistry* **1992**, *31*, 5043-5053.

52) Oesch, B.; Westaway, D.; Walchli, M.; McKinley, M. P.; Kent, S. B.; Aebersold, R.; Barry, R. A.; Tempst, P.; Teplow, D. B.; Hood, L. E.; et al. "A Cellular Gene Encodes Scrapie 27-30 Protein" *Cell* **1985**, *40*, 735-746.

53) Taraboulos, A.; Serban, D.; Prusiner, S. B. "Scrapie Prion Proteins Accumulate in the Cytoplasm of Persistently Infected Cultured Cells" *J. Cell. Biol.* **1990**, *110*, 2117-2132.

54) Pan, K.-M.; Baldwin, M.; Nguyen, J.; Gasset, M.; Serban, A.; Groth, D.; Melhorn, I.; Huang, Z.; Fletterick, R. J.; Cohen, F. E.; Prusiner, S. B. "Conversion of Alpha Helices into Beta-Sheets Features in the Formation of the Scrapie Prion Proteins" *Proc. Natl. Acad. Sci. USA* **1993**, *90*, 10962-10966.

55) Cohen, F. E.; Prusiner, S. B. "Pathologic Conformations of Prion Proteins" *Annu. Rev. Biochem.* **1998**, *67*, 793-819.

56) Gasset, M.; Baldwin, M. A.; Lloyd, D. H.; Gabriel, J. M.; Holtzman, D. M.; Cohen, F.; Fletterick, R.; Prusiner, S. B. "Predicted Alpha-Helical Regions of the Prion Protein When Synthesized as Peptides Form Amyloids" *Proc. Natl. Acad. Sci. USA* **1992**, *89*, 10940-10944.

57) Telling, G. C.; Scott, M.; Mastrianni, J.; Gabizon, R.; Torchia, M.; Cohen, F. E.; DeArmond, S. J.; Prusiner, S. B. "Prion Propagation in Mice Expressing Human and Chimeric PrP Transgenes Implicate the Interaction of Cellular PrP With Another Protein" *Cell* **1995**, *83*, 79-90.

58) Kaneko, K.; Zulianello, L.; Scott, M.; Cooper, C. M.; Wallace, A. C.; James, T. L.; Cohen, F. E.; Prusiner, S. B. "Evidence for Protein X Binding to a Discontinuous Epitope on the Cellular Prion Protein During Scrapie Prion Propagation" *Proc. Natl. Acad. Sci. USA* **1997**, *94*, 10069-10074.

59) Petersen, R. B.; Parchi, P.; Richardson, S. L.; Urig, C. B.; Gambetti, P. "Effect of the D178N Mutation and the Codon 129 Polymorphism on the Metabolism of the Prion Protein" *J. Biol. Chem.* **1996**, *271*, 12661-12668.

60) Taraboulos, A.; Scott, M.; Semenov, A.; Avraham, D.; Laszlo, L.; Prusiner, S. B. "Cholesterol Depletion and Modification of COOH-Terminal Targeting Sequence of the Prion Protein Inhibit Formation of the Scrapie Isoform" *J. Cell. Biol.* **1995**, *129*, 121-132.

61) Hornemann, S.; Glockshuber, R. "A Scrapie-like Unfolding Intermediate of the Prion Protein Domain PrP(121-231) Induced by Acidic pH" *Proc. Natl. Acad. Sci. USA* **1998**, *95*, 6010-6014.

62) Wong, B.-S.; Vénien-Bryan, C.; Williamson, R. A.; Burton, D. R.; Gambetti, P.; Sy, M.-S.; Brown, D. R.; Jones, I. M. "Copper Refolding of Prion Protein" *Biochem Biophys Res Com* **2000**, *276*, 1217-1224.

63) Stöckel, J.; Safar, J.; Wallace, A. C.; Cohen, F. E.; Prusiner, S. B. "Prion Protein Selectively Binds Copper (II) Ions" *Biochemistry* **1998**, *37*, 7185-7193.

64)Ma, J.; Lindquist, S. "De Novo Generation of a PrP-Sc-Like Conformation in Living Cells" *Nat. Cell Biol.* **1999**, *1*, 358-361.

65)Capellari, S.; Zaidi, S. I. A.; Urig, C. B.; Perry, G.; Smithe, M. A.; Petersen, R. B. "Prion Protein Glycosylation is Sensitive to Redox Change" *J. Bio. Chem.* **1999**, *274*, 34846-34850.

66)Welker, E.; Wedermeyer, W. J.; Sheraga, H. A. "A Role for Intermolecular Disulfide Bonds in Prion Diseases" *Proc. Nat. Acad. Sci. USA* **2001**, *98*, 4334-4336.

67)Priola, S. A.; Caughey, B. "Inhibition of Scrapie-Associated PrP Accumulation. Probing the Role of Glycosaminoglycans in Amyloidogenesis" *Mol. Neurobiol.* **1994**, *8*, 113-120.

68)Leteux, C.; Chai, W.; Nagai, K.; Herbert, C.; Lawson, A. M.; Feizi, T. "10E4 antigen of Scrapie Lesions Contains an Unusual Nonsulfated Heparan Motif" *J. Biol. Chem.* **2001**, *276*, 12539-12545.

69)Rudd, P. M.; Wormald, M. R.; Wing, D. R.; Prusiner, S. B.; Dwek, R. A. "Prion Glycoprotein: Structure, Dynamics, and Roles for the Sugars" *Biochemistry* **2001**, *40*, 3759-3766.

70)Lehmann, S.; Harris, D. A. "Blockade of Glycosylation Promotes Acquisition of Scrapie-Like Properties by the Prion Protein in Cultured Cells" *J. Biol. Chem.* **1997**, *272*, 21479-21487.

- 71)Rudd, P. M.; Endo, T.; Colominas, C.; Groth, D.; Wheeler, S. F.; Harvey, D. J.; Wormald, M. R.; Serban, H.; Prusiner, S. B.; Kobata, A.; Dwek, R. A. "Glycosylation Differences Between the Normal and Pathogenic Prion Protein Isoforms" *Proc. Natl. Acad. Sci. USA* **1999**, *96*, 13044-13049.
- 72)Kocisko, D. A.; Come, J. H.; Priola, S. A.; Cheseboro, B.; Raymond, G. J.; Lansbury, P. T.; Caughey, B. "Cell-Free Formation of Protease-Resistant Prion Protein" *Nature* **1994**, *370*, 471-474.
- 73)Riek, R.; Hornemann, S.; Wider, G.; Billeter, M.; Glockshuber, R.; Wuthrich, K. "NMR Structure of the Mouse Prion Protein Domain PrP(121-231)" *Nature* **1996**, *382*, 180-182.
- 74)Taraboulos, A.; Rogers, M.; Borchelt, D. R.; McKinley, M. P.; Scott, M.; Serban, D.; Prusiner, S. B. "Acquisition of Protease Resistance by Prion Proteins in Scrapie-Infected Cells Does not Require Asparagine-Linked Glycosylation" *Proc. Natl. Acad. Sci. USA* **1990**, *87*, 8262-8266.
- 75)Caughey, B.; Raymond, G. J. "The Scrapie-Associated Form of PrP is Made From a Cell Surface Precursor That is Both Protease- and Phospholipase- Sensitive" *J. Biol. Chem.* **1991**, *266*, 18217-18223.
- 76)Nitrini, R.; Rosemberg, S.; Passos-Bueno, M. R.; da Silva, L. S.; Iugheetti, P.; Papadopoulos, M.; Carrilolho, P. M.; Caramelli, P.; Albrecht, S.; Zatz, M.; LeBlanc, A.

"Familial Spongiform Encephalopathy Associated With a Novel Prion Protein Gene Mutation" *Ann. Neurol.* **1997**, *42*, 138-146.

77)Zahn, R.; Liu, A.; Lührs, T.; Riek, R.; Schroetter, C. V.; Gracía, F. L.; Billeter, M.; Calzolari, L.; Wider, G.; Wüthrich, K. "NMR Solution Structure of the Human Prion Protein" *Proc. Natl. Acad. Sci. USA* **2000**, *97*, 145-150.

78)Jackson, G. S.; Hosszu, L. L. P.; Power, A.; Hill, A. F.; Kenney, J.; Saibil, H.; Craven, C. J.; Waltho, J. P.; Clarke, A. R.; Collinge, J. "Reversible Conversion of Monomeric Human Prion Protein Between Native and Fibrillogenic Conformations" *Science* **1999**, *283*, 1935-1937.

79)Knaus, K. J.; Morillas, M.; Swietnicki, W.; Malone, M.; Surewicz, W. K.; Yee, V. C. "Crystal Structure of the Human Prion Protein Reveals a Mechanism for Oligomerization" *Nature Struct. Biol.* **2001**, *8*, 770-774.

## **Chapter 2**

### **Synthesis of Amyloidogenic Glycopeptides**



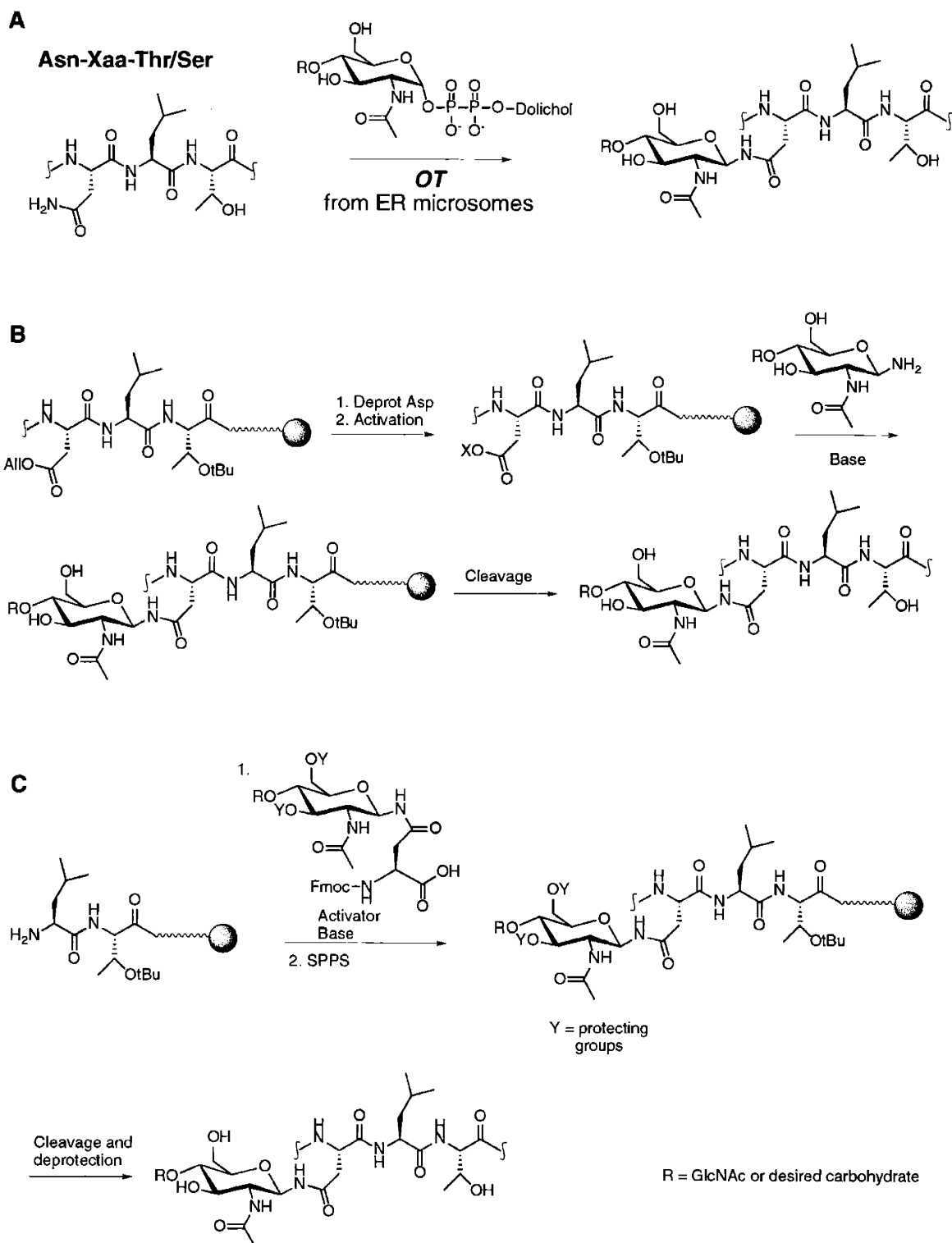
## Introduction

Glycoproteins are involved in many diverse biochemical processes including cell growth regulation,<sup>1</sup> invasion of pathogens,<sup>1</sup> intercellular communication and metastasis.<sup>2</sup> Numerous studies have shown that the saccharide portion of glycoproteins plays an important role in the biological activity and structural properties of the glycoprotein.<sup>3-7</sup> The increased awareness of the important roles of glycoproteins and glycopeptides and their use as possible therapeutic agents<sup>8,9</sup> has generated a major interest for the preparation of such biomolecules. Unfortunately, the isolation of homogeneous glycosylated polypeptides from natural sources is complicated by the large heterogeneity of protein glycoforms. Also, the expression of recombinant glycopeptides in alternate host cells might display altered glycosylation patterns.<sup>10</sup> Therefore, the use of synthetic and semi-synthetic approaches for the preparation of glycopeptides has been of particular interest since they provide for good quantities of homogeneous material.

Presently, three general methods for the preparation of *N*-linked glycopeptides are commonly used; these include the chemoenzymatic,<sup>11</sup> convergent<sup>12</sup> and building block<sup>13</sup> approaches. In the chemoenzymatic method, a crude preparation of the enzyme oligosaccharyl transferase (OT) is used to catalyze the selective transfer of a carbohydrate moiety onto an independently synthesized peptide acceptor (Scheme 2.1A). This conversion requires the pre-assembly of the carbohydrate-dolichol pyrophosphate donor

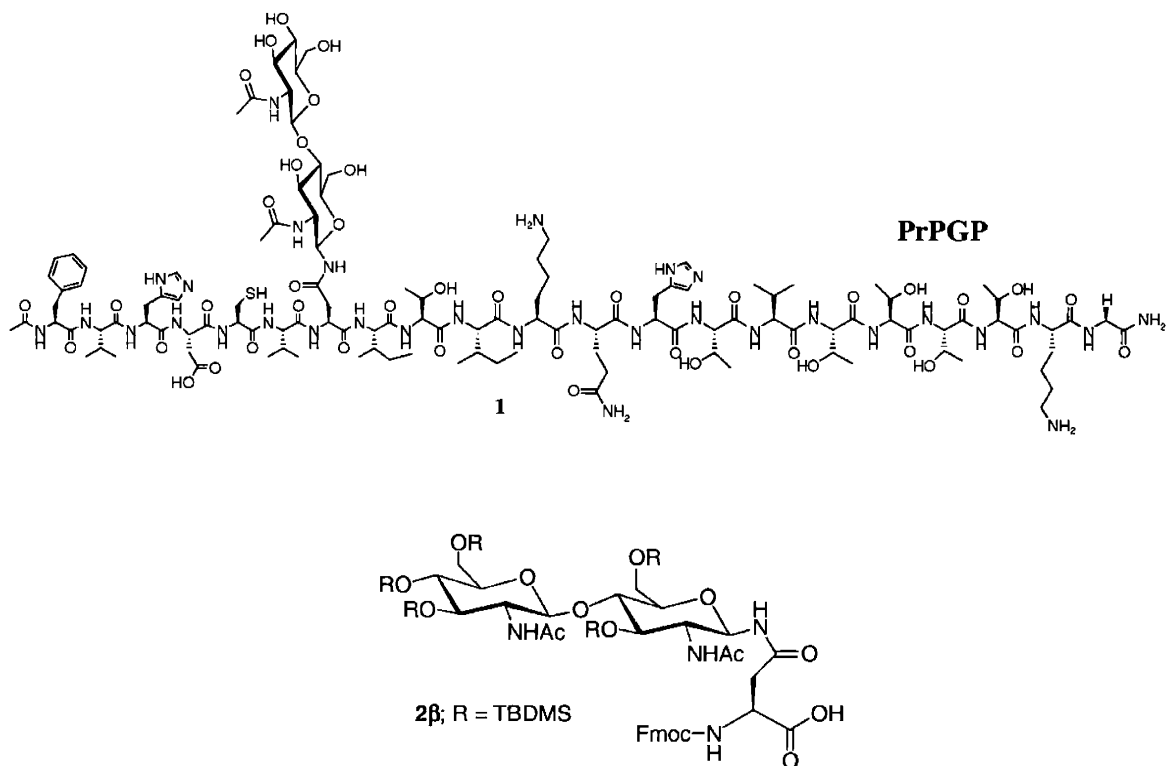
and the acceptor peptide containing the Asn-Xaa-Thr/Ser substrate recognition sequence.<sup>14</sup>

The convergent method involves the preassembly of an unprotected glycosylamine in solution<sup>15</sup> and an immobilized polypeptide on a solid support.<sup>12</sup> An aspartic acid with an orthogonal protecting group is introduced on the peptide at the site where glycosylation is desired and it is selectively deprotected to attach the carbohydrate (Scheme 2.1B). At this time, the aspartic acid is activated and acylation with the glycosylamine is carried out. This last step has been shown to be complicated by aspartimide formation between the preceding backbone amide and  $\beta$ -carboxylic acid of the Asp side chain of the peptide (Scheme 2.3).<sup>16,17</sup> Among these methods, the building block approach is particularly attractive and is presently the most commonly used strategy. In this approach, the glycosylamino acid is first assembled in solution and is then easily incorporated as a standard residue during the solid phase peptide synthesis (SPPS) (Scheme 2.1C).<sup>13,18,19</sup>



**Scheme 2.1.** Schematic representation of the different synthetic approaches for the preparation of *N*-linked glycopeptides. **A.** Chemoenzymatic approach. **B.** Convergent approach. **C.** Building block approach.

With the goal of studying the effects of glycosylation on the structure and stability of prion protein fragments, herein we describe the different approaches used for the preparation of a glycosylated peptide derived from the 175-195 fragment of the human prion protein (**PrPGP**) (Scheme 2.2).<sup>20</sup> Due to the strong evidence that the disaccharide chitobiose is sufficient to impact the secondary structures of glycopeptides,<sup>21,22</sup> this carbohydrate was selected as the sugar moiety for the **PrPGP**. In addition to simplifying the synthesis and manipulation of the glycopeptide, this simple sugar moiety enables subsequent structural analysis. The incompatibility of the chemoenzymatic and the building block approach with base-labile protection for the preparation of amyloidogenic glycopeptides are illustrated with this case. Finally, the stereoselective preparation of a  $\beta$ -linked TBDMS-protected chitobiose asparagine building block **2** and its incorporation onto the peptide are described. The use of this building block provides an impressive increase in the purity and total yield in **PrPGP** synthesis.



**Scheme 2.2.** Structure of **PrPGP** and the Fmoc-L-Asn[ $\beta$ -chitobiose(TBDMS)<sub>5</sub>]-OH building block used for the preparation of the peptide.

## Results

### Chemo-enzymatic approach

Early methods for the preparation of glycopeptides in the Imperiali group employed the use of endoplasmic reticulum-derived microsomes, which include oligosaccharyl transferase (OT), to enzymatically attach the carbohydrate to synthetic

peptides.<sup>11</sup> For this strategy, a semisynthetic GlcNAc-GlcNAc-Dol-P-P is used as the carbohydrate donor and the desired peptide containing the Asx-Xaa-Ser/Thr recognition motif is used as the acceptor. After the enzymatic conversion, the reaction is quenched into a chloroform/ methanol solution separating the dolichol donor from the glycopeptide product. The latter is then easily extracted from the aqueous layer (Figure 2.1A). Our first attempt to prepare **PrPGP** employed this method. First, the unglycosylated peptide (**PrPUP**) was synthesized on a MilliGen/Biosearch 9050 automated peptide synthesizer using standard 9-fluorenylmethoxycarbonyl (Fmoc) chemistry and PAL-PEG-PS resin as the solid support. The peptide was prepared as the C-terminal amide and the N-terminal acetyl derivative to better mimic the internal backbone of the protein. High performance liquid chromatography (HPLC) was used to purify **PrPUP** after cleavage from the resin.

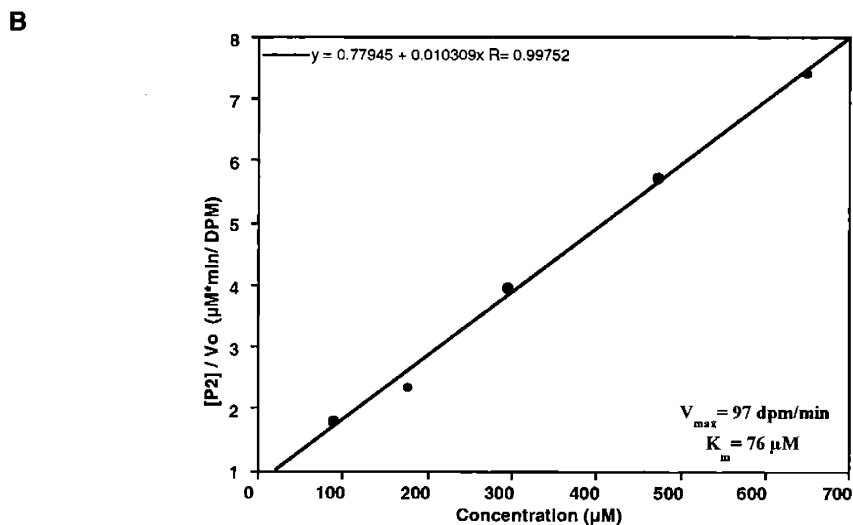
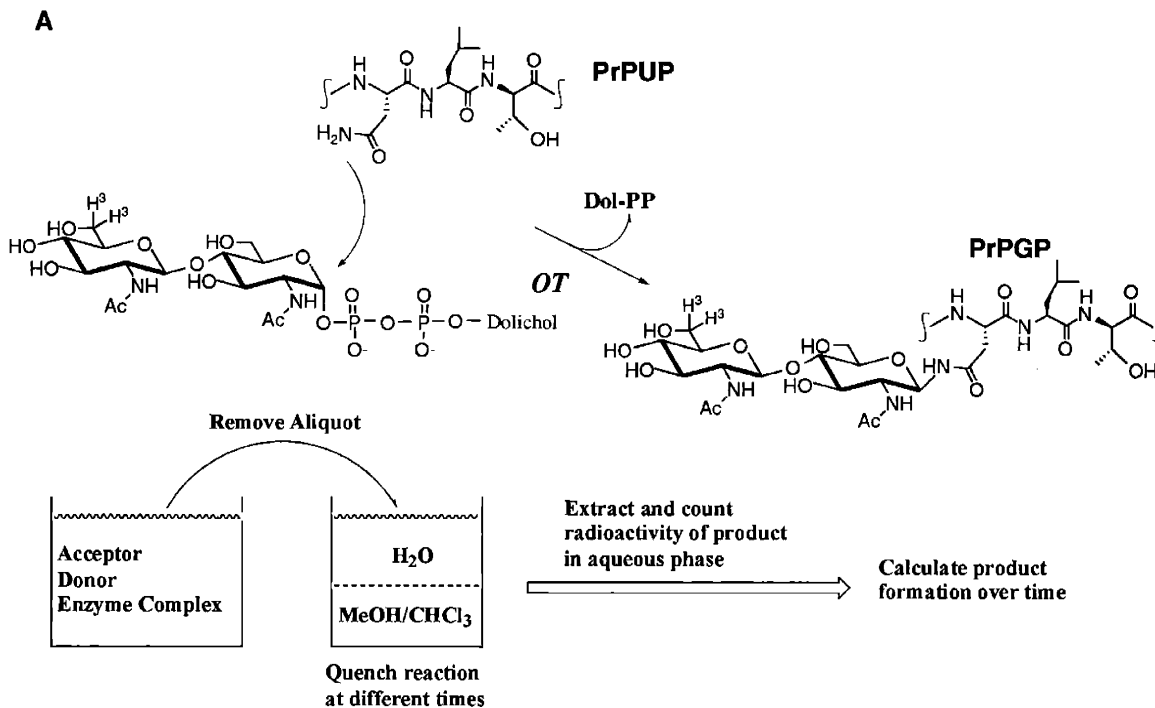


**Figure 2.1.** A. Schematic representation of the experimental approach for monitoring of the chemoenzymatic generation of **PrPGP**. B. Determination of  $K_m$  and  $V_{max}$  for the conversion of **PrPUP** to **PrPGP**.

The unglycosylated peptide (**PrPUP**) was then tested for OT recognition by incubating different peptide concentrations with the radiolabeled [<sup>3</sup>H]-GlcNAc-GlcNAc-

Dol-P-P donor and ER microsomes containing the enzyme. The transfer of the radiolabeled disaccharide to the peptide was monitored as a function of time and the standard enzymatic kinetic parameters of substrate concentration at half maximum velocity ( $K_m$ ) and the maximum velocity ( $V_{max}$ ) were determined. The values of  $K_m$  and  $V_{max}$  were extracted from the slope and y-intercept of the Hanes plot generated from monitoring the conversion of **PrPUP** to **PrPGP** using equation 1.<sup>23</sup>

$$\frac{[P1]}{V_0} = \left( \frac{1}{V_{max}} \right) [P1] + \left( \frac{K_m}{V_{max}} \right) \quad (1)$$

In this equation  $[P1]$  represent the peptide concentration and  $V_0$  is the initial velocity of the reaction.  $K_m$  and relative  $V_{max}$  values of 76  $\mu\text{M}$  and 97 dpm/min were determined for **PrPUP**, suggesting that the peptide is a good substrate for OT (Figure 2.1B).

The scale of the glycopeptide preparation was then increased to generate significant amounts of material. For this, we performed fourteen small-scale reactions in parallel for 80 minutes using 400  $\mu\text{M}$  peptide concentration (approximately five times the  $K_m$ ) and a [ $^3\text{H}$ ]-GlcNAc-GlcNAc-Dol-P-P donor of lower specific activity. Figure 2.2A shows the conversion of **PrPUP** in a small fraction used to monitor the large-scale reaction. After the crude glycopeptide product was separated from the lipid donor by extraction, the fourteen small fractions were combined, pre-purified using a Sep-Pak C<sup>18</sup> column and finally purified by HPLC (Figure 2.3B). Although the transformation of the



peptide was observed in the large scale enzymatic glycosylation, only 0.20 pmol of glycopeptide was isolated. Due to the mM and  $\mu$ M concentrations required for nuclear magnetic resonance (NMR) and CD spectroscopic analysis, the amount of glycopeptide prepared was not sufficient for structural studies.

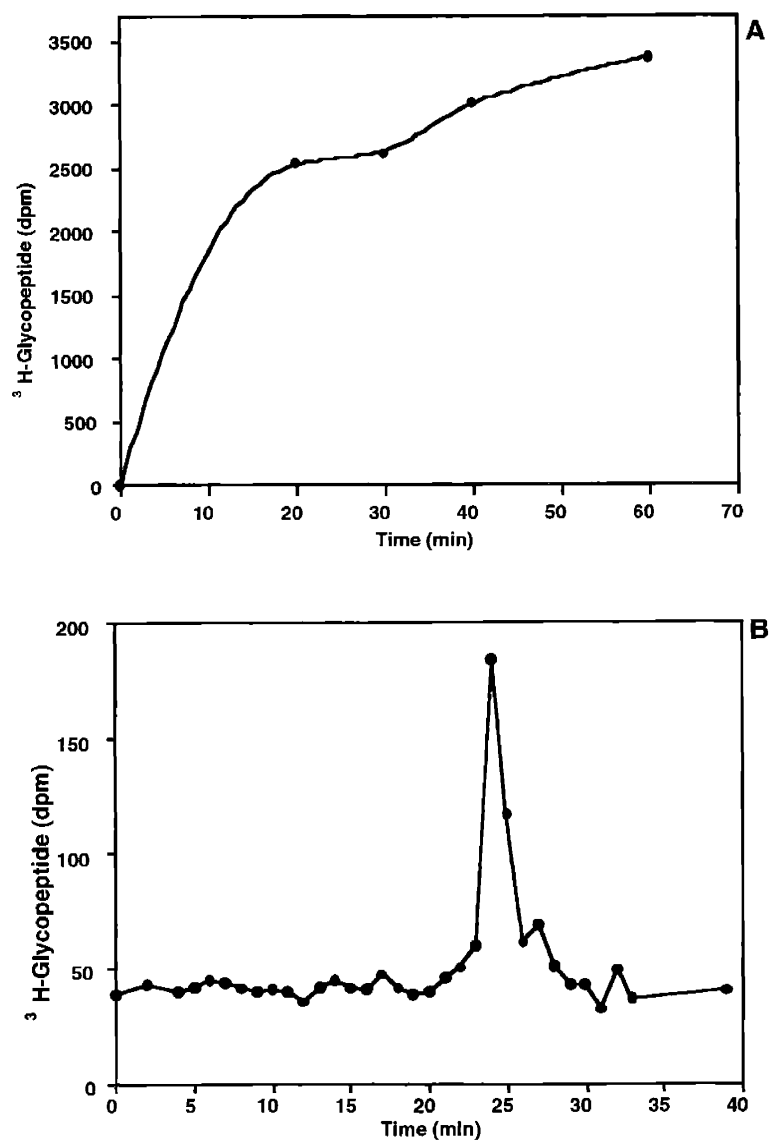
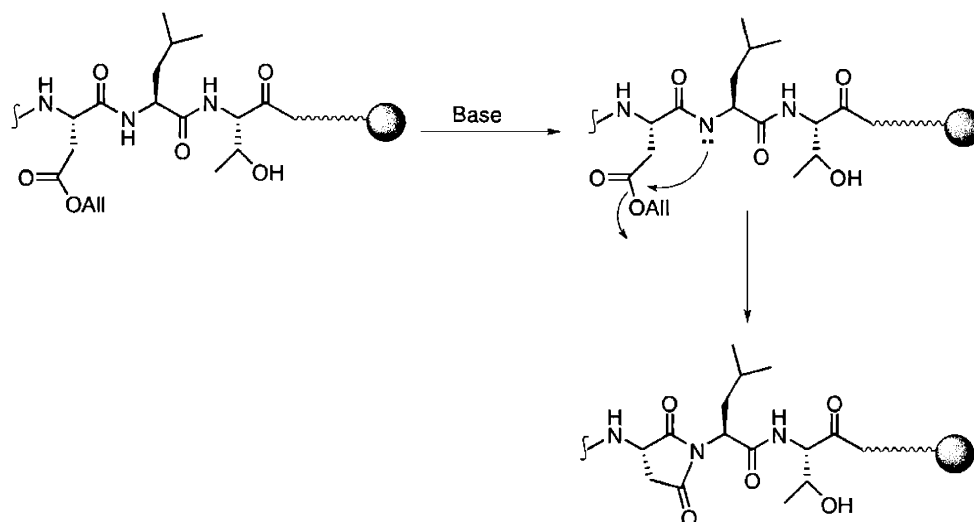


**Figure 2.2.** Large scale enzymatic conversion of PrPUP into PrPGP. A. Monitoring of the transformation as a function of time B. Chromatogram of the final purification of the enzymatic glycosylation shows single labeled peak of the glycopeptide product. Gradient: 0-60%  $\text{CH}_3\text{CN}/\text{H}_2\text{O}$ , 0.1 %TFA.

## **Base-labile building block approach**

### ***Fmoc-L-Asn[ $\beta$ -chitobiose(acetyl)<sub>5</sub>]-OH***

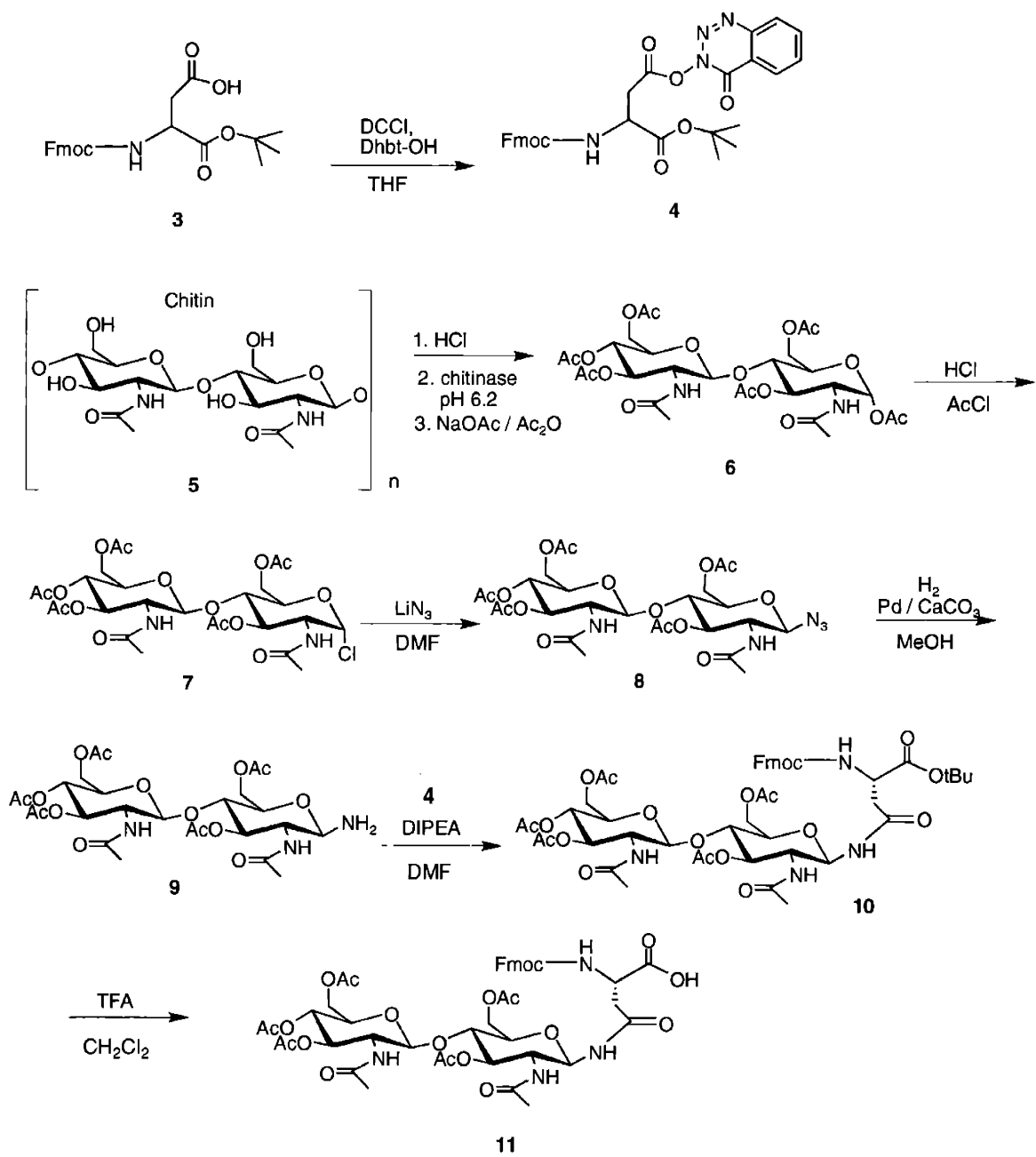
More recently, the convergent approach was employed for the preparation of glycopeptides in the Imperiali group.<sup>21,22</sup> Although this method is relatively simple, undesired aspartimide formation is a major drawback which results in low overall yields (Scheme 2.3). On the other hand, the building block approach offers fewer side reactions during the incorporation of the carbohydrate into the peptide, thus increasing the overall yields. Acetyl protecting groups have been used extensively for the synthesis of glycosylamino acid building blocks and have proved to be successful for the preparation of many important glycoconjugates.<sup>18,24</sup> Despite many advantages, the requirement for a final basic deacetylation of the protected glycopeptide can be detrimental in the preparation of some amyloidogenic peptides because basic conditions can promote fibrillization.



**Scheme 2.3.** Proposed mechanism for aspartimide formation during glycopeptide synthesis using the convergent approach.

Scheme 2.4 illustrates the synthetic scheme for the preparation of the chitobiose building block,  $N^{\alpha}$ -Fmoc- $N^{\beta}$ -(chitobiose heptaacetate)-L-asparagine. Although chitobiose octaacetate (**6**) is commercially available, it is quite expensive to use on large scale. Therefore, chitobiose octaacetate was synthesized in approximately 20% yield from crab shells chitin (**5**) by a combination of enzymatic and standard chemical synthesis.<sup>25</sup> Chlorination of (**6**) with gaseous hydrogen chloride in acetyl chloride (AcCl) generated the 1, $\alpha$ -chloro-chitobioseheptaacetate (**7**) in 84% yield.<sup>26</sup> Compound **7** underwent a bimolecular nucleophilic substitution ( $S_N2$ ) when reacted with lithium azide

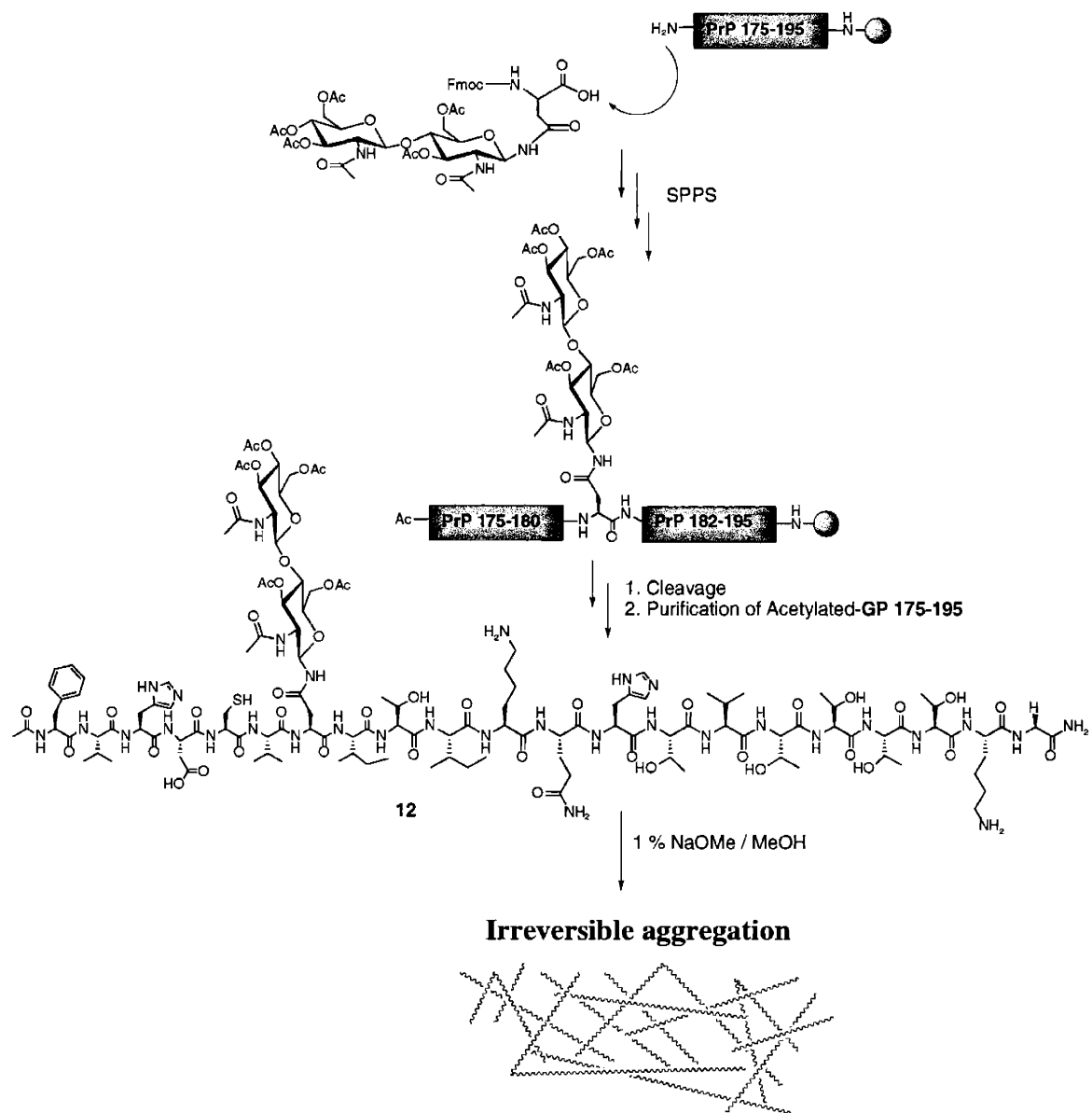
(LiN<sub>3</sub>) to invert the stereochemistry at the anomeric carbon and generate the β-anomer of 1-azido-chitobioseheptaacetate (**8**) in 96% yield.<sup>26</sup> Subsequent reduction of the azido group in **8** produced the chitobiosyl amine (**9**) in a quantitative yield.<sup>26</sup> The side chain of N<sup>α</sup>-Fmoc-L-aspartic acid β-carboxyl O-*tert*-butyl ester (**3**) was activated as the 3,4-dihydro-4-oxo-1,2,3-benzotriazin-3-yl (Dhbt) ester to generate **4** in 98% yield using the 3-hydroxyl precursor of Dhbt (Dhbt-OH).<sup>24</sup> Subsequently, **9** was coupled to the activated side chain of **4** to produce the N<sup>α</sup>-Fmoc-N<sup>β</sup>-(chitobiose heptaacetate)-L-asparagine O-*tert*-butyl ester (**10**) in 80% yield.<sup>24</sup> When ready to use for SPPS the *tert*-butyl group on **10** was cleaved using trifluoroacetic acid (TFA) to give **11** in stoichiometric yield. The use of the Dhbt-activated ester (**4**) demonstrated significantly better results compared with the coupling with N<sup>α</sup>-Fmoc-L-aspartic acid β-chloride OPfp ester,<sup>27</sup> which favored the formation of the succinimide product.



**Scheme 2.4.** Synthetic scheme for the synthesis of Fmoc-L-Asn[β-chitobiose(acetyl)<sub>5</sub>]-OH.

### *Incorporation of the building block onto the peptide*

Standard Fmoc chemistry was performed on a MilliGen/Biosearch 9050 automated peptide synthesizer for the generation of **PrPGP** before the incorporation of the chitobiose building block. For the coupling of **11** and subsequent residues, the couplings were performed "off-line" using manual solid phase synthesis techniques enabling the use of an alternate solvent system. Due to the low solubility of the chitobiose building block in *N,N*-dimethylformamide (DMF), *N*-methylpyrrolidinone (NMP) was used to dissolve and couple **11** to the peptide on the resin. Also, 1-hydroxy-7-azabenzotriazole (HOAT) / *O*-(7-azabenzotriazol-1-yl)-1,1,3,3-tetramethyluronium hexafluorophosphate hydrofluoric acid (HATU) activation was used for this as well as all subsequent couplings. The coupling of **11** and following amino acids required longer reaction times than standard residues apparently due to steric hindrance or the induction of secondary structure of the building block on the peptide. The *N*-terminus of the acetylated **PrPGP** was capped with an acetyl group after the synthesis, followed by cleavage from the resin and HPLC purification.



**Scheme 2.5.** Acetyl-protected building block incorporation and final glycopeptide deprotection. The basic deacetylation in solution causes irreversible aggregation of the PrP peptide.

The final step in the glycopeptide synthesis involved the deacetylation of the acetylated glycopeptide in solution using 1% NaOMe in MeOH (Scheme 2.5). This peptide fragment is stable in aqueous solution at low pH. However, electron microscopy (EM) analysis has demonstrated that the peptide forms fibrils at high pH. (Figure 2.3). Therefore, this step caused the irreversible aggregation and precipitation of the peptide, resulting in a major loss of the synthetic material. The overall yield for the glycopeptide, synthesized in this manner was approximately 1% (2 mg).

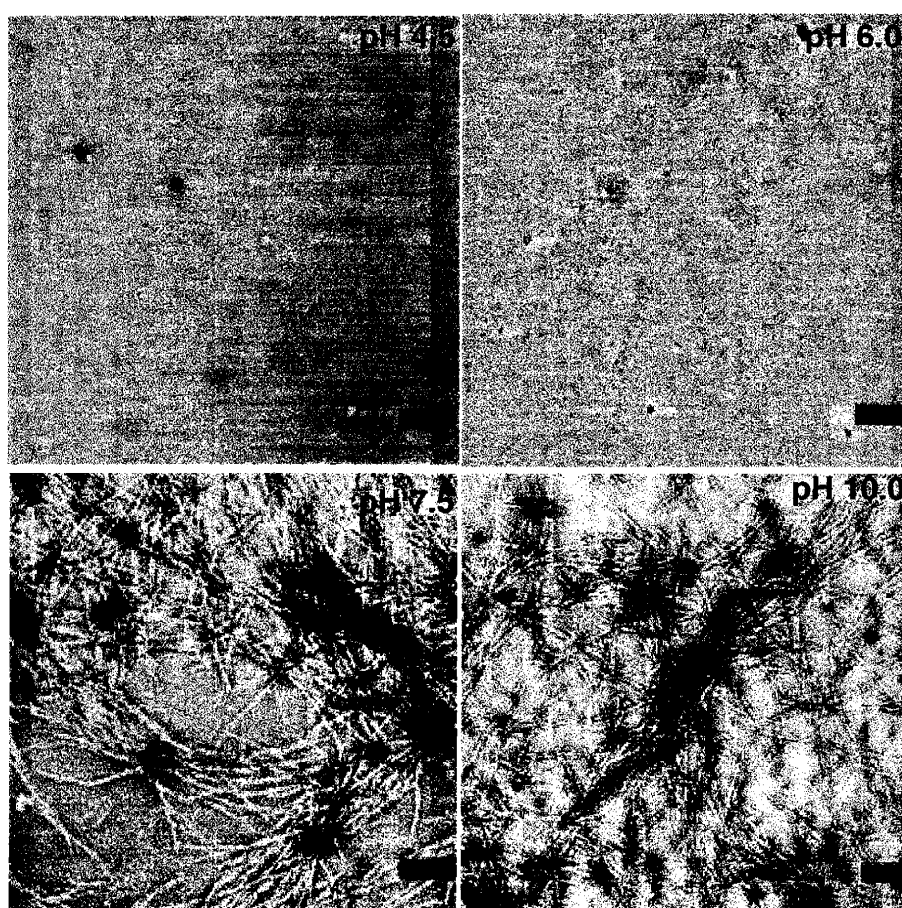


**Figure 2.3.** Electron microscopy of 70  $\mu$ M PrPUP samples after incubation at different pH for 24 hours. Bar size 400 nm.



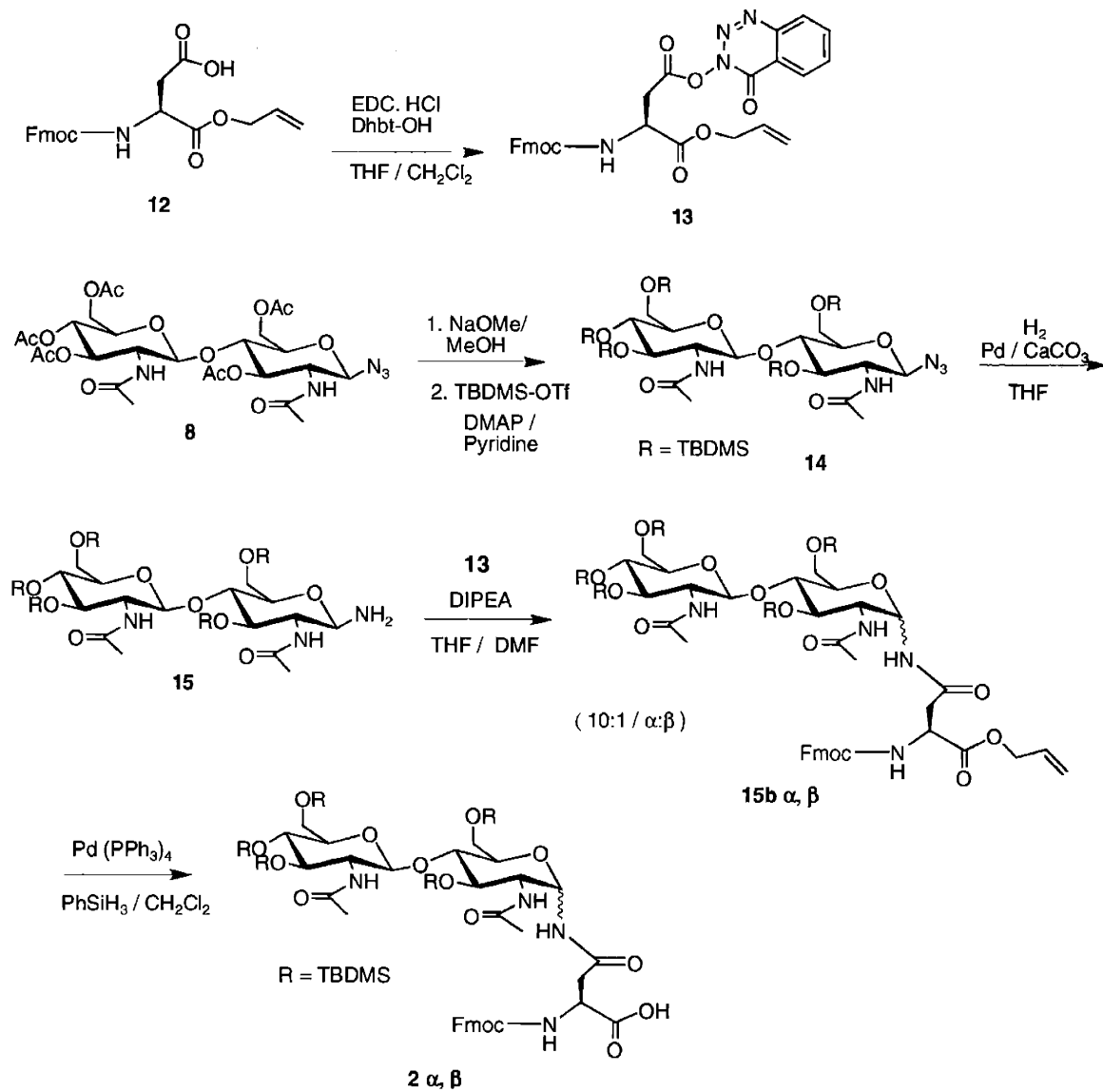
## Acid-labile building block approach

### *Fmoc-L-Asn[ $\alpha$ -chitobiose(TBDMS)<sub>5</sub>]-OH and Fmoc-L-Asn[ $\beta$ -chitobiose(TBDMS)<sub>5</sub>]-OH*

Due to the propensity of this PrP peptide fragment to form irreversible aggregates in solution, the material used for experiments cannot be recycled, therefore, larger quantities of material are desired. We envisioned that an acid-labile protecting group can circumvent the problem we encountered in the previous synthesis. Kihlberg and co-workers have previously shown the use of acid-labile protecting groups for the synthesis of *N*-linked and *O*-linked glycopeptide building blocks.<sup>28,29</sup> The main advantage of using acid-labile protecting groups for glycopeptide synthesis is that a concomitant deprotection of the saccharide moiety can be achieved during the acidic cleavage of the peptide from the resin without further exposure to basic conditions. Unfortunately, in the generation of *N*-linked chitobiose building blocks using *tert*-butyldimethylsilyl (TBDMS) protecting groups, anomerization of the *N*-acetylglucosamine proximal to the amino acid is a major side reaction, giving the undesired  $\alpha$ -anomer as the major product.<sup>28</sup>

For the preparation of Fmoc-L-Asn[ $\beta$ -chitobiose (TBDMS)<sub>5</sub>]-OH we used Kihlberg's preparation.<sup>28</sup> The 1, $\beta$ -azidochitobioseheptaacetate (**8**) was prepared as described in the previous section. Deacetylation of **8** using NaOMe in MeOH, followed

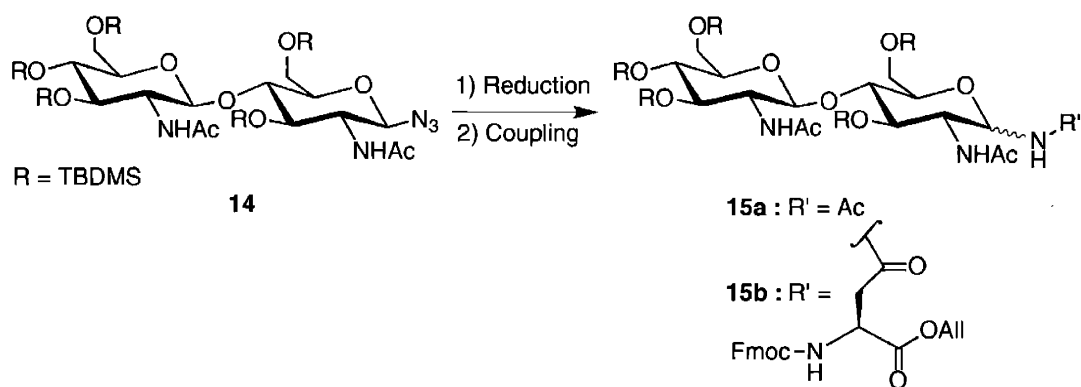
by silylation with *tert*-butyl dimethylsilyl-triflate (TBDMS-OTf) and catalytic amounts of 4-dimethylaminopyridine (DMAP) in pyridine afforded **14** in 88% yield. The TBDMS-protected azidochitobiose (**14**) was then reduced with Pd/CO<sub>3</sub> under H<sub>2</sub> atmosphere in THF followed by coupling with preactivated Fmoc-Asp(Dhbt)-OAll (**13**) in 1:1 THF/DCM. This procedure yielded the  $\alpha$ -linked building block as the major product **15 $\alpha$**  (55%,  $\alpha$  :  $\beta$  = 10:1 after flash column chromatography). The products were then deallylated separately using Pd(PPh<sub>3</sub>)<sub>4</sub> and PhSiH<sub>3</sub> in DCM to give building blocks **2 $\alpha$**  and **2 $\beta$**  in quantitative yield.<sup>30</sup>



**Scheme 2.6.** Synthetic scheme for the preparation of Fmoc-L-Asn[ $\alpha$ -chitobiose(TBDMS)<sub>5</sub>]-OH and Fmoc-L-Asn[ $\beta$ -chitobiose(TBDMS)<sub>3</sub>]-OH

## Stereochemical control for the synthesis of *Fmoc-L-Asn*[ $\beta$ -chitobiose(TBDMS)<sub>5</sub>]-OH

The anomerisation of the first *N*-acetylglucosamine during the synthesis of the *Fmoc-L-Asn*[ $\beta$ -chitobiose(TBDMS)<sub>5</sub>]-OH is apparently induced by the bulky TBDMS groups during the reduction of the protected chitobiosyl-azide and the subsequent coupling of the chitobiosylamine to the aspartic acid.<sup>28,29</sup> In an attempt to reduce the level of anomerisation, different reduction conditions and preactivation of the aspartic acid (instead of *in situ* activation) were used attempted (Scheme 2.7, Table 2.1). Unfortunately, these conditions did not show any significant improvement in the anomeric ratio. Staudinger reactions have also been attempted by others<sup>28</sup> but these approaches have proved unsuccessful.



**Scheme 2.7.** Anomerisation of the TBDMS-protected carbohydrate during the reduction and coupling conditions.

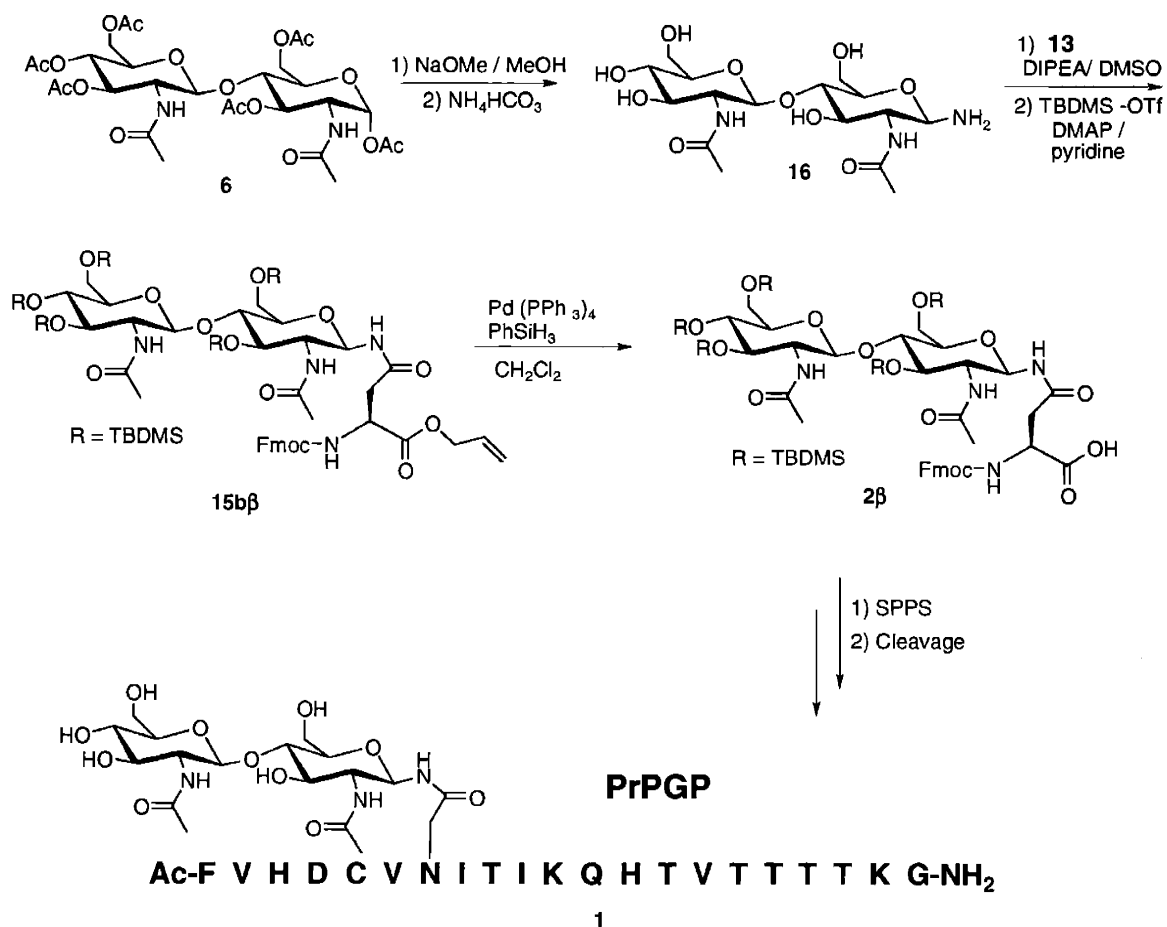
**Table 2.1.** Survey of experimental conditions for the synthesis of the TBDMS-protected,  $\beta$ -linked chitobiose building block.

Reduction	Coupling	$\alpha$ : $\beta$ (%)
H <sub>2</sub> , Pd/C in THF	Pyridine/Ac <sub>2</sub> O (2:1)	75 : 25
H <sub>2</sub> , Pd/CaCO <sub>3</sub> in EtOH	Pyridine/Ac <sub>2</sub> O (2:1)	62 : 38
Raney Ni in EtOH	Ac <sub>2</sub> O/CHCl <sub>3</sub>	43 : 57
Raney Ni in EtOH	Fmoc-Asn(Dhbt)-OAll/CHCl <sub>3</sub>	> 91 : 9
H <sub>2</sub> , Pd/C in THF	Fmoc-Asn(Dhbt)-OAll/CHCl <sub>3</sub>	91 : 9

\* Quantification of the anomeric ratio for **15** was based on the <sup>1</sup>H NMR data for the anomeric protons: <sup>1</sup>H NMR (500 MHz, CD<sub>3</sub>OD)  $\delta$  (ppm): **15a <sub>$\alpha$</sub>**  5.75 (d,  $J=2.2$  Hz, 1H, H-1); **15a <sub>$\beta$</sub>**  4.91 (d,  $J=9.5$  Hz, 1H, H-1)

Since the anomerisation appeared to be promoted by the bulky TBDMS groups, we elected to carry out the coupling of aspartic acid with the free chitobiosylamine prior to carbohydrate protection (Scheme 2.8). Chitobiose octaacetate **6** was prepared as described previously<sup>25</sup> and deacetylated using NaOMe in MeOH to give the free chitobiose. Chitobiosylamine **16** was then generated by stirring free chitobiose in a saturated ammonium hydrogen carbonate solution at 45°C for 2 days.<sup>15</sup> For the preparation of the building block, Fmoc-L-Asp(OH)- $\alpha$ -OAll (**12**) was activated as the 1-oxo-2-hydroxydihydrobenzotriazene (Dhbt) ester **13** and reacted with the free chitobiosylamine **16** in the presence of diisopropylethylamine in DMSO. Silylation of the coupling product using TBDMS-OTf and DMAP in pyridine afforded **15b $\beta$**  in a 50% overall yield after flash column chromatography. This transformation afforded predominantly (>91%) the  $\beta$ -linked building block. Finally, the  $\alpha$ -carboxylic acid was deprotected in quantitative yield using

$\text{Pd}(\text{PPh}_3)_4$  and  $\text{PhSiH}_3$  in  $\text{CH}_2\text{Cl}_2$ .<sup>30</sup> The use of  $\text{PhSiH}_3$  helped to minimize undesired Fmoc deprotection which was observed when morpholine was used.<sup>28</sup>



**Scheme 2.8.** Synthetic scheme for the stereoselective preparation of Fmoc-L-Asn[ $\beta$ -chitobiose(TBDMS)<sub>5</sub>]-OH and the incorporation into **PrPGP**.

### PrPGP synthesis

The incorporation of the TBDMS-protected building block into the peptide and the final cleavage and deprotection processes showed many advantages compared with the acetylated building block approach. First, the solubility of the TBDMS-protected building

block allowed the coupling to be performed in dichloromethane compared with the acetylated counterpart which required *N*-methylpyrrolidinone for the best coupling conditions. Also, the coupling of the building block was more efficient in this case; in addition to proceeding efficiently, no peptide truncation products were observed after cleavage from the resin. On the other hand, the coupling for the acetylated counterpart was very difficult and many deletion products were observed even after triple coupling with 1.5 equivalents of building block for each coupling (Figure 2.4). Most importantly, this approach provided higher yields and fewer side products; particularly because no basic treatment was required for the complete deprotection of the glycopeptide (which causes irreversible aggregation and precipitation) as it is the case when using the acetylated building block. After cleaving the peptide from the resin, only two major products were observed: the expected glycosylated product **PrPGP** (49% peptide after purification) and **PrPGP** with an extra TBDMS protecting group (11%) (Figure 4). The addition of an extra 0.8% water and additional shaking for 45 minutes after the standard 3 hours of cleavage produced the best results for the removal of the protecting groups. This approach provided enough material to carry out a panel of biophysical studies on the system which are described on chapter 4.

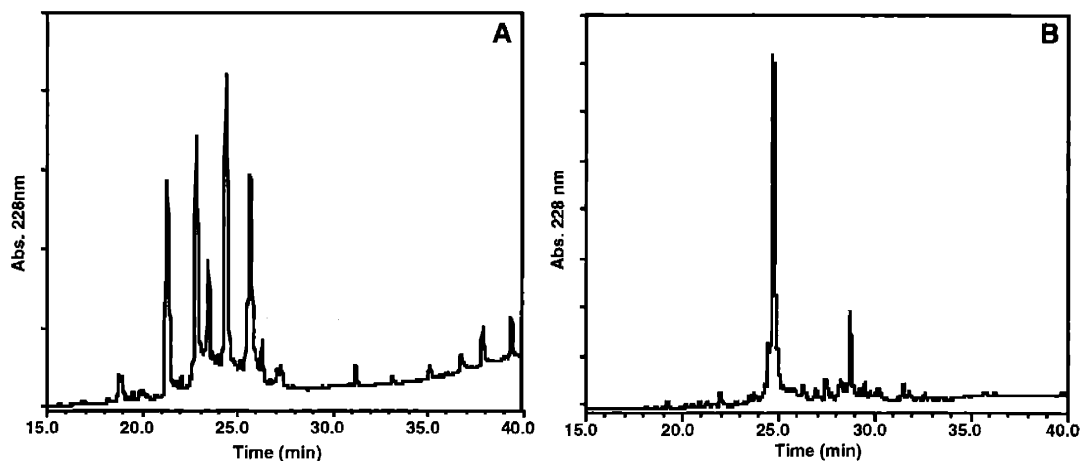


**Figure 2.4.** Comparison of the purity of the crude glycopeptides using the acetylated (**A**) and the silylated (**B**) building blocks. The HPLC analysis was performed on a C<sub>18</sub>-reversed-phase column directly after acidic cleavage from resin and trituration. **A.** Chromatogram shows acetylated glycopeptide ( $t_R=24.2$  minutes,  $[M+3H^+]/3$  1001.2 (obsd.); 1001.1 (calcd.) and many truncation products. Gradient: 0 to 90% CH<sub>3</sub>CN in H<sub>2</sub>O and 0.1 %TFA in 25 minutes. **B.** Chromatogram shows completely deprotected **PrPGP** ( $t_R=24.71$  minutes,  $[M+2H^+]/2$  1396.8 (obsd.); 1396.6 (calcd.) and **PrPGP** with an additional TBDMS ( $t_R=28.75$  minutes,  $[M+2H^+]/2$  1453.4 (obsd.); 1453.7 (calcd.). Gradient: 15 to 70% CH<sub>3</sub>CN in H<sub>2</sub>O and 0.1 %TFA in 30 minutes.

## Discussion

An efficient synthesis of a Fmoc-L-Asn[ $\beta$ -chitobiose(TBDMS)<sub>5</sub>]-OH building block has been achieved *via* the coupling of a free chitobiosylamine and Fmoc-L-Asp(Dhbt)- $\alpha$ -OAll followed by TBDMS protection. This approach avoids the anomerisation of the proximal GlcNAc residue previously encountered. The use of this building block in the synthesis of amyloidogenic peptides was illustrated by incorporation into the 175-195 fragment of the prion protein that has been shown to aggregate into fibrils under neutral and basic conditions. The use of the acid-labile TBDMS-protected building block showed



significant improvement on the synthesis of **PrPGP** when compared with the acetylated building block due to higher coupling efficiency and the elimination of the basic deprotection step after SPPS.

### **Acknowledgements**

This work was supported by a grant from NIH (GM-39334) and by NIH Biotechnology Training Grant to C. J. B. (1999-2001). Part of this work appears in. Bosques, C. J.; Tai, V. W.-F.; Imperiali, B. "Stereoselective Synthesis of  $\beta$ -linked TBDMS-Protected Chitobiose-Asparagine: A Versatile Building Block for Amyloidogenic Glycopeptides" *Tetrahedron Lett.* **2001**, 42, 7207-7210.

## Experimental section

### *Peptide synthesis*

Peptides were synthesized on a MilliGen/Biosearch 9050 automated peptide synthesizer using standard 9-fluorenylmethoxycarbonyl (Fmoc) chemistry. PAL-PEG-PS resin (0.19 meq/g) was used as the solid support and the couplings were performed using HOBT/HBTU as activators. The *N*-terminus Fmoc group was deprotected using 20% piperidine in DMF. The free amine was acetylated using acetic anhydride and diisopropylethylamine in DMF. For the coupling of Cys 179, Fmoc-L-Cys(Trt)-OPfp was used in the absence of base in order to prevent racemization. The peptides were cleaved from the resin using 92:3:3:2 TFA/triisopropylsilane/ethanedithiol/H<sub>2</sub>O, and triturated using ice-cold ethyl ether/hexane 1:1.

### *Peptide purification and characterization*

Peptides were dissolved in 85 : 10 : 5 cold H<sub>2</sub>O : CH<sub>3</sub>CN : DMSO (with 0.1% TFA), filtered through a 0.45 µm filter and purified by reverse-phase HPLC on a Waters Prep LC 4000 system using a 15 -70% gradient in acetonitrile/water, 0.1% TFA for 30 minutes. Peptides were collected (**PrPUP**:  $t_R = 25.7$  minutes; **PrPGP**:  $t_R = 24.7$  minutes) and characterized by electro-spray mass spectrometry (ESMS). **PrPUP**:  $([M+3H^+])/3$

795.7 (obsd); 795.9 (calcd)). **PrPGP**: ( $[M+2H^+]/2 = 1396.8$  (obsd); 1396.6 (calcd)).

Quantitative amino acid analysis (QAA) was used to confirm the amino acid composition of the peptides. Full NMR characterization of **PrPUP** and **PrPGP** is provided in chapter 4.

*Chitobiose octaacetate*(**6**). The preparation of **6** was accomplished following previously published procedures.<sup>25</sup> Commercially available chitin (20 g) from crab shells were digested with 125 ml of concentrated HCl for 90 minutes under sonication. The syrup was diluted with 1.4 liters of ice and water. This mixture was stored overnight at 4 °C. The resulting white powder was filtered, washed with 25 mL of 1 M NaOH solution followed by neutralization with water. The colloidal chitin was subsequently washed with 30 mL of acetone and finally with 30 mL of ethyl ether. The powder was lyophilized to obtain 12.6 g of dry material. This colloidal chitin was used for the enzymatic reaction using commercially available chitinase from *Streptomyces griseus*. Two reactions, each with 6.3 g of colloidal chitin, were performed. For each reaction 34.8 mg of chitinase (460 units/g, or an equivalent to 16 units) were added to a 100 mL 0.1 N Na<sub>2</sub>HPO<sub>4</sub> buffer solution at pH 6.4 which contained the chitin. The mixture was stirred at 40 °C for 15 days followed by filtration and lyophilization of the liquid. Each reaction produced 5.8 g of crude chitobiose, which was acetylated using acetic anhydride (65 mL, 98% pure) and

anhydrous sodium acetate (7 g); the reaction was stirred at 80°C for 2 days. The product was washed with NaHCO<sub>3</sub> and brine and crystallized from MeOH to obtain 2.5 g of pure chitobiose octaacetate mainly in the  $\alpha$ -anomeric form. Recrystallization of the filtrate gave a second batch 740 mg of  $\alpha$ - chitobiose octaacetate.

TLC: [silica, 95:5 CHCl<sub>3</sub>:MeOH, phosphomolybdic acid (PMA) detection] R<sub>f</sub> = 0.31

*1,  $\alpha$ -chloro-chitobiose heptaacetate (7)*. 100 equivalents of distilled acetyl chloride (15.7 ml, 220 mmol) were added to 1.5 g (2.2 mmol) of chitobiose octaacetate (**6**) and gaseous HCl was bubbled into the suspension at -25°C until saturation (approximately 20 minutes). The solution was sealed and allowed to stir at room temperature for 12 hours. The solvent was carefully removed by purging with N<sub>2</sub>. The crude solid was then triturated with cold ethyl ether and acetone to give the chloride **7** in an 84% yield.

Characterization of the product is in agreement previous reports.<sup>26</sup>

TLC: (silica, 95:5 CHCl<sub>3</sub>:MeOH, PMA detection) R<sub>f</sub> = 0.36

*1,  $\beta$ -azidochitobiose heptaacetate (8)*. The chitobiosyl chloride **7** (1.2 g, 1.8 mmol) was dissolved in 12 ml of DMF, 450 mg (9.2 mmol) of LiN<sub>3</sub> were added and the reaction was stirred at 80 °C for 24 hours. The reaction was then concentrated, the product was dissolved in chloroform and washed twice with water. The organic phase was dried with

Na<sub>2</sub>SO<sub>4</sub>, filtered and concentrated to obtain **8** in 96% yield. Characterization of the product is in agreement previous reports.<sup>26</sup>

TLC: (silica, 9:1 CHCl<sub>3</sub>:MeOH, PMA detection) R<sub>f</sub> = 0.45

*1,β-aminochitobiose heptaacetate (9)*. The azido compound **8** (514 mg, 0.78 mmol) was dissolved in a minimum volume of MeOH and EtOH, 5% Pd / CaCO<sub>3</sub> (80 mg) was added and the mixture was stirred at room temperature under H<sub>2</sub> atmosphere for 12 hours. The catalyst was filtered and the solution was concentrated to obtain chitobiosyl amine **9** in 98% yield. Characterization of the product is in agreement previous reports.<sup>26</sup>

TLC: (silica, 9:1 CHCl<sub>3</sub>:MeOH, PMA detection) R<sub>f</sub> = 0.2

*N<sup>α</sup>-Fmoc-L-Aspartic acid-β-4-(3,4-dihydro-4-oxo-1,2,3-benzotriazin-3-yl) O-tert-butyl ester (4)*. To a solution of *N<sup>α</sup>-Fmoc-L-Aspartic acid-β-carboxyl O-tert-butyl ester (3)* (1.93 g, 4.69 mmol) in 9 ml of dry THF at -35 °C, 977 mg (4.69 mmol) of 1,3-dicyclohexyl carbodiimide (99%, Aldrich) was added and stirred for 10 minutes. Dhbt-OH (781 mg, 4.69 mmol) was then added and stirred for 2 hours at -35°C before warming up to room temperature. The product was filtered through celite, concentrated, redissolved in THF, filtered, and concentrated to give 98% yield of the activated ester (**4**). Characterization of the product is in agreement previous reports. <sup>24</sup>

TLC: (silica, 1:2 EtOAc/petroleum ether, PMA and UV detection)  $R_f = 0.57$

*N*<sup>α</sup>-Fmoc-*N*<sup>β</sup>-(chitobiose heptaacetate)-*L*-asparagine *O*-*tert*-butyl ester (**10**). The chitobiosyl amine (**9**) (0.738 mg, 1.17 mmol) was dissolved in 10 ml DMF and 307 μl (1.75 mmol) of *N,N*-diisopropylethylamine (99% Aldrich). The solution was stirred at room temperature for 10 minutes and 0.7781 mg (1.398 mmol) of the Dhbt-activated amino acid (**4**) was added. After 1.5 hours, no starting material was observed by TLC. The reaction mixture was concentrated, dissolved in CHCl<sub>3</sub> and washed with NH<sub>4</sub>Cl. The organic extract was dried with Na<sub>2</sub>SO<sub>4</sub>, filtered and concentrated. The crude product was recrystallization from 49:49:1 CHCl<sub>3</sub>:MeOH:CH<sub>3</sub>CN in 80 % yield. Characterization of the product is in agreement previous reports.<sup>24</sup>

TLC: (silica, 9:1 CHCl<sub>3</sub>:MeOH, PMA, H<sub>2</sub>SO<sub>4</sub> and UV detection)  $R_f = 0.45$ .

*N*<sup>α</sup>-Fmoc-*N*<sup>β</sup>-(chitobiose heptaacetate)-*L*-asparagine (**11**) (351.1 mg, 0.342 mmol) was synthesized by stirring **10** in 50:50 CH<sub>2</sub>CH<sub>2</sub>:TFA (10 ml/10 ml) for 40 minutes. The product was concentrated and co-concentrated with toluene to give the title compound in quantitative yield. Characterization of the product is in agreement previous reports.<sup>24</sup>

TLC: (silica, 9:1 CHCl<sub>3</sub>:MeOH, PMA detection)  $R_f = 0.40$

*2-Acetamido-2-deoxy-4-O-(2-acetamido-2-deoxy-3,4,6-tri-O-tert-butyltrimethylsilyl-β-D-glucopyranosyl)-3,6-di-O-tert-butyltrimethylsilyl-β-D-glucopyranosyl azide (14)*. The azidochitobiose heptaacetate (**8**) (490 mg, 0.74 mmol) was suspended in 40 ml of distilled MeOH and 0.02 M NaOMe/ MeOH (0.02M, 2.5 ml) was added to the mixture. Additional amounts of 0.02 M NaOMe/ MeOH (1.5 ml) were added after 4 and 17 hours. The solution was stirred for 3 days followed by neutralization with dilute HOAc in MeOH. The solvent was then concentrated and co-concentrated with toluene. DMAP (9 mg, 0.07mmol) and pyridine (15 ml) were added, the suspension stirred at 0°C and TBDMS-OTf (2ml, 10.8 mmol) was added slowly. After 1 hour, the solvent was raised to room temperature and stirred for 20 hours. MeOH (3ml) was added and the solution was concentrated and co-concentrated with toluene. Flash column chromatography (3:1 to 2:1 hexane/ ethyl acetate) afforded the desired product **14** in 88% yield. Characterization of the product is in agreement previous reports.<sup>28</sup>

TLC: (silica, 2:1 hexane: ethyl acetate, CAM detection) R<sub>f</sub> = 0.48

*N<sup>α</sup> Fmoc-L-Aspartic acid β-(Dhbt)-OAll (13)*. *N<sup>α</sup> Fmoc-L-aspartic acid -(OH)-OAll (12)* (403.4 mg, 1.0 mmol) was dissolved in 1:1 THF/CH<sub>2</sub>Cl<sub>2</sub> (10 ml). *N*-Ethyl-*N'*-(3-dimethylaminopropyl) carbodiimide.HCl (EDC. HCl, 230mg, 1.2 mmol) was added to the solution and stirred for 10 min. Dhbt-OH (166.47 mg, 1.0 mmol) was then added and

stirred for 3.5 hours. The mixture was washed with 5 mL of 1% HCl/H<sub>2</sub>O, dried with Na<sub>2</sub>SO<sub>4</sub> and filtered to afford compound **13** in a quantitative yield.

<sup>1</sup>H NMR (300 MHz, CDCl<sub>3</sub>) δ (ppm): 8.45-7.89 (m, 4H, Dhbt), 7.78-7.33 (m, 8H, Fmoc-arom.), 6.15 (d, 1H, N<sup>α</sup>H), 5.90 (m, 1H, OCH<sub>2</sub>-CH=CH<sub>2</sub>), 5.40-5.28 (m, 2H, CH=CH<sub>2</sub> *cis, trans*), 4.90-4.75 (m, 3H, OCH<sub>2</sub>-CH=CH<sub>2</sub>, H<sup>α</sup>), 4.45 (m, 2H, FmocCH<sub>2</sub>), 4.30 (t, *J*=7.10Hz, 1H, FmocCH), 3.49 (m, 2H, H<sup>β</sup>)

TLC: (silica, 2:1 petroleum ether: ethyl acetate, PMA and UV detection) R<sub>f</sub> = 0.35

*Allyl-N<sup>4</sup>-[2-acetamido-2-deoxy-4-O-(2-acetamido-2-deoxy-3,4,6-tri-O-tert-butylidimethylsilyl-β-D-glucopyranosyl)-3,6-di-O-tert-butylidimethylsilyl-α-D-glucopyranosyl]-N<sup>2</sup>-(fluoren-9-ylmethoxycarbonyl)-L-aspartate and Allyl-N<sup>4</sup>-[2-acetamido-2-deoxy-4-O-(2-acetamido-2-deoxy-3,4,6-tri-O-tert-butylidimethylsilyl-β-D-glucopyranosyl)-3,6-di-O-tert-butylidimethylsilyl β-D-glucopyranosyl]-N<sup>2</sup>-(fluoren-9-ylmethoxycarbonyl)-L-aspartate (**15bα** and **15bβ**).*

Compound **7** (445.6 mg, 0.44 mmol) was dissolved in THF (20 ml), Pd/ CaCO<sub>3</sub> (10%, 200 mg) was added and the mixture was stirred at room temperature under H<sub>2</sub> atmosphere for 3 hours. The catalyst was filtered and the filtrate was concentrated to a final volume of 2.5 ml. DMF (2.5 ml) and DIPEA were then added (113.5 μL, 0.645 mmol) and stirred for 10 minutes. The activated aspartic acid (**13**) (255.7 mg, 0.47 mmol) was added and the solution turned immediately deep yellowish indicating that the reaction occurred



instantaneously. After stirring for 1 hour, the solution was concentrated, diluted with  $\text{CHCl}_3$  and washed with saturated  $\text{NaHCO}_3$ . The organic layer was dried with  $\text{MgSO}_4$ , filtered and concentrated. Flash column chromatography (3.5:1 to 3:1 to 2.5:1  $\text{CHCl}_3/\text{CH}_3\text{CN}$ ) afforded **15b $\alpha$**  (50%) and **15b $\beta$**  (5%).

Characterization of **15b $\alpha$**  and **15b $\beta$**  is in agreement previous reports.<sup>28</sup>

TLC: (silica, 3:1  $\text{CHCl}_3/\text{CH}_3\text{CN}$ ; CAM and UV detection) **15b $\alpha$**  :  $R_f = 0.24$  and **15b $\beta$**  :  $R_f = 0.33$

*1,β-aminochitobiose* (**16**). Chitobiose octaacetate (**6**) (372 mg, 0.55 mmol) and NaOMe (596 mg, 11.0 mmol) were dissolved in dry MeOH (24 mL) and stirred at room temperature for 3.5 hours. The reaction was neutralized using Dowex resin (pyridinium form), filtrated concentrated, coconcentrated with toluene and the trace of solvent were removed under vacuum overnight. Saturated ammonium hydrogen carbonate (27 mL) was added to free chitobiose (223.9 mg, 0.53 mmol) and the mixture was stirred at 45°C for 2 days. Additional amounts of solid  $\text{NH}_4\text{HCO}_3$  were added during the reaction to ensure saturation. After successful conversion to the aminochitobiose, the solution was diluted with water and concentrated to half the volume. This process was repeated (5 times) until no further ammonia was detected. The chitobiosylamine was then repetitively frozen, lyophilized and dissolved until constant weight was achieved. Due to the instability of glycosylamines, **16** was used for the next step without further purification.

TLC: (silica, 4:3:2 ethyl acetate/MeOH/water; CAM and 10% H<sub>2</sub>SO<sub>4</sub> detection) unprotected chitobiose (R<sub>f</sub> = 0.73) and **16** (R<sub>f</sub> = 0.33).

ESMS: [M+H<sup>+</sup>] = 424.1 (obsd) 424.4 (calc).

<sup>1</sup>H NMR **16** (500 MHz, D<sub>2</sub>O) δ (ppm): 4.55 (d, *J* = 8.5 Hz, 1H, H-1'), 4.12 (d, 1H, *J* = 8.5 Hz, H-1), 3.90-3.40 (m, 13H), 2.04 (s, 3H, NAc), 2.01 (s, 3H, NAc)

Allyl-N<sup>4</sup>-[2-acetamido-2-deoxy-4-O-(2-acetamido-2-deoxy-3,4,6-tri-O-*tert*-butyldimethylsilyl-β-D-glucopyranosyl)-3,6-di-O-*tert*-butyldimethylsilyl-β-D-glucopyranosyl]-N<sup>2</sup>-(fluoren-9-ylmethoxycarbonyl)-L-aspartate (**15bβ**). The unprotected amine (**16**) (211.7 mg, 0.50 mmol) was dissolved in DMSO to a concentration of 0.1 M, DIPEA (104.5 μL, 0.6 mmol) was added and the solution was stirred for 10 min. The activated aspartic acid (**13**) (270.3 mg, 0.5 mmol) was added and the solution turned immediately deep yellowish indicating that the reaction occurred instantaneously. The reaction was monitored by TLC, HPLC and ESMS. After complete consumption of the starting material the solution was lyophilized. Pyridine (2.4 mL, 30 mmol) and catalytic amounts of DMAP (9.1 mg, 0.075 mmol) were added and the mixture was cooled to 0°C. TBDMS-OTf (2.3 mL, 10 mmol) was added slowly and stirred at low temperature for 1 hour before raising it to room temperature. The solution was stirred for 20 hours, diluted with 12 mL of MeOH, concentrated, concentrated with toluene and the trace solvent was dried under high vacuum. Flash column chromatography (3.5:1 to 3:1 to 2.5:1 CHCl<sub>3</sub>/CH<sub>3</sub>CN) afforded **15bβ** (50%).

HPLC and ESMS of unprotected building block. Gradient 0-70% CH<sub>3</sub>CN / H<sub>2</sub>O, 0.1%

TFA:  $t_R$  = 28.4 min; [M+H<sup>+</sup>] = 8002.8 (obsd) 8002.0 (calc).

<sup>1</sup>H NMR **15b $\beta$**  (500 MHz, CDCl<sub>3</sub>)  $\delta$  (ppm): 7.76-7.33 (m, 8H, Fmoc-arom.), 6.86 (d,  $J$ =7.5 Hz, 1H,  $\gamma$ NH), 6.60 (d,  $J$ =9.0 Hz, 1H, NHAc), 6.14 (d,  $J$ =9.0 Hz, 1H, N $\alpha$ H), 5.90 (m, 1H, OCH<sub>2</sub>-CH=CH<sub>2</sub>), 5.75 (d,  $J$ =10.4 Hz, 1H, NHAc'), 5.34 (dd,  $J$ =17.4, 1.5 Hz, 1H, CH=CHH<sub>trans</sub>), 5.24 (dd,  $J$ =10.3, 1.2 Hz, 1H, CH=CHH<sub>cis</sub>), 4.96 (t,  $J$ =7.6 Hz, 1H, H-1), 4.65 (m, 3H, OCH<sub>2</sub>-CH=CH<sub>2</sub>, H $\alpha$ ), 4.55 (d,  $J$ =7.0 Hz, 1H, H-1'), 4.43 (dd,  $J$ =10.0, 7.0 Hz, 1H, FmocCH<sub>2</sub>), 4.29-4.21 (m, 2H, FmocCH<sub>2</sub>, FmocCH), 4.13 (m, 1H, H-2'), 4.02-3.98 and 3.85-3.65 (m, 11H), 3.02 (dd,  $J$ =16.5, 4.3 Hz, 1H, H <sup>$\beta$</sup> ), 2.68 (dd,  $J$ =16.5, 4.0 Hz, 1H, H <sup>$\beta'$</sup> ), 2.05 (s, 3H, NAc), 1.96 (s, 3H, NAc), 0.93-0.87 (5s, 9H each, tBu), 0.17-0.02 (10s, 3H each, Si-CH<sub>3</sub>)

*N*<sup>4</sup>-[2-acetamido-2-deoxy-4-*O*-(2-acetamido-2-deoxy-3,4,6-tri-*O*-*tert*-butyldimethylsilyl- $\beta$ -*D*-glucopyranosyl)-3,6-di-*O*-*tert*-butyldimethylsilyl- $\alpha$ -*D*-glucopyranosyl]-*N*<sup>2</sup>-(fluoren-9-ylmethoxycarbonyl)-*L*-aspartic acid (**2b $\alpha$**  and **2b $\beta$** ). Compound **15b $\alpha$**  and **15b $\beta$**  (1 eq) were separately dissolved in CH<sub>2</sub>Cl<sub>2</sub> (5 mL), Pd (PPh<sub>3</sub>)<sub>4</sub> (0.02 eq.) and PhSiH<sub>3</sub> (2 eq.) was added and the solution was stirred for 45 min. Water (0.15 ml) was added and after 30 minutes the solution was concentrated. Flash column chromatography (95:4.5:0.5 CHCl<sub>3</sub>/MeOH/ AcOH) followed by size exclusion chromatography (LH-20) (2 drops/min) (2:1 CHCl<sub>3</sub>/MeOH) afforded **2b $\alpha$**  and **2b $\beta$**  in quantitative yields.<sup>30</sup>

Characterization of **2b $\alpha$**  and **2b $\beta$**  is in agreement previous reports.<sup>28</sup>

TLC: (silica, 95:4.5:0.5 CHCl<sub>3</sub>/ MeOH/ AcOH; CAM and UV detection) R<sub>f</sub> = 0.21.

### *Glycosylation Assay*

The radiolabelled carbohydrate substrate [<sup>3</sup>H]-GlcNAc-GlcNAc-Dol-P-P (50,000 dpm) was dissolved in 10 μL DMSO. Assay buffer (150 μL of 50 mM Hepes, pH 7.5, 140 mM sucrose, 1.2% Triton X-100, 0.5 mg/mL PC, 10 mM MnCl<sub>2</sub>) and 30 μL of OT containing microsomes from *Saccharomyces cerevisiae* were added to the carbohydrate substrate. The assay was initiated by adding 10 μL of different concentrations of **PrPUP**. During the course of the experiment the enzyme was gently agitated. Reaction aliquots (4 x 40μL) were removed at two minute intervals and quenched into 3:2:1 chloroform:methanol:4 mM MgCl<sub>2</sub>. The tritiated glycopeptide was separated from the unreacted glycolipid through a series of extractions. The upper aqueous layer was removed and the organic layer was extracted twice with 0.6 mL Theoretical Upper Phase (TUP) with salt (TUP: 12/192/186/2.69 chloroform/methanol/water/0.25 M MgCl<sub>2</sub>). The combined aqueous layers were quantitated for tritium content in 5.5 mL EcoLite (ICN) as desintegrations per minute (dpm).<sup>11</sup>

### *Large scale enzymatic glycosylation*

Yeast microsomes were used instead of pig liver microsomes because a better turnover was observed with the *S. cerevisiae* microsomes. Fourteen small reactions were performed in parallel using 400  $\mu\text{M}$  peptide concentration (5  $K_m$ ) and a 1:20 mixture of tritium-labeled and unlabeled Dol-PP-chitobiose. One of the reactions was used to monitor the sugar transfer by counting the radioactivity in the aqueous layer. The reactions were stopped after 80 minutes and the phases were separated. The aqueous phases of the reactions were combined and the product was purified by Sep-Pak, followed by standard HPLC. The product eluted from the column at 25 minutes using a 0-60%  $\text{CH}_3\text{CN}/\text{H}_2\text{O}$ , 0.1 %TFA gradient. Only 0.20 pmol of glycopeptide was obtained.<sup>11</sup>

### **Negative Staining Electron Microscopy (EM)**

Five  $\mu\text{l}$  aliquots were taken from the incubation samples (70  $\mu\text{M}$ , 24 hours) and placed on carbon-coated 300-mesh nickel grids and adsorbed for 2 minutes. The grids were then stained with 2% uranyl acetate for 2 minutes and after drying, were viewed in a Philips EM 410 operated at 80 KV at magnifications 10,000 X.

## References

- 1) Bahl, O. P. *An Introduction to Glycoproteins*; Marcel Dekker: New York, 1992.
- 2) Kobata, A. "Structure and Functions of Sugar Chains in Glycoproteins" *Eur. J. Biochem.* **1992**, *209*, 483-501.
- 3) Dennis, J. W.; Warren, C. E.; Granovsky, M.; Demetriou, M. "Genetic Defects in N-Glycosylation and Cellular Diversity in Mammals" *Curr. Opin. Struct. Biol.* **2001**, *11*, 601-607.
- 4) Fiete, D.; Srivastava, V.; Hindsgaul, O.; Baenziger, J. U. "A Hepatic Reticuloendothelial Cell Receptor Specific for SO<sub>4</sub>-4GalNAc $\beta$ 1,4GlcNAc $\beta$ 1, Man $\alpha$  that Mediates Rapid Clearance of Lutropin" *Cell* **1991**, *67*, 1103-1110.
- 5) Takeuchi, M.; Kobata, A. "Structures and Functional Roles of the Sugar Chains of Human Erythropoietins" *Glycobiology* **1991**, *1*, 337-346.
- 6) Rudd, P. M.; Joao, H. C.; Coghill, E.; Fiten, P.; Saunders, M. R.; Opdenakker, G.; Dwek, R. A. "Glycoforms Modify the Dynamic Stability and Functional Activity of an Enzyme" *Biochemistry* **1994**, *33*, 17-22.
- 7) Imperiali, B. "Protein Glycosylation: The Clash of the Titans" *Acc. Chem. Res.* **1997**, *30*, 452-459.

- 8) Danishefsky, S. J.; Allen, J. "From the Laboratory to the Clinic: A Retrospective on Fully Synthetic Carbohydrate-Based Anticancer Vaccines" *Angew. Chem. Int. Ed. Engl.* **2000**, *39*, 836-863.
- 9) Lohof, E.; Planker, E.; Mang, C.; Burkhart, F.; Dechantsreiter, M. A.; Haubner, R.; Wester, H.; Schwaiger, M.; Hölzemann, G.; Goodman, S.; Kessler, H. "Carbohydrate Derivatives for Use in Drug Design: Cyclic  $\alpha_V$ -Selective RGD Peptides" *Angew. Chem. Int. Ed. Engl.* **2000**, *39*, 2761-2763.
- 10) Seitz, O. "Glycopeptide Synthesis and Effects of Glycosylation on Protein Structure and Activity" *ChemBiochem* **2000**, *1*, 214-246.
- 11) Imperiali, B.; Rickert, K. W. "Conformational Implications of Asparagine-Linked Glycosylation" *Proc. Nat. Acad. Sci. USA* **1995**, *92*, 97-101.
- 12) Ainsfeld, S. T.; Lansbury, P. T. "A Convergent Approach to the Chemical Synthesis of Asparagine-Linked Glycopeptides" *J. Org. Chem.* **1990**, *55*, 5560-5562.
- 13) Arsequell, G.; Valencia, G. "Recent Advances in the Synthesis of Complex N-Glycopeptides" *Tetrahedron: Asymmetry* **1999**, *10*, 3045-3094.
- 14) Silberstein, S.; Gilmore, R. "Biochemistry, Molecular Biology, and Genetics of the Oligoaccharyl Transferase" *FASEB J.* **1996**, 849-858.

- 15)Likhoshesterov, L.; Novikova, O.; Derevitskaja, V.; Kochetkov, N. "A New Simple Synthesis of Amino Sugar  $\beta$ -D-Glycosylamines" *Carbohydr. Res.* **1986**, *146*, C1-C5.
- 16)Bodnansky, M.; Kwei, J. Z. "Side Reactions in Peptide Synthesis VII" *Intl. J. Pep. Prot. Res.* **1978**, *12*, 69-74.
- 17)Yang, Y.; Sweeny, W. V.; Schneider, K.; Thornquist, S.; Chait, B. T.; Tam, J. P. "Aspartimide Formation in Base Driven 9-Fluorenylmethoxycarbonyl Chemistry" *Tetrahedron Lett.* **1994**, *35*, 9689-9692.
- 18)Christiansen-Brams, I.; Meldal, M.; Bock, K. "Protected-mode Synthesis of N-Linked Glycopetides: Single-step Preparation of Building Blocks as Peracetyl Glycosylated N $^{\alpha}$  Fomc Asparagine OPfp Esters" *J. Chem. Soc. Perkin Trans.* **1993**, *1*, 1461-1471.
- 19)Jobron, L.; Hummel, G. "Solid-Phase Synthesis of Unprotected N-Glycopeptide Building Blocks for Spot Synthesis of N-linked Glycopeptides" *Angew. Chem. Int. Ed.* **2000**, *39*, 1621-1624.
- 20)Zahn, R.; Liu, A.; Lührs, T.; Riek, R.; Schroetter, C. V.; Gracia, F. L.; Billeter, M.; Calzolari, L.; Wider, G.; Wüthrich, K. "NMR Solution Structure of the Human Prion Protein" *Proc. Natl. Acad. Sci. USA* **2000**, *97*, 145-150.
- 21)O'Connor, S. E.; Imperiali, B. "Conformational Switching by Asparagine-linked Glycosylation" *J. Am. Chem. Soc.* **1997**, *119*, 2295-2296.



- 22)O'Connor, S. E.; Imperiali, B. "A Molecular Basis for Glycosylation Induced Conformational Switching" *Chem. Biol.* **1998**, *5*, 427-437.
- 23)Ferscht, A. *Enzyme Structure and Mechanism*; W. H. Freeman: New York, 1985.
- 24)Meinjohanns, E.; Meldal, M.; Paulsen, H.; Dwek, R. A.; Bock, K. "Novel Sequential Solid-Phase Synthesis of N-Linked Glycopeptides From Natural Sources" *J. Chem. Soc. Perkin Trans. 1* **1998**, 549-560.
- 25)Terayama, H.; Takahashi, S.; Kuzuhara, H. "Large-Scale Preparation of N,N'-Diacetylchitobiose by Enzymatic Degradation of Chitin and its Chemical Modifications" *J. Carbohydr. Chem.* **1993**, *12*, 81-93.
- 26)Thiem, J.; Wiemann, T. "Combined Chemoenzymatic Synthesis of N-Glycoprotein Building Blocks" *Angew. Chem. Int. Ed. Engl.* **1990**, *29*, 80-82.
- 27)Meinjohanns, E.; Meldal, M.; Paulsen, H.; Bock, K. "Dithiasuccinoyl (Dts) Amino-protecting Group used in Syntheses of 1,2-trans-Amino Sugar Glycosides" *J. Chem. Soc. Perkin Trans. 1* **1995**, 405-415.
- 28)Holm, B.; Linse, S.; Kihlberg, J. "Synthesis of an N-linked Glycopeptide from Vitamin K-dependent Protein S" *Tetrahedron* **1998**, *54*, 11995-12006.

29) Broddefalk, J.; Bergquist, K.; Kihlberg, J. "Use of Acid-labile Protecting Groups for Carbohydrate Moieties in Synthesis of Glycopeptides Related to Type II Collagen"

*Tetrahedron* **1998**, *54*, 12047-12070.

30) Dessolin, M.; Guillerez, M. G.; Thieriet, N.; Guibé, F.; Loffet, A. "New Allyl Group Acceptors for Palladium Catalyzed Removal of Allylic Protections and Transacylation of Allyl Carbamates" *Tetrahedron Lett.* **1995**, *36*, 5741-5744.

## **Chapter 3**

### **Effects of Carbohydrate Stereochemistry on Glycopeptide Structure**

## Introduction

*N*-linked glycosylation plays an important role in many biological events. For example, the carbohydrate moieties of glycoproteins can be involved in cell-cell communication, immune response, cell adhesion, intracellular targeting, protease resistance.<sup>1-3</sup> The carbohydrates can also impart several physicochemical properties to the protein such as hydration, stability, hydrophilicity and structure.<sup>4,5</sup> In *N*-linked glycosylation, a triantennary tetradecasaccharide is transferred from the Glc<sub>3</sub>Man<sub>9</sub>GlcNAc<sub>2</sub>-PP-dolichol donor to the carboxamide side chain of asparagine when it is found within the Asn-Xaa-Thr/Ser consensus sequence.<sup>6-8</sup> The OT-orchestrated transfer is very specific generating the beta linkage between the anomeric carbon of the carbohydrate and the nitrogen of the asparagine carboxamide.<sup>9</sup> This process occurs co-translationally while the nascent polypeptide is being synthesized on the ribosome. Therefore, it is conceivable that the attachment of the 2000 Da saccharide unit could have a significant role in the protein folding pathway. In fact, the biosynthesis of many glycoproteins leads to misfolding and aggregation when transfer of the saccharide to the polypeptide is suppressed.<sup>10-19</sup>

The study of the molecular effects of *N*-linked glycans on the conformation of small glycopeptide fragments has recently provided significant evidence about the specific effect of the sugar moiety.<sup>20-24</sup> These glycopeptides provide an excellent model system

for these studies since the specific structural effects can be evaluated in the absence of stabilizing long-range protein contacts. These studies use peptide sequences derived from conserved glycosylation sites known to be essential for the structure and function of the protein. One particular system is a glycopeptide derived from the 285 glycosylation site of the A subunit of the hemagglutinin protein (Figure 3.1B and scheme 3.1).<sup>20,21,23</sup> The hemagglutinin protein is an essential component for the binding and membrane fusion of the influenza virus to the host cell.<sup>25,26</sup> In this membrane bound homo-trimer, seven saccharide chains decorate the surface of each subunit (Figure 3.1B). Furthermore, asparagine-linked glycosylation has been shown to be essential for the correct folding of this protein.<sup>14</sup>

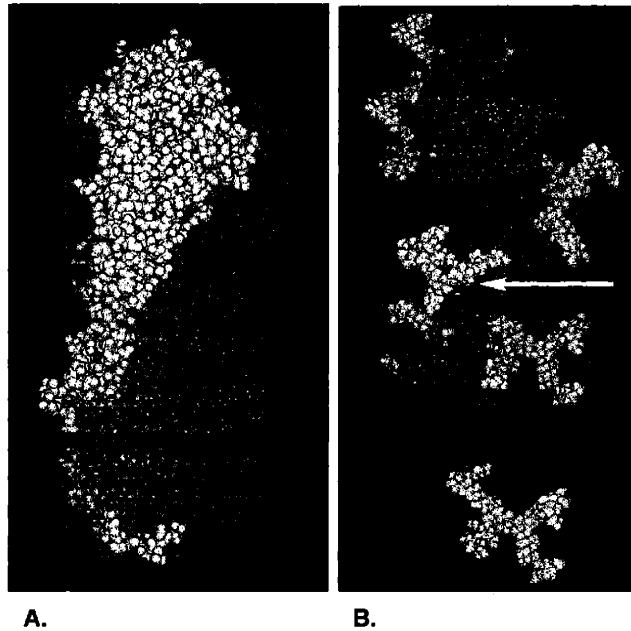
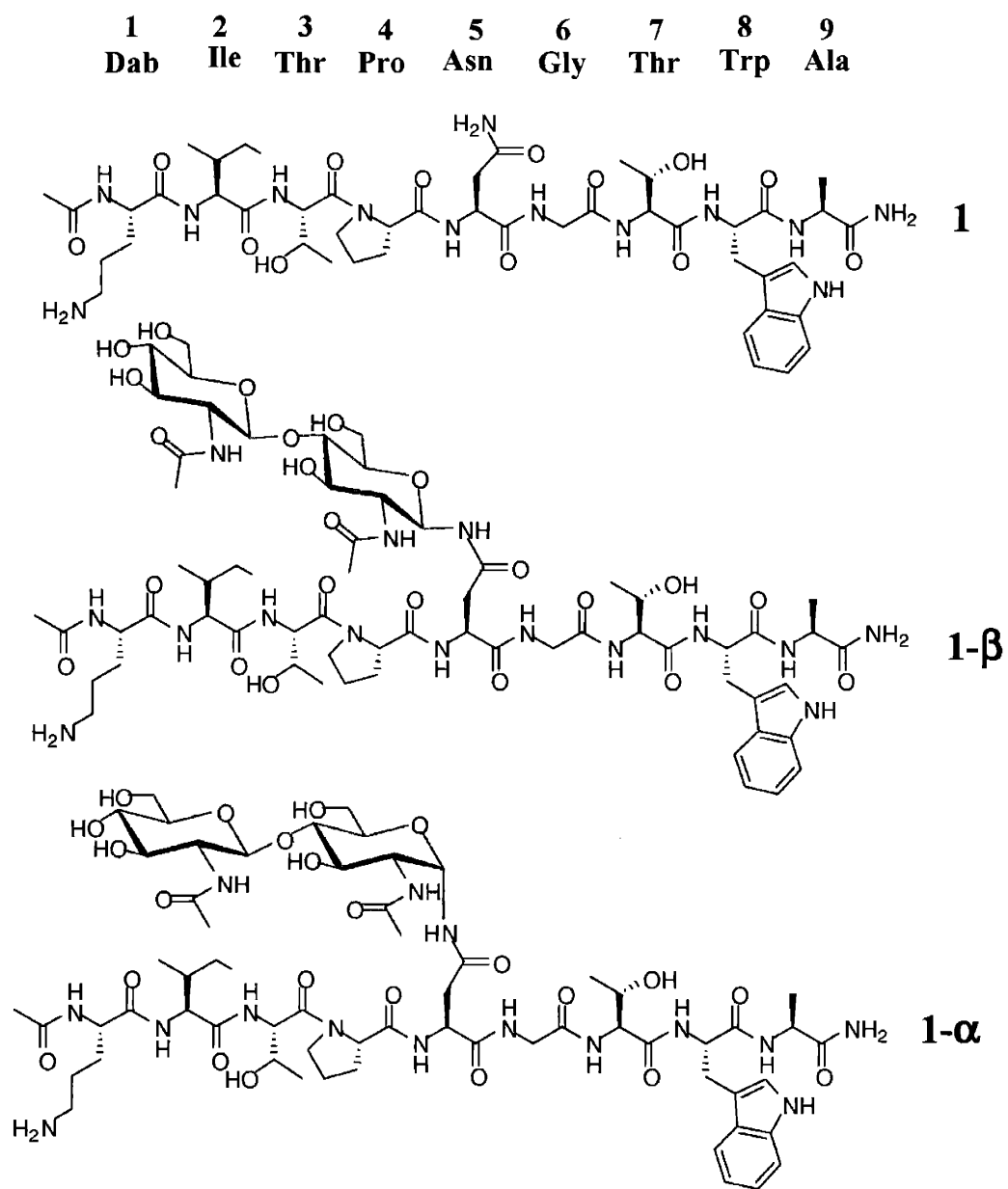


**Figure 3.1** A. Crystal structure of the hemagglutinin protein from the A/Hong Kong/1968 virus.<sup>26</sup> B. Structure of the heavily glycosylated subunit A from the hemagglutinin trimer. Protein is shown in purple and the *N*-linked carbohydrates are shown in white. The arrow highlights the 285 glycosylation site. Figure adapted from <sup>27</sup>.

Despite the diversity of the outer carbohydrates, the core (GlcNAc- $\beta$ -GlcNAc- $\beta$ ) structure remains conserved in all *N*-linked glycoproteins. Previous studies from the Imperiali group on a hemagglutinin glycopeptide derived from the A281-288 fragment showed that this fragment adopts a more compact conformation after modification with the disaccharide chitobiose (GlcNAc- $\beta$ -GlcNAc- $\beta$ ).<sup>23</sup> Two dimensional NMR techniques were then used to study the atomic composition on the *N*-linked glycan required to induce a specific conformational change on the glycopeptide backbone.<sup>20,21</sup> It was shown that the two C2 *N*-acetamido groups on the natural (GlcNAc- $\beta$ -GlcNAc- $\beta$ ) core are specific in

inducing a well defined type I  $\beta$ -turn to the peptide backbone similar to that observed in the native protein.<sup>21</sup> Replacement of the C2 and C2' N-acetyl with hydroxy groups resulted in less ordered conformations.<sup>21</sup> These *N*-acetyl moieties seem to provide a specific steric hindrance in *N*-linked glycoproteins that propagates a precise peptide conformation.

The  $\beta$  stereochemistry of the anomeric carbon of the proximal *N*-acetyl-D-glucosamine (GlcNAc) is also conserved in all *N*-linked glycoproteins. This suggest that stereochemistry of the carbohydrate-protein linkages may also transmit specific structural or functional information to the glycoprotein. In this study we examine how the stereochemistry at the anomeric center of the proximal GlcNAc affects the backbone conformation of the glycopeptide product. To address this question we probe the structural impact of the naturally-encountered chitobiose core on the hemagglutinin peptide previously studied in our laboratory<sup>20,21,23</sup> but in this case, linked with  $\alpha$ -stereochemistry to the Asn side chain (Scheme 3.1). Glycopeptide **1- $\alpha$**  was prepared through a building block approach using modified procedures from the literature<sup>28</sup> to improve the selectivity for the  $\alpha$ -anomer. The structure of this  $\alpha$ -linked glycopeptide is compared to the structures of the unglycosylated peptide (**1**) as well as the  $\beta$ -linked glycopeptide (**1- $\beta$** ).(Scheme 3.1)



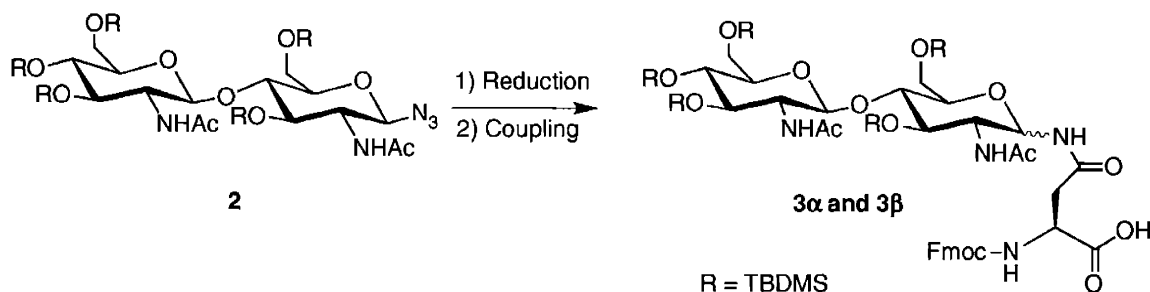
**Scheme 3.1** Chemical structures of peptide **1** and glycopeptide **1-β** and **1-α**. Peptide **1-β** is peptide **2** in reference <sup>20</sup> and glycopeptide **1** in reference <sup>21</sup>.



## Results

### Glycopeptide synthesis

Our previous observations concerning the anomerization induced by the TBDMS protecting groups on the carbohydrate during the reduction of the azidochitobiose (**2**) to the amine and the subsequent coupling to the activated aspartic acid (Scheme 3.2)<sup>29</sup> allow us to use this effect to our advantage in the preparation of an  $\alpha$ -linked TBDMS-protected chitobiose-asparagine (**3 $\alpha$** ). Modified procedures from Holm, et.al.<sup>28</sup> facilitated the production of the  $\alpha$ -anomer of the chitobiose building block with improved selectivity (10:1  $\alpha$ : $\beta$ ). The preparation of the  $\alpha$ -linked building block **3 $\alpha$**  was discussed in chapter 2.



**Scheme 3.2.** Anomerization of TBDMS-protected carbohydrate during the reduction of azidochitobiose and subsequent coupling of the aminochitobiose to the activated aspartic acid.<sup>29</sup>

The glycosylated building block was coupled as a standard amino acid to the peptide during solid phase peptide synthesis using PyAOP as activator and 2,4,6-collidine as base.<sup>29</sup> The coupling of the building block was very efficient, requiring only 1.2 equivalents of **3 $\alpha$**  in DCM to get complete coupling. The peptide was cleaved from the resin using 92:3:3:2 TFA / triisopropylsilane / ethanedithiol / H<sub>2</sub>O, and triturated using ice-cold ethyl ether/hexane 1:1. The addition of an extra 0.8% water during the cleavage and additional shaking for 45 minutes after the standard 3 hours produced the best results for the removal of the protecting groups.

### **Biophysical characterization**

In order to compare the differences between the effects of the  $\alpha$  and  $\beta$  linkage on the glycopeptide structure, we used circular dichroism (CD) and 2D-nuclear magnetic resonance (NMR) spectroscopy. We focus especially on NMR spectroscopy due to the advantage that this one provides atomic-level information.

### **Circular dichroism**

The CD spectra of glycopeptide **1- $\alpha$**  was recorded using the same conditions previously used for the unglycosylated peptide **1** and the  $\beta$ -linked glycopeptide **1- $\beta$** .<sup>27</sup> As

expected, the CD spectra of 20  $\mu\text{M}$  glycopeptide **1- $\alpha$**  displayed mainly random coil characteristics (Figure 3.2A).<sup>30</sup> This result agrees with previous data from peptide **1** and glycopeptide **1- $\beta$**  since most of the peptide is in an unordered conformation and the only structural elements displayed by the peptides is around the glycosylation site. Therefore, CD provides limited information about the minor structural differences occurring near the glycosylation site.

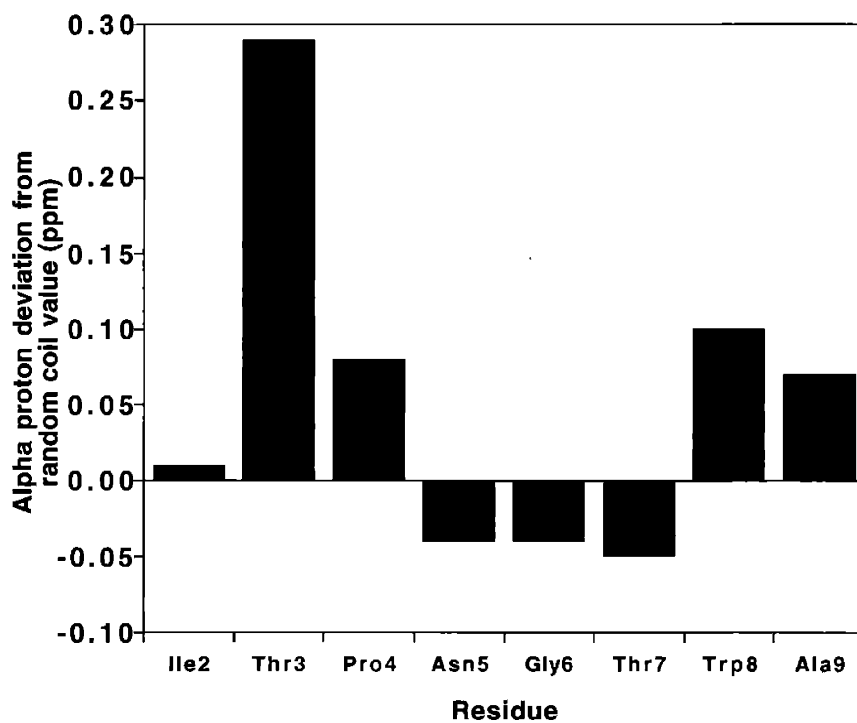
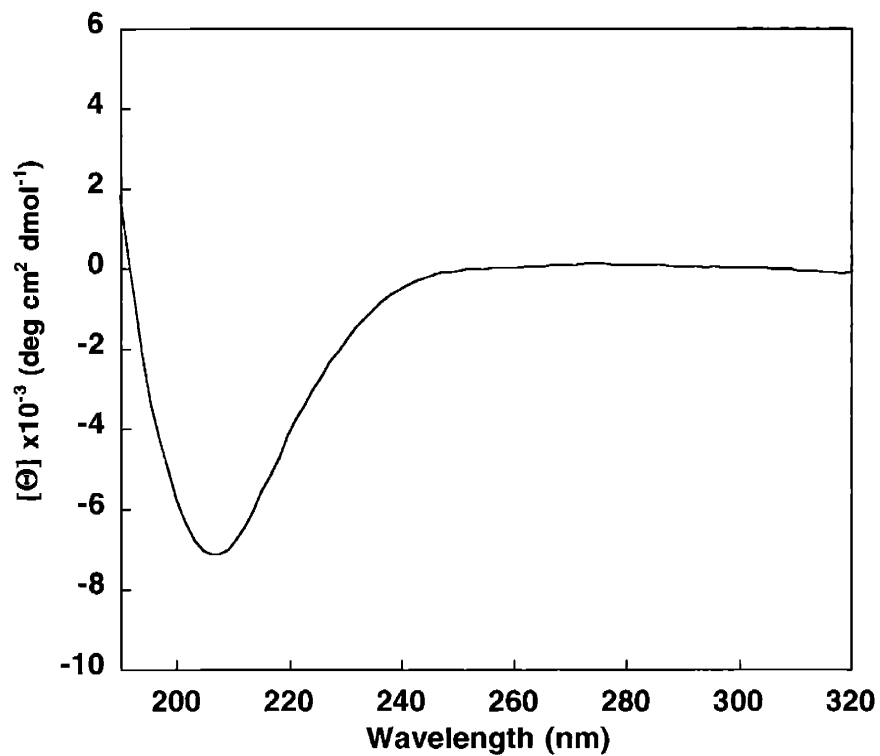
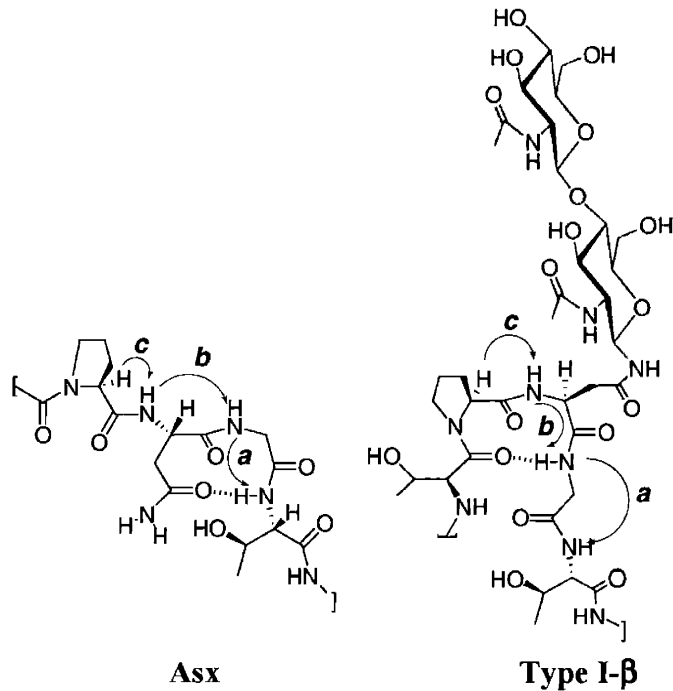


**Figure 3.2** A. CD spectra of 20  $\mu\text{M}$  glycopeptide **1- $\alpha$**  at 25  $^{\circ}\text{C}$  in water, pH 4.5. B. Alpha proton deviation from random coil values for glycopeptide **1- $\alpha$** .<sup>31</sup>



**Scheme 3.3.** Structures of Asx and Type I  $\beta$ -turn and their NOE patterns. Figure adapted from O'Connor, et. al.<sup>20</sup>

### Two-dimensional nuclear magnetic resonance spectroscopy (2D-NMR)

Total correlation spectroscopy (TOCSY)<sup>32</sup> and rotating frame overhauser spectroscopy (ROESY)<sup>33</sup> spectra were used to characterize glycopeptide **1- $\alpha$**  and assign all the spin systems (see experimental section). As expected from the CD results and previous NMR studies on peptide **1** and glycopeptide **1- $\beta$** , NMR data for glycopeptide **1- $\alpha$**  displayed random coil characteristics. As revealed by the  $H_{\alpha}$  chemical shift deviations from random coil, all residues showed values close to 0 ppm (Figure 3.2B).<sup>31</sup> However,

detailed analysis of NOE patterns,  $^3\text{JNH}\alpha$  coupling constants and amide proton variable temperature (VT) coefficients reveal that glycopeptide **1- $\alpha$**  is structured near the region that includes the glycosylation site (Asn<sup>5</sup>). It was observed that this central region of glycopeptide **1- $\alpha$**  display similar characteristics to the unglycosylated peptide **1**, which has an Asx-turn structure, but significantly different to the  $\beta$ -linked glycopeptide **1- $\beta$** , which has a type I  $\beta$ -turn structure around the carbohydrate moiety.<sup>20</sup> As depicted in scheme 3.3, a type I  $\beta$ -turn displays several measurable differences from the Asx-turn. For this peptide, the interproton distance *a* between the Gly<sup>6</sup>-Thr<sup>7</sup> amides [ $d_{\text{NN}}(\text{Gly}^6, \text{Thr}^7)$ ] is expected to be shorter for a Asx-turn than for a type I  $\beta$ -turn.<sup>20</sup> On the other hand, the Asn<sup>5</sup>-Gly<sup>6</sup> amide distance [ $d_{\text{NN}}(\text{Asn}^5, \text{Gly}^6)$ ] *b* is expected to be shorter for a type I  $\beta$ -turn than for a Asx-turn.<sup>20</sup> As observed from table 1, the ROESY spectra of glycopeptide **1- $\alpha$**  displays the particular  $d_{\text{NN}}(\text{Gly}^6, \text{Thr}^7)$  NOE present in unglycosylated peptide **1** but absent in the  $\beta$ -linked glycopeptide **1- $\beta$** .<sup>20</sup> Furthermore, in contrast to glycopeptide **1- $\beta$** , the ROESY spectra for glycopeptide **1- $\alpha$**  revealed a weak  $d_{\text{NN}}(\text{Asn}^5, \text{Gly}^6)$  NOE as in the unglycosylated peptide (Table 3.1).

**Table 3.1** Comparison of the relative intensities of the diagnostic ROESY crosspeaks in the turn region of peptides **1**, **1-β**, and **1-α**. Data for peptide **1** and **1-β** was taken from<sup>20</sup>.

	NOE	Peptide <b>1</b>	Peptide <b>1-β</b> *	Peptide <b>1-α</b>
<i>a</i>	$d_{\text{NN}}(\text{Gly}^6, \text{Thr}^7)$	weak	absent	weak
<i>b</i>	$d_{\text{NN}}(\text{Asn}^5, \text{Gly}^6)$	weak	strong	weak
<i>c</i>	$d_{\alpha\text{N}}(\text{Pro}^4, \text{Asn}^5)$	strong	strong	strong

Amide proton variable temperature (VT) coefficients can provide clues about whether an exchangeable proton is protected from solvent exchange by involvement in a hydrogen bond.<sup>34</sup> Usually, low VT coefficients (below -7.0 ppb/K) are associated with protons involved in hydrogen bonding. A major characteristic expected for an Asx turn is a hydrogen bond between the carboxamide carbonyl of the Asn side chain and the backbone amide of the Thr or Ser two residues after (in this case Thr<sup>7</sup>) (Scheme 3.4).<sup>20</sup> Therefore, a low VT coefficient will be expected for the Thr<sup>7</sup> amide proton for a peptide in a Asx-turn like conformation. Only two amide protons in the glycopeptide **1-α** structure displayed values lower than -7.0 ppb/K. As observed from figure 3.3 and table 3.2, the calculated VT coefficient for Thr<sup>7</sup> amide of glycopeptide **1-α** was -5.9 ppb/K, a value in good agreement with the presence of a hydrogen bond. Also, a similar low VT was observed for the γNH of the Asn<sup>5</sup> side chain (-5.8 ppb/K). These values are similar to those observed in peptide **1** which showed VT values of -6.2 and -5.4 ppb/K for the Thr<sup>7</sup>

amide and one of the Asn<sup>5</sup>  $\gamma$ NH<sub>2</sub> protons respectively. On the other hand, peptide **1- $\beta$**  exhibited a higher VT value for the Asn<sup>5</sup>  $\gamma$ NH<sub>2</sub> proton (-7.2 ppb/K) (table 3.2).<sup>20</sup> Although a low VT coefficient for the Thr<sup>7</sup> amide is also observed for glycopeptide **1- $\beta$** , this has been previously explained by an unusual and strong  $d_{\text{NH}\alpha}(\text{Gly}^6, \text{Thr}^7)$  NOE which indicated that Thr<sup>7</sup> may fold back, thus protecting the Gly<sup>6</sup> amide.<sup>20</sup>

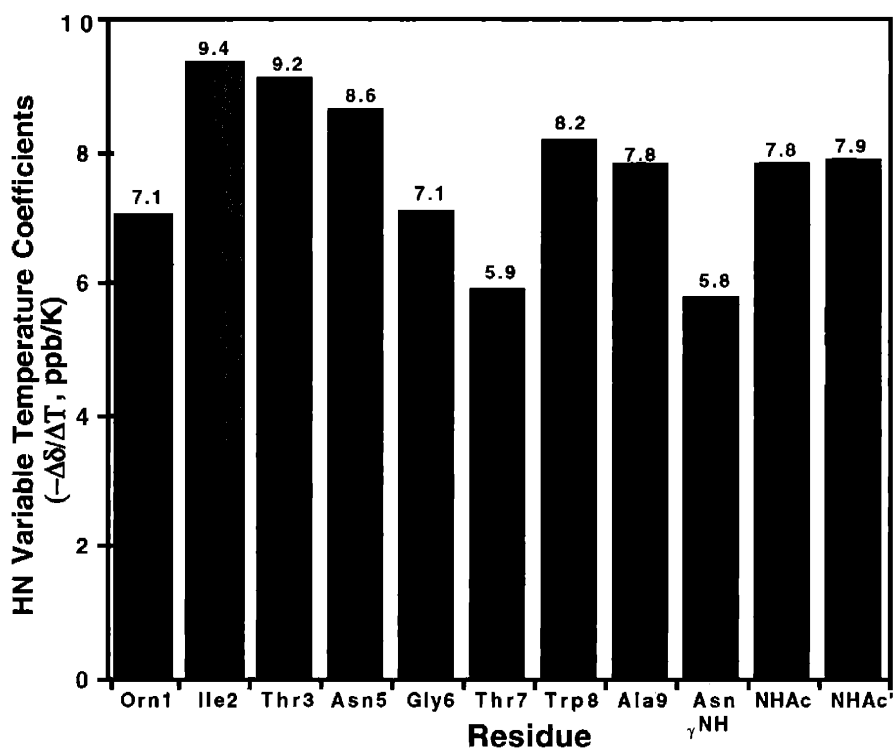


**Figure 3.3.** Complete list of Variable temperature coefficients of amide protons for glycopeptide **1- $\alpha$** .



**Table 3.2.** Comparison of the amide proton variable temperature coefficients ( $-\Delta\delta/\Delta T$ , ppb/K) for peptides **1**, **1- $\beta$**  and **1- $\alpha$** . Data for peptide **1** and **1- $\beta$**  was taken from <sup>20</sup> and <sup>27</sup>. Data points were taken at 5° C increments from 280 to 300 K.

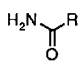
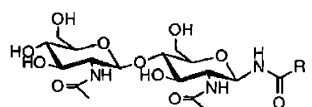
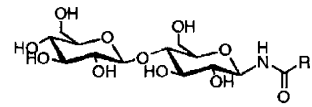
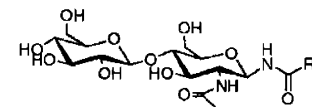
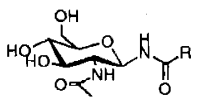
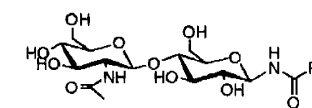
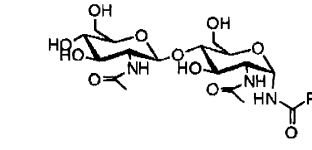
Residue	Peptide <b>1</b>	Peptide <b>1-<math>\beta</math></b>	Peptide <b>1-<math>\alpha</math></b>
Asn <sup>5</sup>	7.0	8.6	8.6
Gly <sup>6</sup>	7.8	6.8	7.1
Thr <sup>7</sup>	6.2	6.0	5.9
Asn $\gamma$ NH <sub>2</sub>	5.4, 7.0	7.2	5.8
GlcNAc	n.a.	6.4	7.8
GlcNAc'	n.a.	7.6	7.9

Many glycopeptide derivatives containing different carbohydrate composition attached to the hemagglutinin peptide were previously studied in our laboratory.<sup>21</sup> Among the different glycopeptides, only the natural core (GlcNAc- $\beta$ -GlcNAc- $\beta$ ) was able to induced a well-defined type I  $\beta$ -turn.<sup>21</sup> One of the most distinct features suggesting that glycopeptide **1- $\beta$**  adopts such a turn was the elevated  $^3J_{\text{HN}\alpha}$  coupling constant for asparagine 5 (9.6 Hz). The  $^3J_{\text{HN}\alpha}$  coupling constant is associated with the amino acid dihedral angles through the Karplus equation.<sup>35</sup> As shown in table 3.3, the corresponding value for glycopeptide **1- $\alpha$**  is 7.5 Hz, a closer value to the 7.0 Hz observed for the unglycosylated peptide **1** than the 9.6 Hz value found for glycopeptide **1- $\beta$** . Also,

the  $^3J_{\text{HN}\alpha}$  value for Asn<sup>5</sup> in glycopeptide **1- $\alpha$**  was the same as for glycopeptide **6** which also displays an extended conformation.<sup>21</sup> Together, these results suggest that glycopeptide **1- $\alpha$**  adopts an extended conformation (as the unglycosylated peptide **1**)<sup>20</sup> rather than a type I  $\beta$ -turn structure exhibited by the  $\beta$ -linked glycopeptide **1- $\beta$** .<sup>20</sup> These data also reinforce the notion that the (GlcNAc- $\beta$ -GlcNAc- $\beta$ ) moiety is uniquely able to induce the type I  $\beta$ -turn structure.<sup>20,21</sup>

**Table 3.3.** Comparison of the  $^3J_{HN\alpha}$  (Hz) of Asn5 for different glycopeptides.

Data for peptide 1-6 was taken from <sup>20</sup> and <sup>27</sup>. Coupling constants were calculated from DQF COSY experiment at 7°C.

Carbohydrate attached	Peptide	$^3J_{HN\alpha}$ Asn <sup>5</sup>
	1	7.0
	1-β	9.6
	3	6.4
	4	6.6
	5	6.9
	6	7.5
	1-α	7.5

## Solution-state structure

The solution-state structure of glycopeptide **1- $\alpha$**  was solved by a simulated annealing protocol using similar conditions as for peptide **1** and glycopeptide **1- $\beta$** .<sup>20,21,27,36</sup> A total of 100 NOE distance and 21 chiral restraints were included in the simulated annealing protocol. As expected from the alpha proton chemical shift deviations, the greater fraction of the peptide was unordered. However, the backbone residues near the glycosylation site adopted a well ordered conformation (figure 3.4). From the simulated annealing results, 10/10 structures displayed an extended conformation near the glycosylation site. Three of the structures displayed a shorter distance from Thr<sup>7</sup> to the Asn<sup>5</sup> side chain but the rest of the structures showed wider structures (figure 3.4). Similar NOE intensities from the carbohydrate to the Asn  $\gamma$ NH resulted in the expected unordered carbohydrate moiety from the annealing. The extended structure displayed by glycopeptide **1- $\alpha$**  is similar to the Asx turn observed for peptide **1**, although somewhat wider, and very different from glycopeptide **1- $\beta$** .(figure 3.5) The wider Asx turn-like structure is expected for glycopeptide **1- $\alpha$**  (in comparison to peptide **1**) since the carbohydrate moiety and the organized water molecules associated with the sugar will occupy extra space between the Asn side chain and the backbone near Thr<sup>7</sup>. These results suggest that the minor variation on the stereochemistry at the anomeric center of the proximal GlcNAc can have major effects on the glycopeptide structure.



**Figure 3.4.** Structures derived from a simulated annealing protocol for glycopeptide 1- $\alpha$ . The two major populations are shown. The peptide backbone is shown in gray and the carbohydrate is shown in red. Residues Pro<sup>4</sup> through Thr<sup>7</sup> are displayed.

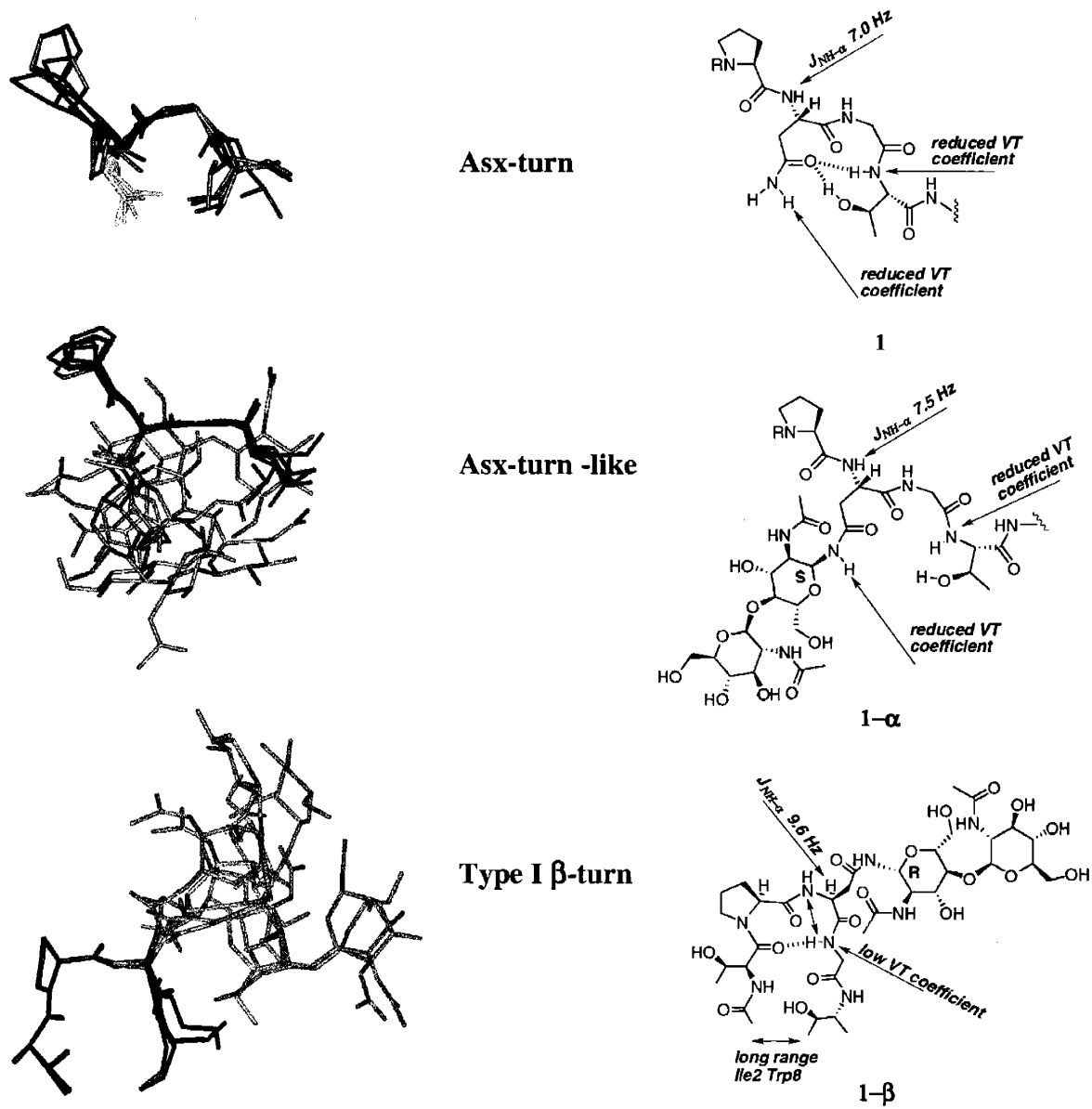


**Figure 3.5.** Comparison of the solution state structure among peptide **1** and glycopeptides **1- $\beta$**  and **1- $\alpha$** . Peptide **1** and glycopeptide **1- $\alpha$**  are shown from Pro<sup>4</sup> to Thr<sup>7</sup>. Glycopeptide **1- $\beta$**  is shown from Thr<sup>3</sup> to Thr<sup>7</sup>. Structures of peptide **1** and **1- $\beta$**  were taken from <sup>20</sup> and <sup>21</sup>.

## Discussion

In this work an  $\alpha$ -linked chitobiose glycopeptide was prepared through the building block approach. The modified procedure for the preparation of the asparagine-chitobiose building block demonstrated improved selectivity for the  $\alpha$ -anomer of the carbohydrate-amino acid linkage. Two-dimensional homonuclear NMR was used to compare the structure of this  $\alpha$ -linked glycopeptide to those of the unglycosylated peptide as well as the  $\beta$ -linked glycopeptide. The NMR results provided information on how the stereochemistry at the anomeric center of the carbohydrate affects the backbone conformation of the glycopeptide. It was shown that although the  $\alpha$ -linked glycopeptide poses the same atomic composition as the  $\beta$ -linked glycopeptide, the first showed an extended structure instead of the type I  $\beta$ -turn displayed by the  $\beta$ -linked glycopeptide. These results reinforce previous conclusions that carbohydrate composition is important for the induction of the particular type I  $\beta$ -turn. Furthermore, these results indicate that it is not only the composition of the carbohydrate attached to the peptide but also the stereochemistry of the linkage that is important for the induction of the turn.

## **Acknowledgements**

A computational part of this project is now in progress in collaboration with Dr. Robert J. Woods and Sarah Wittkopp from the Complex Carbohydrate Research Center at the University of Georgia. This work was supported by a grant from the NIH (GM-39334). We like to thank Dr. Sarah O'Connor, Dr. Jeniffer Ottesen and Dr. Jebrell Glover for their assistance with NMR spectroscopy.



## Experimental section

### *Glycopeptide Synthesis*

Glycopeptide **1- $\alpha$**  was synthesized using the same procedure as in.<sup>29</sup> The addition of an extra 0.8% water and additional shaking for 45 minutes after the standard 3 hours of cleavage produced the best results for the removal of the protecting groups. The peptide was purified by HPLC ( $t_r$ =23.31 minutes; gradient: 10 to 70% CH<sub>3</sub>CN in H<sub>2</sub>O and 0.1 %TFA in 30 minutes) and characterized by ESMS {[M+H<sup>+</sup>] 1421.6 (obsd.); 1421.5 (calcd.)}and QAA.

### *Circular Dichroism*

Samples were prepared using the same conditions used for peptide **1** and glycopeptide **1- $\beta$** .<sup>27</sup> Peptide solutions of 20  $\mu$ M concentration in water were pH to 4.5 and the CD spectra was recorded using a 0.1 cm cuvette. The spectra were recorded on an Aviv Instrument model 202 CD spectrophotometer.

### *NMR studies*

NMR spectra were acquired using the same conditions used in <sup>20,21,27</sup>. One to three millimolar peptide concentrations in 90:10 H<sub>2</sub>O:D<sub>2</sub>O at pH 4.5 were used. DMSO was used as internal reference. TOCSY, ROESY and DQF COSY spectra were recorded on a 600 MHz Bruker Advance spectrometer. TOCSY spectra were recorded at 7, 12, 17, 22 and 27°C were used to calculate the amide proton variable temperature (VT) coefficients. ROESY spectra were acquired using 400 ms mixing times with WATERGATE gradient suppressions. The NMR data was processed using Felix 97 software.

**Table 3.4.** <sup>1</sup>H assignment for glycopeptide 1- $\alpha$ .

Residue	HN	H $\alpha$	H $\beta$	Others				
Ac				Ac 2.01				
Orn1	8.36	4.30	1.80, 1.72	$\gamma$ CH <sub>2</sub> 2.99 $\delta$ NH <sub>2</sub> 7.62				
Ile2	8.45	4.24	1.82	$\gamma$ CH <sub>2</sub> 1.46,1.17 $\gamma$ CH <sub>3</sub> 0.85 $\delta$ CH <sub>3</sub> 0.83				
Thr3	8.51	4.64	4.19	$\gamma$ CH <sub>3</sub> 1.24				
Pro4		4.38	2.03,2.31	$\gamma$ CH <sub>2</sub> 1.89,1.97 $\delta$ CH <sub>2</sub> 3.72,3.89				
Asn5	8.56	4.71	2.94,2.87	$\gamma$ NH 8.83				
Gly6	8.35	3.93						
Thr7	8.09	4.30	4.14	$\gamma$ CH <sub>3</sub> 1.12				
Trp8	8.35	4.66	3.25,3.28	2H 7.25 4H 7.63 5H 7.14 6H 7.23 7H 7.48 NH 10.18				
Ala9	8.16	4.17	1.22					
CONH <sub>2</sub>				NH <sub>2</sub> 6.93, 6.75				
	NH	H1	H2	H3	H4	H5	H6	Ac
GlcNAc	8.20	5.71	4.05	3.90	3.65	3.58	3.89,3.65	1.93
GlcNAc'	8.54	4.57	3.78	3.56	3.50	3.46	3.76,3.48	2.05

**Table 3.5.**  $^3\text{JHN}\alpha$  coupling constants for all residues in glycopeptide **1- $\alpha$** .

Residue	$^3\text{JHN}\alpha$ (Hz)
Orn 1	7.2
Ile 2	7.9
Thr 3	7.4
Asn 5	7.5
Gly 6	12.0
Thr 7	7.5
Trp 8	6.3
Ala 9	7.1
NHAc-H2	8.2
NHAc'-H2'	9.7

### *Simulated Annealing*

The solution state structure of glycopeptide **1- $\alpha$**  was solved by a simulated annealing protocol using similar conditions as for peptide **1** and glycopeptide **1- $\beta$** .<sup>20,27</sup> The structure was generated using the Biopolymer option of Insight II. ROESY crosspeaks volumes were measured and sorted into strong and weak bins. The strong peaks were assigned a distance range of 1 to 3 Å and the weak peaks were assigned a distance range of 2 to 4 Å. An additional distance restraint of 2.0 to 5.0 Å between Thr<sup>7</sup> amide and the

Asn<sup>5</sup> carboxamide was justified by the decreased VT coefficient observed for Thr<sup>7</sup> and the Asn  $\gamma$ NH.<sup>20</sup> A total of 100 NOE distance and 21 chiral restraints were included in the simulated annealing protocol.

**Table 3.6.** Simulated Annealing Schedule.

Stage	Procedure	Force Constant	Length	Temp (K)
1	randomize coordinates	0.00001	100 iterations	1000
2	minimization	0.001	500 iterations	1000
3	Dynamics Scale: NMR	NMR 0.001->1.0 Chiral 0.001->0.15 Cov 0.0002->0.15	40 ps	1000
4	Covalent	Cov 0.15->1.0 Chiral 0.15->1.0 NB 0.0001->0.015	10 ps	1000
5	Non-bonds	NB 0.015->0.25 NMR 1.0->2.0	40 ps	1000
6	dynamics	NMR 2.0 Cov 1.0 NB 0.25	4 ps	650
7	dynamics	same	4 ps	475
8	dynamics	same	4 ps	385
9	dynamics	same	4 ps	340
10	dynamics	same	4 ps	300
11	minimization	same	100 iterations	300
12	minimization	same	500 iterations	300
13	minimization	NMR 1.0 Cov 1.0 NB 1.0	100 iterations	300
14	minimization	same	1500 iterations	300

**Table 3.7.** Distance restraints for glycopeptide 1- $\alpha$ .

Atom 1	Atom 2	Lower Bound	Upper Bound	Restraint Strength
1:Orn_1:HD1	1:Orn_1:HG1	2.00	4.00	weak
1:Orn_1:HD2	1:Orn_1:HG2	2.00	4.00	weak
1:Orn_1:HD2	1:Orn_1:HB2	2.00	4.00	weak
1:Orn_1:HD2	1:Orn_1:HA	2.00	4.00	weak
1:Orn_1:HN	1:ACE_1B:HA3	1.00	3.00	strong
1:Orn_1:HN	1:Orn_1:HB2	2.00	4.00	weak
1:Orn_1:HN	1:Orn_1:HB1	1.00	3.00	strong
1:Orn_1:HN	1:Orn_1:HA	1.00	3.00	strong
1:Ile_2:HA	1:Ile_2:HG21	2.00	4.00	weak
1:Ile_2:HA	1:Ile_2:HG22	2.00	4.00	weak
1:Ile_2:HA	1:Ile_2:HG23	2.00	4.00	weak
1:Ile_2:HA	1:Ile_2:HD1	2.00	4.00	weak
1:Ile_2:HA	1:Ile_2:HD2	2.00	4.00	weak
1:Ile_2:HA	1:Ile_2:HD2	2.00	4.00	weak
1:Ile_2:HA	1:Ile_2:HG11	2.00	4.00	weak
1:Ile_2:HA	1:Ile_2:HG12	2.00	4.00	weak
1:Ile_2:HA	1:Ile_2:HB	2.00	4.00	weak
1:Ile_2:HB	1:Ile_2:HD13	1.00	3.00	strong
1:Ile_2:HB	1:Ile_2:HD12	1.00	3.00	strong
1:Ile_2:HB	1:Ile_2:HD11	1.00	3.00	strong
1:Ile_2:HG11	1:Ile_2:HG21	1.00	3.00	strong
1:Ile_2:HG11	1:Ile_2:HG22	1.00	3.00	strong
1:Ile_2:HG11	1:Ile_2:HG23	1.00	3.00	strong
1:Ile_2:HG12	1:Ile_2:HG21	1.00	3.00	strong
1:Ile_2:HG12	1:Ile_2:HG22	1.00	3.00	strong
1:Ile_2:HG12	1:Ile_2:HG23	1.00	3.00	strong
1:Ile_2:HN	1:Ile_2:HG21	2.00	4.00	weak
1:Ile_2:HN	1:Ile_2:HG22	2.00	4.00	weak
1:Ile_2:HN	1:Ile_2:HG23	2.00	4.00	weak
1:Ile_2:HN	1:Ile_2:HG12	2.00	4.00	weak
1:Ile_2:HN	1:Ile_2:HG11	2.00	4.00	weak
1:Ile_2:HN	1:Ile_2:HD13	2.00	4.00	weak
1:Ile_2:HN	1:Ile_2:HD12	2.00	4.00	weak
1:Ile_2:HN	1:Ile_2:HD11	2.00	4.00	weak
1:Ile_2:HN	1:Ile_2:HB	1.00	3.00	strong
1:Ile_2:HN	1:Orn_1:HA	1.00	3.00	strong
1:Ile_2:HA	1:Thr_3:HN	1.00	3.00	strong
1:Ile_2:HN	1:Ile_2:HA	1.00	3.00	strong
1:Thr_3:HB	1:Thr_3:HG21	1.00	3.00	strong
1:Thr_3:HB	1:Thr_3:HG22	1.00	3.00	strong
1:Thr_3:HB	1:Thr_3:HG23	1.00	3.00	strong
1:Thr_3:HN	1:Thr_3:HA	2.00	4.00	weak

1:Thr_3:HN	1:Thr_3:HG21	2.00	4.00	weak
1:Thr_3:HN	1:Thr_3:HG22	2.00	4.00	weak
1:Thr_3:HN	1:Thr_3:HG23	2.00	4.00	weak
1:Thr_3:HN	1:Ile_2:HD11	2.00	4.00	weak
1:Thr_3:HN	1:Ile_2:HD12	2.00	4.00	weak
1:Thr_3:HN	1:Ile_2:HD13	2.00	4.00	weak
1:Thr_3:HN	1:Ile_2:HB	2.00	4.00	weak
1:Pro_4:HD2	1:Thr_3:HB	2.00	4.00	weak
1:Pro_4:HD1	1:Thr_3:HB	2.00	4.00	weak
1:Pro_4:HD1	1:Thr_3:HA	2.00	4.00	weak
1:Pro_4:HD2	1:Thr_3:HA	2.00	4.00	weak
1:Pro_4:HD1	1:Pro_4:HD2	1.00	3.00	strong
1:Pro_4:HA	1:Pro_4:HB1	1.00	3.00	strong
1:Pro_4:HA	1:Pro_4:HB2	1.00	3.00	strong
1:Pro_4:HD1	1:Pro_4:HB1	2.00	4.00	weak
1:Pro_4:HD1	1:Pro_4:HB2	2.00	4.00	weak
1:Pro_4:HD2	1:Pro_4:HG2	2.00	4.00	weak
1:Pro_4:HB1	1:Pro_4:HG1	1.00	3.00	strong
1:Pro_4:HB2	1:Pro_4:HG1	1.00	3.00	strong
1:Pro_4:HA	1:Asn_5:HN	1.00	3.00	strong
1:Asn_5:HN	1:Gly_6:HN	2.00	4.00	weak
1:Asn_5:HA	1:Asn_5:HB2	2.00	4.00	weak
1:Asn_5:HA	1:Asn_5:HB1	2.00	4.00	weak
1:Asn_5:HN	1:Asn_5:HB1	2.00	4.00	weak
1:Asn_5:HN	1:Asn_5:HB2	2.00	4.00	weak
1:Gly_6:HN	1:Asn_5:HA	2.00	4.00	weak
1:Asn_5:H4	1:Asn_5:H10	2.00	4.00	weak
1:Asn_5:HN1	1:Asn_5:H151	1.00	3.00	strong
1:Asn_5:HN1	1:Asn_5:H152	1.00	3.00	strong
1:Asn_5:HN1	1:Asn_5:H153	1.00	3.00	strong
1:Asn_5:HN2	1:Asn_5:H71	1.00	3.00	strong
1:Asn_5:HN2	1:Asn_5:H72	1.00	3.00	strong
1:Asn_5:HN2	1:Asn_5:H73	1.00	3.00	strong
1:Asn_5:HN1	1:Asn_5:H10	2.00	4.00	weak
1:Asn_5:HD2	1:Asn_5:H2	2.00	4.00	weak
1:Asn_5:HD2	1:Asn_5:H3	2.00	4.00	weak
1:Asn_5:HD2	1:Asn_5:H4	2.00	4.00	weak
1:Asn_5:HD2	1:Asn_5:H5	2.00	4.00	weak
1:Asn_5:H1	1:Asn_5:H2	2.00	4.00	weak
1:Asn_5:H1	1:Asn_5:H3	2.00	4.00	weak
1:Asn_5:HN	1:Asn_5:HA	2.00	4.00	weak
1:Asn_5:HN1	1:Asn_5:H11	2.00	4.00	weak
1:Asn_5:HN1	1:Asn_5:H4	2.00	4.00	weak
1:Asn_5:HN1	1:Asn_5:H12	2.00	4.00	weak
1:Asn_5:HN1	1:Asn_5:H13	2.00	4.00	weak

1:Asn_5:HN2	1:Asn_5:H2	2.00	4.00	weak
1:Asn_5:HN2	1:Asn_5:H3	2.00	4.00	weak
1:Asn_5:HN2	1:Asn_5:H4	2.00	4.00	weak
1:Asn_5:H3	1:Asn_5:H2	2.00	4.00	weak
1:Asn_5:H4	1:Asn_5:H2	2.00	4.00	weak
1:Asn_5:H5	1:Asn_5:H2	2.00	4.00	weak
1:Asn_5:H12	1:Asn_5:H11	2.00	4.00	weak
1:Asn_5:H13	1:Asn_5:H11	2.00	4.00	weak
1:Asn_5:H9	1:Asn_5:H11	2.00	4.00	weak
1:Asn_5:H3	1:Asn_5:H141	2.00	4.00	weak
1:Asn_5:H3	1:Asn_5:H142	2.00	4.00	weak
1:Asn_5:H3	1:Asn_5:H13	2.00	4.00	weak
1:Asn_5:H3	1:Asn_5:H9	2.00	4.00	weak
1:Asn_5:H10	1:Asn_5:H12	2.00	4.00	weak
1:Asn_5:H10	1:Asn_5:H13	2.00	4.00	weak
1:Asn_5:HN2	1:Asn_5:HD2	2.00	4.00	weak
1:Asn_5:HN2	1:Asn_5:H1	2.00	4.00	weak
1:Asn_5:HD2	1:Asn_5:H1	2.00	4.00	weak
1:Asn_5:HD2	1:Asn_5:HB1	2.00	4.00	weak
1:Asn_5:HD2	1:Asn_5:HB2	2.00	4.00	weak
1:Gly_6:HN	1:Thr_7:HN	2.00	4.00	weak
1:Gly_6:HN	1:Gly_6:HA1	2.00	4.00	weak
1:Gly_6:HN	1:Gly_6:HA2	2.00	4.00	weak
1:Thr_7:HA	1:Thr_7:HG21	1.00	3.00	strong
1:Thr_7:HA	1:Thr_7:HG22	1.00	3.00	strong
1:Thr_7:HA	1:Thr_7:HG23	1.00	3.00	strong
1:Thr_7:HB	1:Thr_7:HG21	1.00	3.00	strong
1:Thr_7:HB	1:Thr_7:HG22	1.00	3.00	strong
1:Thr_7:HB	1:Thr_7:HG23	1.00	3.00	strong
1:Thr_7:HB	1:Thr_7:HA	1.00	3.00	strong
1:Thr_7:HN	1:Gly_6:HA1	2.00	4.00	weak
1:Thr_7:HN	1:Gly_6:HA2	2.00	4.00	weak
1:Thr_7:HN	1:Asn_5:HD2	2.00	5.00	v.weak
1:Trp_8:HN	1:Thr_7:HB	2.00	4.00	weak
1:Trp_8:HN	1:Trp_8:HA	1.00	3.00	strong
1:Trp_8:HN	1:Thr_7:HG21	2.00	4.00	weak
1:Trp_8:HN	1:Thr_7:HG22	2.00	4.00	weak
1:Trp_8:HN	1:Thr_7:HG23	2.00	4.00	weak
1:Trp_8:HB1	1:Trp_8:HE3	1.00	3.00	strong
1:Trp_8:HB2	1:Trp_8:HE3	2.00	4.00	weak
1:Trp_8:HN	1:Trp_8:HB2	2.00	4.00	weak
1:Trp_8:HA	1:Trp_8:HE3	1.00	3.00	strong
1:TRp_8:HN	1:Thr_7:HN	2.00	4.00	weak
1:Trp_8:HN	1:Trp_8:HD1	2.00	4.00	weak
1:Ala_9:HN	1:Trp_8:HB2	2.00	4.00	weak



---

1:Ala_9:HN	1:Trp_8:HA	1.00	3.00	strong
1:Ala_9:HN	1:Ala_9:HB1	1.00	3.00	strong
1:Ala_9:HN	1:Ala_9:HB2	1.00	3.00	strong
1:Ala_9:HN	1:Ala_9:HB3	1.00	3.00	strong
1:Ala_9:HA	1:Ala_9:HB1	1.00	3.00	strong
1:Ala_9:HA	1:Ala_9:HB2	1.00	3.00	strong
1:Ala_9:HA	1:Ala_9:HB3	1.00	3.00	strong

---

## References:

- 1)Varki, A. "Biological Roles of Oligosaccharides: all of the Theories are Correct" *Glycobiology* **1993**, 3, 97-130.
- 2)Dwek, R. A. "Glycobiology: Toward Understanding the Function of Sugars" *Chem. Rev.* **1996**, 96, 683-720.
- 3)Reuter, G.; Gabius, H. J. "Eukaryotic Glycosylation: Whim of Nature or Multipurpose Tool?" *Cel. Mol. Life Sci.* **1999**, 55, 368-422.
- 4)O'Connor, S. E.; Imperiali, B. "Modulation of Protein Structure and Function by Asparagine-Linked Glycosylation" *Chem. Biol.* **1996**, 3, 803-812.
- 5)Imperiali, B.; O'Connor, S. E. "Effect of *N*-linked Glycosylation on Glycopeptide and Glycoprotein Structure" *Curr. Opin. Chem. Biol.* **1999**, 3, 643-649.
- 6)Silberstein, S.; Gilmore, R. "Biochemistry, Molecular Biology, and Genetics of the Oligosaccharyl Transferase" *FASEB J.* **1996**, 849-858.
- 7)Burda, P.; Aebi, M. "The Dolichol Pathway of *N*-linked Glycosylation" *Biochim. Biophys. Acta* **1999**, 1426, 239-257.
- 8)Imperiali, B.; Spenser, J. R.; Struthers, M. D. "Structural and Functional Characterization of a Constrained Asx-Turn Motif" *J. Am. Chem Soc.* **1994**, 116, 8424-8425.

- 9)Imperiali, B. "Protein Glycosylation: The Clash of the Titans" *Acc. Chem. Res.* **1997**, *30*, 452-459.
- 10)Rieder, M. A.; Hinnen, A. "Removal of *N*-Glycosylation Sites of the Yeast Acid Phosphatase Severely Affects Protein Folding" *J. Bacter.* **1991**, *173*, 3539-3546.
- 11)Powell, L. M.; Pain, R. H. "Effects of Glycosylation on the Folding and Stability of Human, Recombinant and Cleaved Alpha-1-Antitrypsin" *J. Mol. Biol.* **1992**, *224*, 241-252.
- 12)Danielson, E. M. "Folding of Intestinal Brush Border Enzyme. Evidence that High Mannose Glycosylation is an Essential Early Event" *Biochemistry* **1992**, *31*, 2266-2272.
- 13)Kern, G.; Kern, D.; Jaenicke, R.; Seckler, R. "Kinetics of Folding and Association of Differently Glycosylated Variants of Invertase from *Saccharomyces Cerevisiae*" *Prot. Sci.* **1993**, *2*, 1862-1868.
- 14)Roberts, P. C.; Garten, W.; Klenck, H.-D. "Role of Conserved Glycosylation Sites in Maturation and Transport of Influenza A Virus Hemagglutinin" *J. Virol.* **1993**, *67*, 3048-3060.
- 15)Letourneur, O.; Sechi, S.; Willette-Brown, J.; Robertson, M. W.; Kinet, J.-P. "Glycosylation of Human Truncated FCεRIα Chain is Necessary for Efficient Folding in the Endoplasmic Reticulum" *J. Biol. Chem.* **1995**, *270*, 8249-8256.

- 16)Ruddon, R. W.; Sherman, S. A.; Bedows, E. "Protein Folding in the Endoplasmic Reticulum: Lessons from the Human Chorionic Gonadotropin Subunit" *Prot. Sci.* **1996**, *5*, 1443-1452.
- 17)Fan, H.; Meng, W. M.; Kilian, C.; al., e. "Domain Specific *N*-Glycosylation of the Membrane Protein Dipeptidylpeptidase IV (CD26) Influences its Subcellular Trafficking, Biological Stability, Enzyme Activity and Potein Folding" *Eur. J. Biochem.* **1997**, *246*, 243-251.
- 18)Beggah, A. T.; Jaunin, P.; Geering, K. "Role of Glycosylation and Disulfide Bond Formation in the beta Subunit in the Folding and Functional Expression of Na, K-AtPase" *J. Biol. Chem.* **1997**, *272*, 10318-10326.
- 19)Marquardt, T.; Helenius, A. "Misfolding and Aggregation of Newly Synthesized Proteins in the Endoplasmic Reticulum" *J. Cell Biol.* **1992**, *117*, 505-513.
- 20)O'Connor, S. E.; Imperiali, B. "Conformational Switching by Asparagine-linked Glycosylation" *J. Am.Chem. Soc.* **1997**, *119*, 2295-2296.
- 21)O'Connor, S. E.; Imperiali, B. "A Molecular Basis for Glycosylation Induced Conformational Switching" *Chem. Biol.* **1998**, *5*, 427-437.

- 22)Live, D. H.; Kumar, R. A.; Beebe, X.; Danishefsky, S. J. "Conformational Influences of Glycosylation of a Peptide: A Possible Model for the Effect of Glycosylation on the Rate of Protein Folding" *Proc. Natl. Acad. Sci. USA* **1996**, *93*, 12759-12761.
- 23)Imperiali, B.; Rickert, K. W. "Conformational Implications of Asparagine-Linked Glycosylation" *Proc. Nat. Acad. Sci. USA* **1995**, *92*, 97-101.
- 24)Rickert, K. W.; Imperiali, B. "Analysis of the Conserved Glycosylation Site in the Nicotinic Acetylcholine Receptor: Potential Roles in Complex Assembly" *Chem. Biol.* **1995**, *2*, 751-759.
- 25)Wilson, I. A.; Lander, R. C.; Skehel, J. J.; Wiley, D. C. "The Structure and Role of the Carbohydrate Moieties of Influenza Virus Hemagglutinin" *Biochem. Soc. Trans.* **1983**, *11*, 145-147.
- 26)Wilson, I. A.; Skehel, J. J.; Wiley, D. C. "Structure of the Hemagglutinin Membrane Glycoprotein of Influenza Virus at 3Å Resolution" *Nature* **1981**, *289*, 366-373.
- 27)O'Connor, S. E. *Conformational Effects of Asparagine-Linked Glycosylation*; Massachusetts Institute of Technology: Cambridge, 2000, pp 28.
- 28)Holm, B.; Linse, S.; Kihlberg, J. "Synthesis of an N-linked Glycopeptide from Vitamin K-dependent Protein S" *Tetrahedron* **1998**, *54*, 11995-12006.

- 29)Bosques, C. J.; Tai, V. W.-F.; Imperiali, B. "Stereoselective Synthesis of  $\beta$ -linked TBDMS-Protected Chitobiose-Asparagine: a Versatile Building Block for Amyloidogenic Peptides" *Tetrahed. Lett.* **2001**, *42*, 7207-7210.
- 30)Johnson, W. C. "Protein Secondary Structure and Circular Dichroism" *Proteins* **1990**, *7*, 205-214.
- 31)Wuthrich, K. *NMR of Proteins and Nucleic Acids*; Wiley: New York, 1986.
- 32)Griesenger, C.; Otting, G.; Wuthrich, K.; Ernst, R. R. "Clean TOCSY for H1 Spin Ssystem Identification in Macromolecules" *J. Am. Chem. Soc.* **1988**, *110*, 7870-7872.
- 33)Bothnerby, A. A.; Stephens, R. L.; Lee, J. M.; Warren, C. D.; Jeanloz, R. W. "Structure Determination of a Tetrasaccharide - Transient Nuclear Overhauser Effects in the Rotating Frame" *J. Am. Chem. Soc.* **1984**, *106*, 811-813.
- 34)Ohnishi, O. M.; Urry, D. W. "Temperature Dependence of Amide Proton Chemical Shifts: The Secondary Structures of Gramicidin S and Valinomycin" *Biochem. Biophys. Res. Comm.* **1969**, *36*, 194-202.
- 35)Pardi, A.; Billeter, M.; Wüthrich, K. "Calibration of the Angular Dependence of the Amide Proton-C $\alpha$  Proton Coupling Constants,  $^3J_{HN\alpha}$ , in a Globular Protein" *J. Mol. Biol.* **1984**, *180*, 741-751.

36) Holak, T. A.; Nilges, M.; Prestegard, J. H.; Gronenborn, A. M.; Clore, G. M. "3-Dimensional Structure of Acyl Carrier Protein in Solution Determined by Nuclear Magnetic Resonance and the Combined use of Dynamical Simulated Annealing and Distance Geometry" *Eur. J. Biochem* **1988**, *175*, 9-15.

## **Chapter 4**

**The Interplay of Glycosylation and Disulfide Formation Influences**

**Fibrillization in a Prion Protein Fragment**



## Introduction

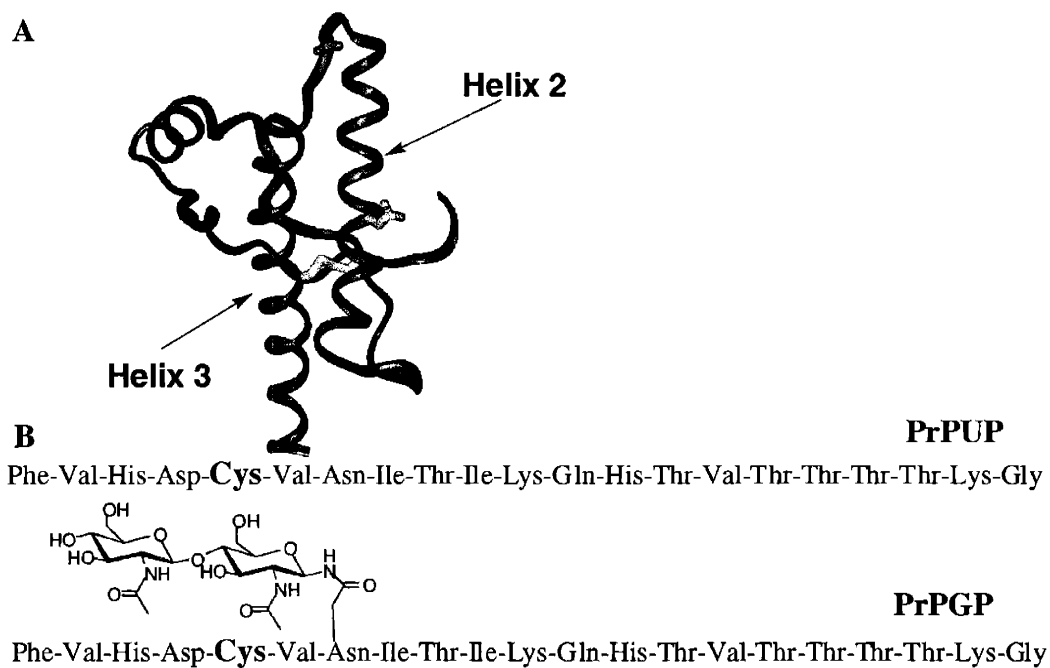
Spongiform encephalopathies are a group of fatal neurodegenerative diseases that can be manifested sporadically, genetically inherited, or in some cases transmitted<sup>1-3</sup>. In contrast to many diseases where the nature of the infectious particle is virus or bacterium, currently, the only agent associated with these conditions is the structural isoform of the cellular prion protein (PrP<sup>C</sup>) known as the scrapie conformation (PrP<sup>Sc</sup>)<sup>1,4</sup>. PrP<sup>C</sup> is an N-linked glycoprotein that is normally attached to the cell membrane by a glycosylphosphatidylinositol (GPI) anchor<sup>5</sup>. PrP<sup>C</sup> also contains an intramolecular disulfide bond (Cys179-Cys214) that provides structural stability to the C-terminus of the protein<sup>6,7</sup>. Secondary structure analyses have shown that PrP<sup>C</sup> is a predominantly helical protein, whereas PrP<sup>Sc</sup> is mainly  $\beta$ -sheet, suggesting that the conversion into PrP<sup>Sc</sup> involves a major structural change<sup>8</sup>. Although the structure of the unglycosylated PrP<sup>C</sup> monomer has been solved by nuclear magnetic resonance (NMR) spectroscopy<sup>7,9</sup>, elucidation of the PrP<sup>Sc</sup> structure has been hampered by its highly aggregated state.

As with many membrane-associated proteins, initiation of the biosynthesis of PrP begins with translocation into the endoplasmic reticulum (ER) where the amino-terminal signal sequence is cleaved<sup>1</sup>. The ER houses the machinery for asparagine-linked glycosylation as well as for disulfide formation<sup>10,11</sup>. Proteins in the secretory pathway that are misfold in the ER<sup>12,13</sup> are subject to retrograde transport into the cytosol where

they are degraded by proteasomes <sup>14,15</sup>. In particular, protein isoforms (or mutants) that are less stable during their maturation are most likely to undergo this retrograde transport <sup>14</sup>. Lindquist and coworkers have recently shown that inhibition of the proteasome causes PrP to accumulate in the cytosol, where it can adopt a PrP<sup>Sc</sup> like conformation <sup>16,17</sup>. Furthermore, expression of an unglycosylated, cytosolic form of PrP has extremely toxic effects on neuroblastoma cells as well as in transgenic mice <sup>17,18</sup>. It has also been shown that inhibition of glycosylation using tunicamycin or exposure of neuroblastoma cells expressing PrP to dithiothreitol (DTT) can cause the protein to acquire PrP<sup>Sc</sup>-like conformations <sup>18</sup>.

Many factors have been associated with the conversion of PrP<sup>C</sup> to PrP<sup>Sc</sup>. For example, fluctuations in metal ion concentrations <sup>19,20</sup>, GPI anchor stability <sup>21</sup>, extracellular molecules such as glycosaminoglycans <sup>22,23</sup>, pH <sup>24</sup>, *N*-linked glycosylation <sup>18,25</sup>, and the redox environment have all been proposed to be implicated <sup>18,26,27</sup>. Some of these factors (eg. variations in pH, post-translational modifications, or redox environment in the secretory pathway) <sup>13,17</sup> could also be associated with protein localization or processing within the cell. Therefore, the available data suggest that the structural transition between PrP<sup>C</sup> and PrP<sup>Sc</sup> might not be induced simply by one specific factor, but rather due to the additive effect of a combination of factors. In some cases, there is a possibility that these factors could be interrelated and affecting each other. The

evidence showing that a reducing environment can promote the generation of PrP<sup>Sc</sup>-like species<sup>6,16-18</sup> suggests that factors affecting the stability of the disulfide bridge could also have an effect in preventing or promoting the PrP<sup>C</sup> to PrP<sup>Sc</sup> transition. Previous glycopeptide studies reveal that N-linked glycosylation can impact the conformation of protein fragments<sup>28-30</sup>. In particular, we have shown that glycosylation can alter the thermodynamics of disulfide bond formation, favoring the oxidized form<sup>31</sup>. In this study we prepare a peptide and a glycopeptide corresponding to residues 175-195 of the human PrP in order to investigate the effects of the core carbohydrate unit (chitobiose) of N-linked glycans on the stability and conformational properties of the fragment. The 175-195 segment is derived from helix 2 of the prion protein and contains one of the two glycosylation sites (Asn181) found in the protein and a cysteine at position 179 (Scheme 4.1)<sup>7</sup>. Our results show that N-linked glycosylation, with the disaccharide chitobiose, has a significant effect on the fibril formation capabilities of the PrP175-195 fragment; glycosylation significantly decelerates the rate of fibrillization. Furthermore, the carbohydrate moiety appears to alter the redox properties of C179 causing the peptide to be stabilized as the intermolecular disulfide homodimer, which is highly resistant to fibril formation.



**Scheme 4.1.** (A) Ribbon diagram generated from the human PrP 121-230 NMR structure.<sup>7</sup> Asn 181 and Asn 197 (glycosylation sites) are colored by atom. Disulfide bridge between Cys 179 and Cys 214 is colored in yellow. Fragment 175-195 is colored in blue. (B) Synthetic unglycosylated (**PrPUP**) and glycosylated (**PrPGP**) peptides derived from the PrP 175-195 fragment.

## Results

### Circular Dichroism and FTIR of PrPUP and PrPGP

Peptide stock solutions were prepared by dissolving the peptides in water to a concentration of 210  $\mu\text{M}$  at pH 4 in order to prevent rapid fibril formation (see electron microscopy results in chapter 2). Aliquots of the peptides were then mixed with sodium phosphate buffer pH 7.5 and DTT to final concentrations of 70  $\mu\text{M}$  peptide, 1 mM buffer and 1 mM DTT. Spectra taken immediately after dissolution displayed random-coil characteristics for both unglycosylated (**PrPUP**) and glycosylated (**PrPGP**) peptides (Figure 4.1A). However, after incubation for 24 hours, the CD spectra displayed a characteristic  $\beta$ -sheet signature (Figure 4.1A). Precipitates were also noted in the samples at this stage. Since CD spectroscopy does not provide structural information on the precipitated material, the total secondary structure in the suspension was examined by Fourier-transform infrared spectroscopy (FTIR). The maxima at 1615  $\text{cm}^{-1}$  for both peptide and glycopeptide confirmed the presence of aggregated  $\beta$ -sheets as the major secondary structure present in the suspension (Fig. 4.1B). These results reflect the natural tendency of both **PrPUP** and **PrPGP** to undergo a structural transition into aggregated  $\beta$ -sheets.

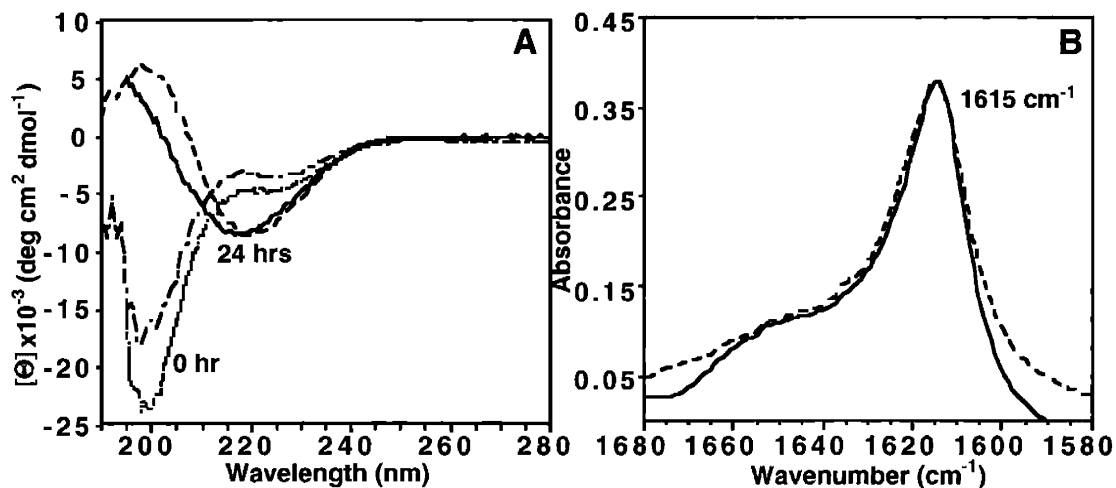


**Figure 4.1** (A) CD spectra of PrPUP at 0 (dotted line) and 24 hours (solid line) and PrPGP at 0 (intermediate dashed line) and 24 hours (dashed line) of incubation in 1mM phosphate buffer pH 7.5 and 1mM DTT. (B) Amide I' region of the FTIR spectra for PrPUP (solid line) and PrPGP (dashed line) after aggregation at pH 7.5 and 5mM DTT.

### Effect of Glycosylation on the Kinetics of Aggregation and Disulfide Stabilization

Previous studies suggest that glycosylation delays the PrP<sup>C</sup> to PrP<sup>Sc</sup> transition in cells<sup>32</sup>. It has also been demonstrated that disulfide stability in PrP<sup>C</sup> can play an important role in stabilizing the native fold of the protein<sup>6</sup>. Although fragment 175-195 includes only one cysteine residue, Cys 179 has the potential to form intermolecular disulfide bonds that could affect the ability of the PrP fragment to form fibrils. To study the effects of glycosylation and reducing environment on the aggregation kinetics of the PrP fragment we studied the fibrillization of the peptides at various DTT concentrations. A summary of the aggregation lag times for both peptide and glycopeptide are shown in

Table 4.1. The aggregation kinetics for both peptides showed a well-defined dependence on DTT concentrations. For both, **PrPUP** and **PrPGP**, the aggregation lag time decreased with increasing concentrations of DTT. However, **PrPGP** showed slower aggregation than **PrPUP** when incubated at similar DTT concentrations (Figure 4.2). **PrPGP** also showed a higher resistance to aggregation at lower DTT concentrations. Although at higher DTT concentrations the difference between the aggregation lag times for **PrPUP** and **PrPGP** was not so dramatic (3.4 hours for **PrPUP** and 6.2 hours **PrPGP** at 10 mM DTT), the difference in the aggregation lag times was dramatically increased at lower DTT concentrations or in the absence of DTT. While **PrPUP** begins to aggregate at 6.9 hours in the absence of DTT, no aggregation was observed for **PrPGP** by 5 days under comparable conditions. It required one hundred times more DTT to accelerate the aggregation kinetics of **PrPGP** to be similar to **PrPUP** (0.1 mM for **PrPUP** and 10 mM DTT for **PrPGP**). Also, no major decrease in the aggregation lag time was observed for **PrPUP** after the DTT concentration was increased above 1 mM. On the other hand, the aggregation lag times for **PrPGP** continued to decrease between 1.0 and 10.0 mM DTT concentrations. These results show that for both species, a reducing environment accelerates fibril formation. However, the glycopeptide appears to be more stable in the soluble form than the unglycosylated peptide in a reducing environment .

The effect of reduced and oxidized glutathione on the aggregation kinetics of the peptides was also investigated. In the cell, oxidized and reduced glutathione levels are regulated to maintain control of the redox environment. Similar conditions to those used for studies with DTT were employed. Both peptides (**PrPUP** and **PrPGP**) were incubated in 1mM sodium phosphate pH 7.5 buffer and 0.1 mM reduced or oxidized glutathione and the aggregations kinetics were monitored. Peptide solutions incubated with oxidized glutathione displayed complete inhibition of aggregation with both **PrPUP** and **PrPGP**. In contrast, when the peptides were incubated with reduced glutathione, **PrPUP** showed significant aggregation (with aggregation lag time of  $4.6 \pm 0.8$  hours) while **PrPGP** aggregation was inhibited at least for 5 days (Table 4.1). These results reinforce the proposal that the glycopeptide has a higher resistance to the redox environment than the unglycosylated peptide.



**Table 4.1.** Summary of aggregation lag times for 70  $\mu\text{M}$  PrPUP and PrPGP in 1mM sodium phosphate buffer pH 7.5 and different reducing conditions.

Reducing agent	PrPUP lag time (hours)	PrPGP lag time (hours)
none	$6.9 \pm 0.8$	$> 120$
0.1 mMDTT	$5.9 \pm 0.9$	$> 24$
1.0 mM DTT	$3.4 \pm 0.6$	$8.8 \pm 0.2$
10.0 mM DTT	$3.4 \pm 0.2$	$6.2 \pm 0.5$
0.1 mM GSH	$4.6 \pm 0.8$	$> 120$

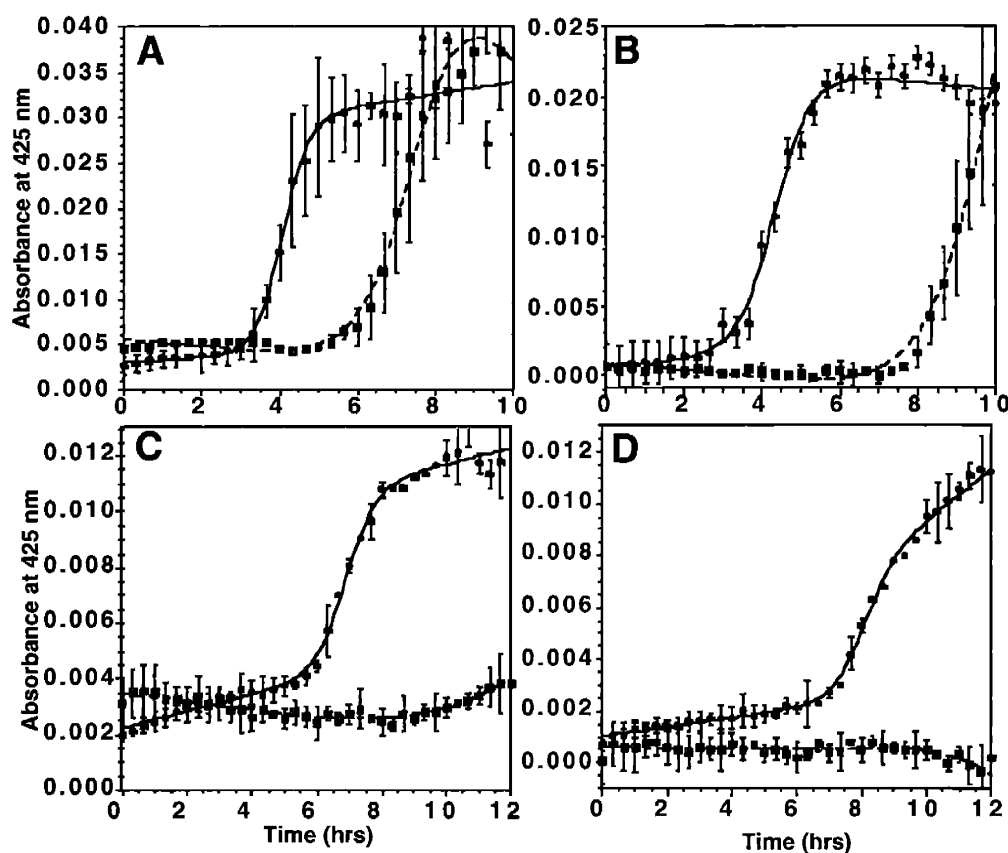


**Fig. 4.2.** Comparison of aggregation kinetics for 70  $\mu\text{M}$  PrPUP (black solid line) and 70  $\mu\text{M}$  PrPGP (red dashed line) in 1mM phosphate buffer pH 7.5 and different DTT concentrations. (A) 10 mM DTT (B) 1mM DTT (C) 0.1 mM DTT (D) no DTT.

### **Congo red reactivity to PrPUP and PrPGP solutions**

Congo red has been widely used to monitor the presence of amyloid fibrils.<sup>33</sup> Incubation of amyloid fibrils with Congo red is associated with a change in the dye color from orange-red to pink. Spectrophotometrically, the binding of amyloid fibrils to the dye is associated with a red shift of the Congo red excitation maxima. Aliquots of solutions used for the aggregation studies were taken after one day of incubation, mixed with a Congo red solution at pH 7.5 and color changes were monitored. As shown in the inset of figure 4.3A, rapidly after mixing, all the **PrPUP** solutions that have been incubated at pH 7.5 (with and without DTT) displayed a more pink color compared to the Congo red solution without peptide. Similar results were observed for **PrPGP** solutions that have been incubated with DTT. However, **PrPGP** solutions incubated without DTT did not display significant color changes in the presence of Congo red (inset of Figure 4.3B).

The same solutions were then examined by UV-Vis spectroscopy. **PrPUP** and **PrPGP** peptide solutions incubated with DTT showed a significant red shift in the excitation maxima of the Congo red spectra from 488 nm to 525 nm for **PrPUP** and 530 nm for **PrPGP** (Figure 4.3A). However, although **PrPUP** incubated in the absence of DTT showed a significant red shift from 488 nm to 525 nm (37 nm), the **PrPGP** solution under the same conditions showed only a minor red shift from 488 to 498 nm (10 nm) of

the Congo red spectra (Figure 4.3B). These data suggest that **PrPUP** and **PrPGP** are capable of forming amyloid fibrils within a period of 24 hours when incubated with high concentrations of DTT. However, although **PrPUP** can also form amyloid fibrils in this time period in the absence of DTT, the glycopeptide does not form fibrils to the same extent.

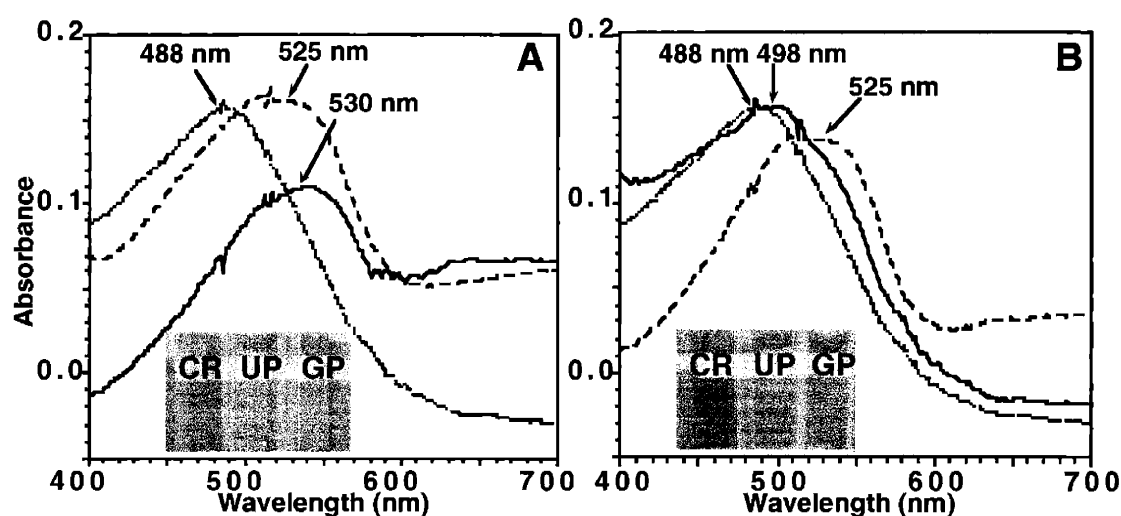


**Figure 4.3.** Congo red binding assay for **PrPUP** and **PrPGP** after incubation for 24 hours in 1mM phosphate buffer pH 7.5 with (A) and without (B) DTT. Congo red (dotted lines), **PrPUP** (dashed line) and **PrPGP** (solid line). Although the spectra were subtracted by the peptide aggregates, the high baselines are the result of the heterogeneous nature of the peptide suspensions. **Inset.** Photos of congo red samples after titrating the peptides that have been incubated for 24 hours with or without DTT respectively. In this picture: **CR** = Congo red without peptide, **UP** = **PrPUP** and **GP** = **PrPGP**.

### Electron Microscopy analysis of **PrPUP** and **PrPGP**

Electron microscopy (EM) studies were implemented to provide direct information about the specific macromolecular structures generated with **PrPUP** and

**PrPGP**. EM analysis for **PrPUP** and **PrPGP** solutions incubated with 1mM DTT for 24 hours indicated the presence of fibrils (Figure 4.4A top and bottom respectively). Only minor differences are noted in the analyses; in general, **PrPUP** solutions displayed more extended fibril networks than **PrPGP**, and **PrPGP** showed a higher quantity of small-sized filaments near the major fibrils. On the other hand, **PrPUP** and **PrPGP** solutions incubated in the absence of DTT showed significant differences (Figure 4.4B top and bottom). **PrPUP** grids showed a high concentration of fibrils. In contrast, no major fibrils, only minor precipitates, were observed for **PrPGP** under the same conditions. These results were also corroborated by the Congo red assay (supplementary material) <sup>33</sup>. Similarly, EM analysis of **PrPUP** incubated with 0.1 mM reduced glutathione displayed fibrils while only minor precipitates were observed for **PrPGP** under similar conditions (Figure 4.4C top and bottom). No fibrils were observed in the peptide solutions incubated with oxidized glutathione. These results are in good agreement with the aggregation kinetics and congo red studies and suggest that fibril formation could be inhibited by oxidation of the peptide. Additionally, the *N*-linked chitobiose moiety may alter the properties of the glycopeptide, rendering it more resistant to fibril formation. This effect is more pronounced in a non-reducing environment, where the glycosylated peptide (**PrPGP**) is inhibited from forming fibrils (in contrast to the unglycosylated peptide).

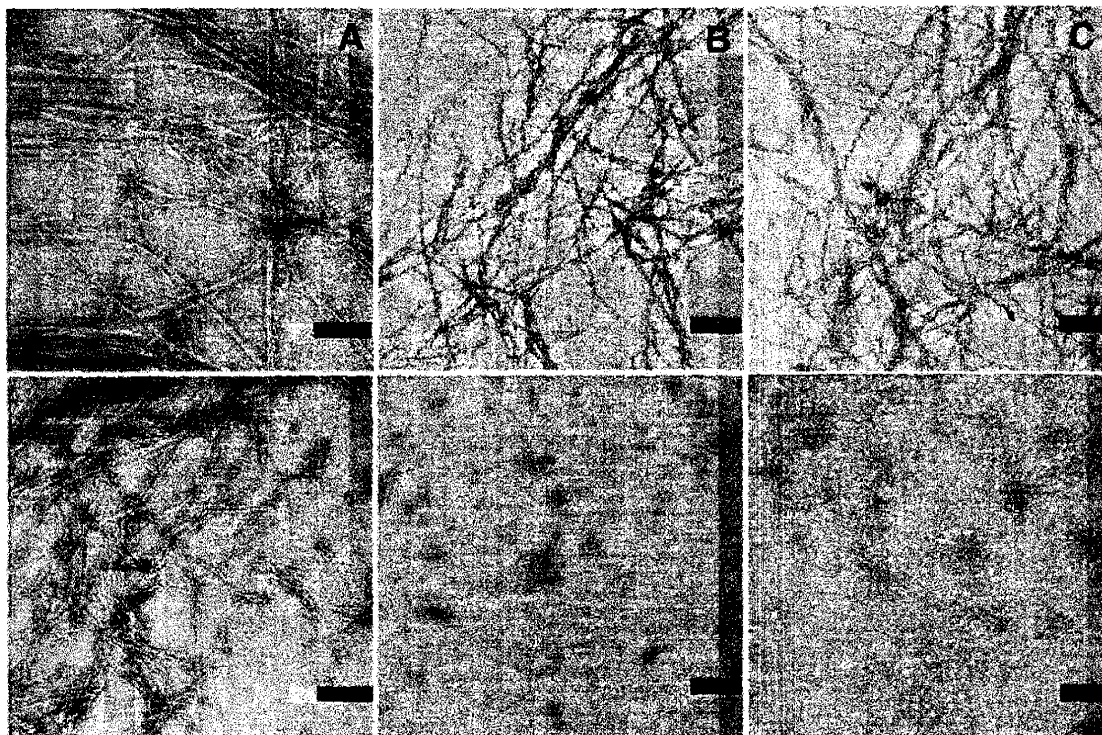


**Figure 4.4.** EM pictures for **PrPUP** (top) and **PrPGP** (bottom). (A) Peptides incubated for 24 hours in 1mM phosphate buffer pH 7.5 and 1mM DTT (bar=100 nm). (B) Peptides incubated for 24 hours in 1mM phosphate buffer pH 7.5 in the absence of DTT (bar=200 nm). (C) Peptides incubated for 24 hours in 1mM phosphate buffer pH 7.5 and 0.1 mM GSH (bar=200 nm).

### **Effect of C179S mutation**

In order to confirm that the inhibition of fibril formation in the peptide fragment is related to Cys 179 (probably by cystine formation), we synthesized the **C179S** mutant of the unglycosylated PrP 175-195 peptide fragment. Aggregation kinetics, Congo red binding assays and EM analyses were performed on this mutant and compared to the native unglycosylated peptide. Interestingly, aggregation kinetics showed that the **C179S**

mutant aggregates instantaneously without a significant lag time. Also, the aggregation kinetics for the mutant did not show any significant dependence on DTT concentration (Figure 4.5A). Similar results were observed when incubation was carried out with oxidized glutathione; while oxidized glutathione inhibits the fibrillization of **PrPUP**, it did not have any effect on the aggregation kinetics of **C179S**. Visual inspection of the peptide solutions incubated with the Congo red dye showed a very intense pinkish-red color for the **C179S** mutant compared with the wild type **PrPUP** (inset of Figure 4.5B). The high reactivity of the mutant with Congo red was then corroborated by UV-Vis analysis (Figure 4.5B). The wild type and the **C179S** mutant caused a significant red shift on the Congo red maxima from 488 nm to 520 nm (32 nm). However, titrating similar amounts of peptides into the Congo red solution caused a noticeably higher absorbance. In addition, EM analysis of the mutant revealed a high amount of entangled fibrils (Figure 4.6). These results indicate that the **C179S** mutant is more “aggressive” in the fibrillization process and suggest that Cys179 plays a major role in controlling the formation of fibrils. These results also reinforced the idea that the fibrillization pathway can be inhibited by intermolecular cystine formation.

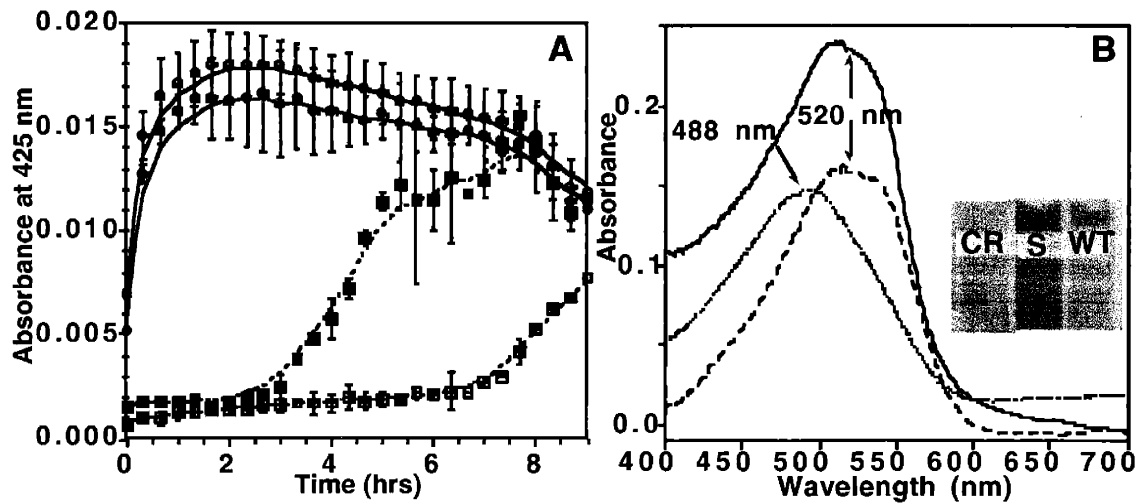


**Figure 4.5.** Effect of C179S mutation on the fibril formation of the PrP175-195 fragment. (A) Aggregation kinetics for C179S in the presence of 10 mM DTT (red) and absence of DTT (blue) and for WT PrPUP incubated with 10 mM DTT (dashed line-closed squares) and absence of DTT (dashed line-open squares). (B) UV-Vis spectra of Congo red (dotted line) and Congo red titrated with C179S (solid line) and PrPUP (dashed line) after 24 hours of incubation in the absence of DTT. **Inset.** Visual inspection of Congo red solutions titrated with the mutant (S) and WT solutions after 24 hours of incubation in the absence of DTT.

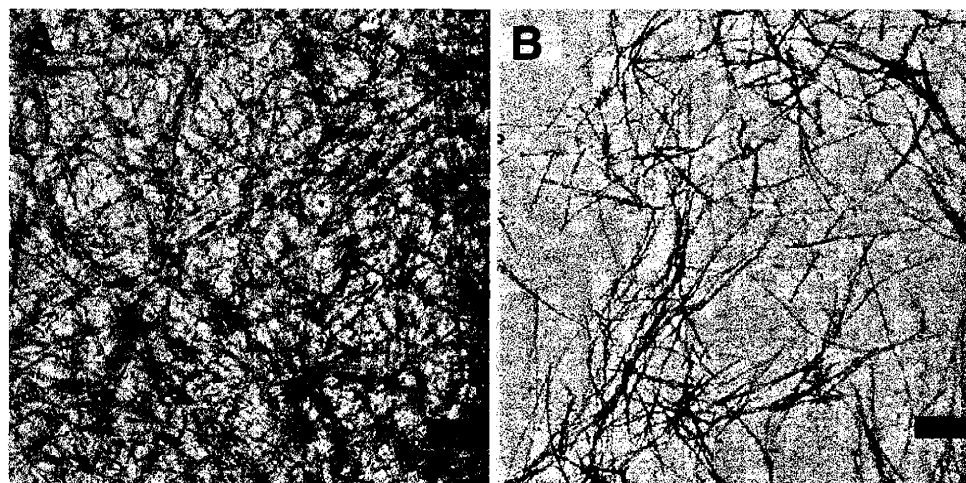


**Figure 4.6.** Electron microscopy of C179S (A) compared to wild type PrPUP (B). Both samples were placed on the EM grid 24 hours after incubation in 1mM phosphate buffer pH 7.5 in the absence of DTT. Bars represent 200 nm.

### **Evidence for a redox mechanism by mass spectrometry**

The previous data suggest that a peptide oxidation could be involved in the inhibition of fibril formation and that glycosylation promotes this oxidation. Therefore, we examined the solutions in which fibrillization was inhibited after 5 days of incubation by electrospray mass spectrometry (ESMS). Although **PrPUP** formed fibrils in the absence of DTT, the suspension was analyzed to compare the results with **PrPGP** incubated in the absence of DTT. For this case, it was necessary to first centrifuge the **PrPUP** suspension to remove major precipitates and only use the supernatant for the analysis. Although most of the unglycosylated sample was aggregated, a minor peak corresponding to the **PrPUP** monomer ( $[M+3H^+]/3$  795.7 (obsd); 795.9 (calcd)) was observed in the supernatant (Figure 4.7A). On the other hand, ESMS analysis of the **PrPGP** solution showed masses corresponding to the cystine-linked glycopeptide dimer ( $[M+5H^+]/5$  1117.7 (obsd); 1117.0 (calcd),  $[M+6H^+]/6$  931.4 (obsd); 931.0 (calcd),  $[M+7H^+]/7$  798.3 (obsd); 798.2 (calcd)) (Figure 4.7B). The presence of the intermolecular cystine dimer in the glycopeptide sample and its absence in the unglycosylated peptide sample, suggest that this is the major species responsible for inhibition of the peptide self-assembly into fibrils. Therefore, dimerization via intermolecular cystine formation could serve as an alternate process that competes with fibril formation. These observations correlate with the previous results showing the



dependence of the reductive environment on fibril formation and the enhanced effect of the carbohydrate moiety against the fibrillization pathway, potentially by promoting the oxidation.

ESMS analysis of solutions incubated with oxidized glutathione showed similar results for both peptides; the peptide-glutathione adduct linked *via* disulfide bond was the major species present in the samples (Figure 4.7C and 4.7D). For **PrPUP** we observed:  $[M+3H^+]/3$  897.4 (obsd); 897.7 (calcd),  $[M+4H^+]/4$  673.3 (obsd); 673.5 (calcd). For **PrPGP** samples incubated with oxidized or reduced glutathione, the peptide-glutathione adduct linked through the disulfide bond was observed (Figure 4.7D).

Only minor precipitates were observed in the **PrPGP** sample incubated with reduced glutathione after the 5 days of incubation. The masses observed for **PrPGP** incubated with oxidized glutathione were:  $[M+3H^+]/3$  775.3 (obsd); 775.1 (calcd),  $[M+4H^+]/4$  1033.4 (obsd); 1033.1 (calcd). When incubated with reduced glutathione we observed:  $[M+3H^+]/3$  775.1 (obsd); 775.1 (calcd),  $[M+4H^+]/4$  1033.1 (obsd); 1033.1 (calcd). These results reinforce the idea that an alternate mechanism promoting the formation of intermolecular disulfide (either to form a homodimer or a mixed disulfide with glutathione) could play a major role in inhibiting the fibril formation pathway in this prion peptide fragment. These observations also strengthen the proposal that

glycosylation could be decelerating the fibrillization mechanism by promoting this alternate intermediate.

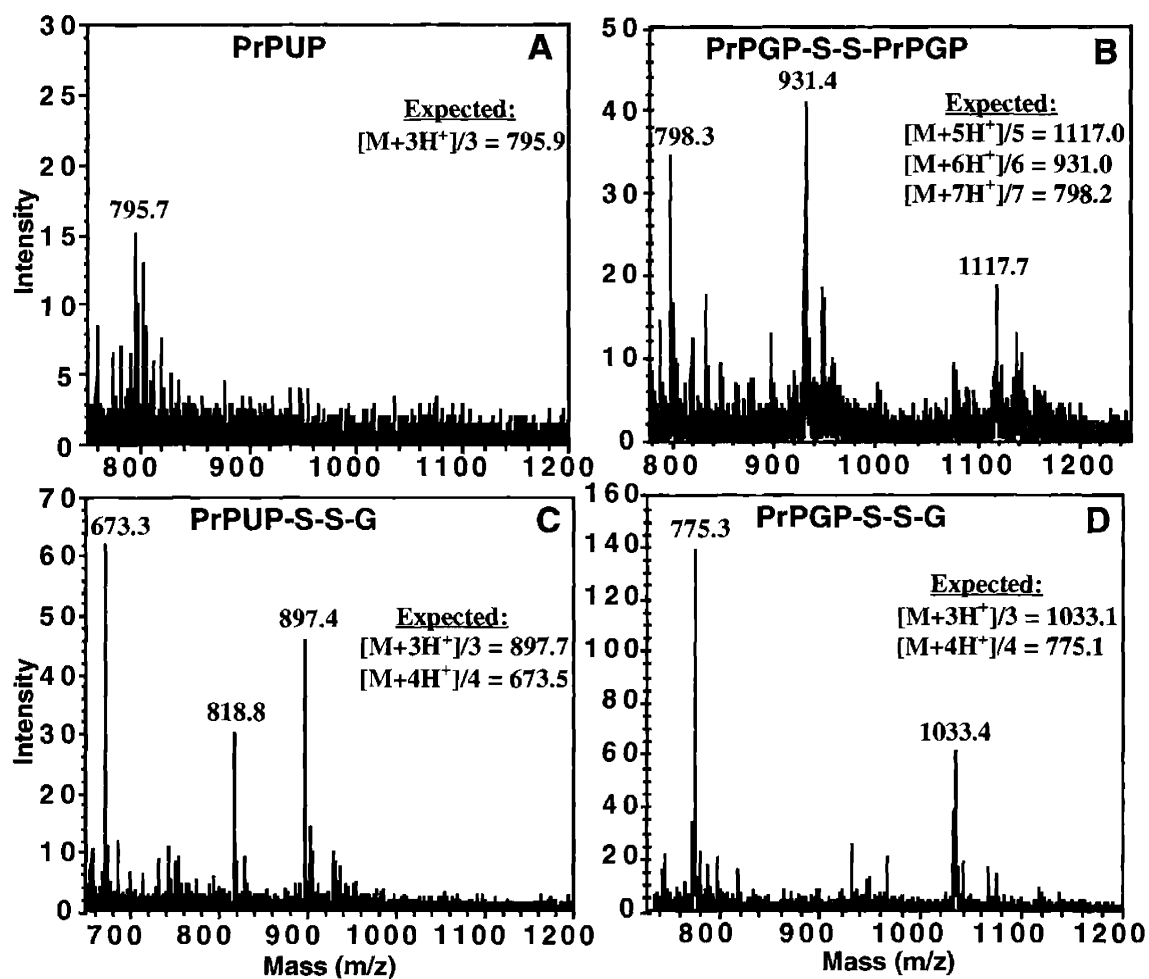


**Figure 4.7.** ESMS spectra of peptide solutions after five days of incubation at pH 7.5. (A) Supernatant of PrPUP after incubation in the absence of DTT. (B) PrPGP after incubation in the absence of DTT. (C) PrPUP after incubation with 0.1 mM oxidized glutathione. (D) PrPGP after incubation with 0.1 mM oxidized glutathione.

## Structural differences between PrPUP and PrPGP by NMR

Previous studies have shown that N-linked glycosylation can impact the local structure of peptides by promoting adoption of a more compact conformations<sup>34</sup>. In systems where the peptide local conformations are affected, but not the complete secondary structure,  $^3J_{\text{HN}\alpha}$  coupling constants have provided an indication of local conformational preferences<sup>34-36</sup>. Although both **PrPUP** and **PrPGP** displayed unstructured characteristics, comparison of the  $^3J_{\text{HN}\alpha}$  coupling constants between the peptides only showed noticeable differences near the glycosylation site (at Asn 181) (Table 4.2, Figure 4.8). A significant increase in the  $^3J_{\text{HN}\alpha}$  coupling constants at Asn 181 from 7.0 Hz in **PrPUP** to 8.7 Hz in **PrPGP** was observed. Since  $^3J_{\text{HN}\alpha}$  coupling constants provide information about the dihedral angles of the peptide backbone, similar elevations on this parameter in analogous systems have been previously attributed to the induction of more compact local structures<sup>34-36</sup>.

The observed differences suggest that a minor local conformational change in the peptide near the glycosylation site may be caused by the chitobiosyl moiety. Although this minor effect does not seem to influence the total peptide structure significantly, it could potentially be related to the induction of intermolecular cystine formation with Cys 179, which is only two residues away from the glycosylation site.

**Table 4.2.** Comparison of the  $^3J_{\text{HN}\alpha}$  (Hz) values for PrPGP and PrPUP.

Residue	PrPGP $^3J_{\text{HN}\alpha}$ (Hz)	PrPUP $^3J_{\text{HN}\alpha}$ (Hz)
F 175	7.3	7.1
V 176	8.8	8.8
H 177	7.2	7.1
D 178	7.2	7.0
C 179	8.7	8.7
V 180	8.6	7.4
<b>N 181</b>	8.7	7.0
I 182	8.8	8.7
T 183	8.8	7.0
I 184	8.8	7.1
K 185	8.8	8.8
Q 186	7.0	7.1
H 187	7.1	8.8
T 188	7.1	7.0
V 189	8.8	8.8
T 190	8.7	8.7
T 191	7.2	7.1
T 192	7.1	7.1
T 193	7.1	7.1
K 194	7.0	7.1
G 195	12.3	12.3

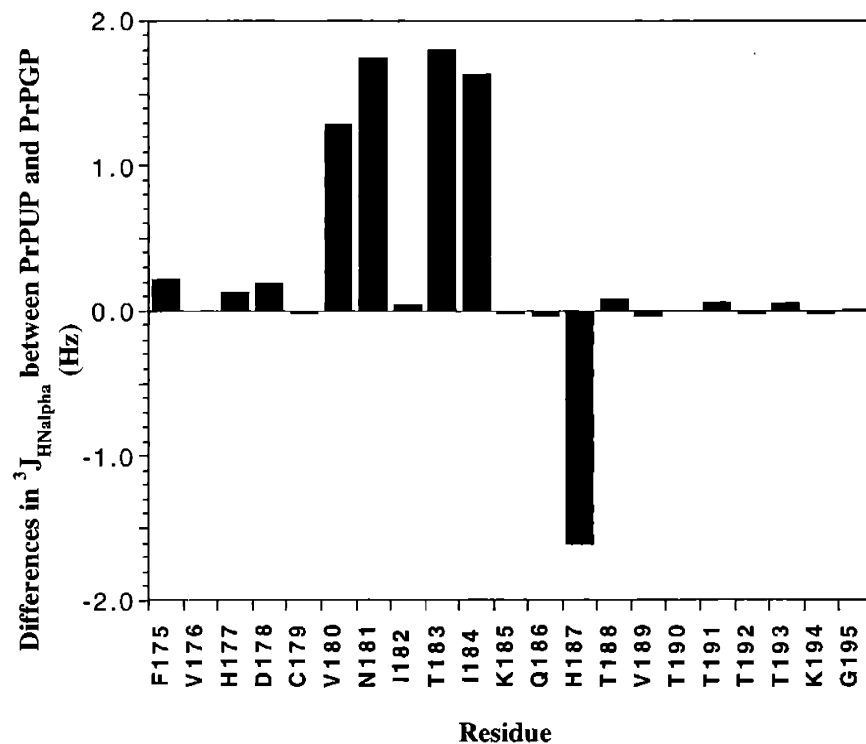


**Figure 4.8.** Differences in  $^3J_{HN\alpha}$  (Hz) values between PrPGP and PrPUP.

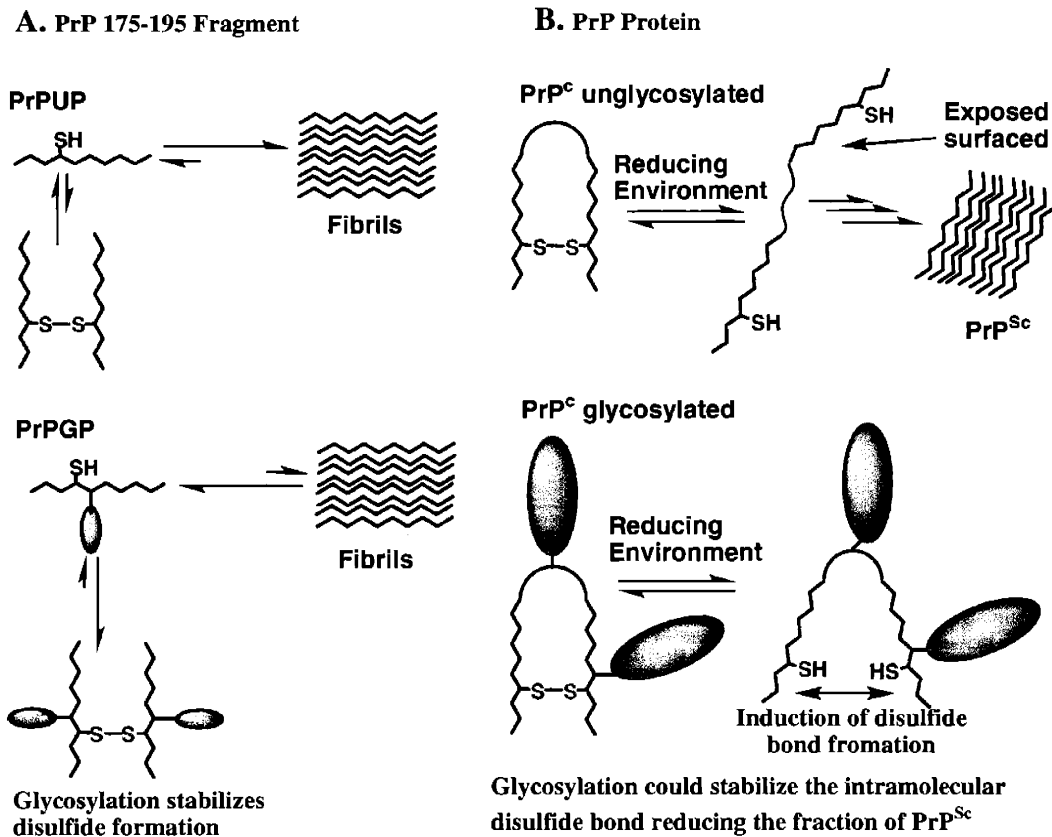
## Discussion

In this study we have synthesized and studied unglycosylated and glycosylated peptides corresponding to the 175-195 fragment of the human prion protein. The glycosylated peptide was modified with the core chitobiose disaccharide found in all N-linked glycoproteins. Comparison of the structure, aggregation kinetics, fibril formation capabilities and redox susceptibility of Cys 179 has provided insight into the effects of the N-linked carbohydrate on the stability of the PrP fragment. Although both peptides

are capable of undergoing a random coil to  $\beta$ -sheet transition to form fibrils at and above physiological pH, glycosylation caused a significant deceleration in the rate of fibril formation. The fibrillization of both peptides also showed a major dependence on reductive environment; however, the glycopeptide showed a higher resistance to aggregation under similar reducing conditions. Mass spectrometry then confirmed that the greater stability displayed by the glycopeptide was due to a higher tendency of this peptide to exist as the intermolecular homodimer linked *via* a disulfide bond (Figure 4.7). The proposal that intermolecular disulfide bond formation stabilizes the peptide as a soluble species was also supported by the aggressive fibrillization of the **C179S** mutant.

The fact that the PrP 175-195 fragment is capable of forming fibrils at physiological pH, but the fibrilization is inhibited when the peptide is dimerized through disulfide formation is noteworthy when put in the context of the intact protein. In the native protein, part of this fragment is occluded by helix 3. Masking of the peptide surface is strongly stabilized by the Cys 179-Cys 214 disulfide bond (Scheme 4.1A). Therefore, if exposure of a surface of the 175-195 fragment can induce fibrilization (as displayed by the peptide), in order to expose that peptide surface, the disulfide must first be reduced. This is in agreement with our results on the peptide fragment and previous reports on the total protein that show that a reducing environment promotes the fibrilization process or a PrP<sup>Sc</sup>-like conformation<sup>6,16-18</sup>. Together these results suggest

that factors stabilizing the Cys 179-Cys 214 disulfide are of extreme importance in preventing the PrP<sup>C</sup> to PrP<sup>Sc</sup> transition. As observed from the primary sequence and the NMR structure of the prion protein <sup>7</sup>, the two glycosylation sites are in close proximity to the disulfide bond. Asn 181 is only two residues away from Cys 179 and the other glycosylation site (Asn 197) is located at the turn between the two helices held together by the disulfide (Scheme 4.1). Although for the 175-195 fragment, formation of the disulfide bond must be intermolecular, a similar behavior is observed; the formation of the disulfide bond inhibits the fibrillization process. Therefore, these results suggest that glycosylation may have a similar effect in the native protein; stabilizing the PrP<sup>C</sup> isoform in an indirect manner by promoting the intramolecular disulfide stability. Scheme 4.2 summarizes the effects of glycosylation on the PrP 175-195 fragments and the possible effects that glycosylation might have on the prion protein.



**Scheme 4.2.** Disulfide stabilization by N-linked glycans in the PrP 175-195 fragment (A) and in the context of the protein (B). In the 175-195 fragment, glycosylation promotes the formation of the intermolecular cysteine which inhibits the fibrilization of the peptide. Glycosylation could have a similar effect on the prion protein by stabilizing the intramolecular disulfide bond.

In the peptide fragment, intermolecular disulfide bond formation competes with fibrillization (Scheme 4.2A). The N-linked chitobiose moiety seems to drive the fragment towards the dimer state by promoting the disulfide bond stability. In the intact protein, exposure to a reducing environment, as for example in the cytoplasm when the protein is retrograde transported<sup>14,16,17</sup>, the intramolecular disulfide bond can be reduced. The



surface of the 175-195 fragment with high propensity for fibrillization is then exposed which promotes the protein fibrillization. It is also possible that final intermolecular disulfide rearrangements can then take place to form the ultimate, protease resistant PrP<sup>Sc</sup> <sup>27</sup>. Although exposure to a reducing environment can also induce PrP<sup>Sc</sup> formation on the glycosylated PrP<sup>C</sup>, glycosylation could stabilize the intramolecular disulfide bond in the protein decreasing the fraction of PrP<sup>Sc</sup> formation. In the intact protein, the glycans could have a significant impact on the properties of the disulfide bond. They could shield the cystine, which would stabilize the oxidized form of the protein, or they could perturb the redox potential of the cysteines, thus promoting the oxidation <sup>31</sup>.

With the results presented here, several proposals can be put forward to explain how glycosylation might affect the fibrillization mechanism. 1. The carbohydrate moiety could cause a minor destabilization on the peptide structure required for the specific intermolecular interactions leading to fibril formation. 2. Glycosylation could cause a steric effect that inhibits intermolecular association leading to fibrillization. Although this could be a non-specific factor, this effect could be very significant considering that the size of the PrP carbohydrates in vivo are large and occupy a significant surface area of the protein. 3. N-linked glycosylation could also be diverting the fibrillization mechanism by indirectly affecting other aspects of the peptide structure. For example, it could

influence the oxidation potential of the cysteine residue thus promoting the formation of the intermolecular cystine dimer that could compete with fibril formation.

**Acknowledgements.**

This work was supported by the NIH (GM-39334). Part of this chapter was submitted to

*Proc. Natl. Acad. Sci. USA*, **2003**.

## **Materials and Methods**

### **Peptide Synthesis**

The unglycosylated peptide (**PrPUP**) was synthesized on PAL-PEG-PS resin using a MilliGen/Biosearch 9050 automated peptide synthesizer. The peptides were prepared as the C-terminal amide and the N-terminal acetyl derivative to better mimic internal sequences in **PrP**. Standard 9-fluorenylmethoxycarbonyl (Fmoc) chemistry and HBTU/HOBT activation was used for all residues except cysteine. In this case, pre-activated Fmoc-L-Cys(Trt)-OPfp was employed in the absence of base in order to prevent racemization. For glycopeptide synthesis, incorporation of the GlcNAc-GlcNAc disaccharide was achieved using a pre-synthesized Fmoc-L-Asn[ $\beta$ -chitobiose(TBDMS)<sub>5</sub>]-OH derivative<sup>37</sup>. Peptides were cleaved from the resin using 92% TFA, 2% triisopropylsilane, 3% ethanedithiol and 3% H<sub>2</sub>O, purified using preparative RP-HPLC and characterized using electrospray mass spectrometry (ESMS) and quantitative amino acid analysis (QAA). The C179S mutant was synthesized using similar procedures.

### **Peptide purification and characterization**

Peptides were dissolved in 85 : 10 : 5 cold H<sub>2</sub>O : CH<sub>3</sub>CN : DMSO (with 0.1% TFA), filtered through a 0.45  $\mu$ m filter and purified by reverse-phase HPLC on a

Waters Prep LC 4000 system using a 15 -70% gradient in acetonitrile/0.1% TFA for 30 minutes. Peptides were collected (**PrPUP**:  $t_R = 25.7$  minutes; **PrPGP**:  $t_R = 24.7$  minutes) and characterized by electro-spray mass spectrometry (ESMS). **PrPUP**: ( $[M+3H^+]/3$  795.7 (obsd); 795.9 (calcd)). **PrPGP**: ( $[M+2H^+]/2 = 1396.8$  (obsd); 1396.6 (calcd)). Quantitative amino acid analysis (QAA) was used to confirmed the amino acid composition of the peptides. NMR characterization is provided below.

### **Circular Dichroism**

CD spectra were recorded at 25°C on an Aviv 202 CD spectrophotometer in Quartz cuvettes with an optical path length of 0.1 cm. The buffer and DTT contribution were subtracted for all spectra. Any contribution to the signal from the carbohydrate was subtracted using chitobiose amine as a standard. The signal was normalized to mean residue ellipticity based on the peptide concentration.

### **Fourier Transform Infrared Spectroscopy (FTIR)**

FTIR spectra were recorded on a Nicolet Magna 560 IR spectrometer using a rectangular cuvette with  $\text{CaF}_2$  windows and 50  $\mu\text{m}$  spacers. Peptides were dissolved in  $\text{D}_2\text{O}$  (pD approximately 3.9) and lyophilized twice before analysis to remove residual  $\text{H}_2\text{O}$ . For analysis, peptides were redissolved in  $\text{D}_2\text{O}$  to a concentration of 1.3 mM (pD

3.9) and deuterated phosphate buffer (pD 7.9) and DTT were added to a concentration of 5 mM buffer and DTT. FTIR spectra were recorded after aggregation.

### **Negative Staining Electron Microscopy (EM)**

Samples used for EM analysis were obtained from aggregation studies (usually 24 hours after incubation). Five  $\mu$ l aliquots were taken from the incubation samples and placed on carbon-coated 300-mesh nickel grids and adsorbed for 2 minutes. The grids was then stained with 2% uranyl acetate for 2 minutes and after drying, were viewed in a Philips EM 410 operated at 80 KV at magnifications of 55,000, 24,000 and 10,000 X.

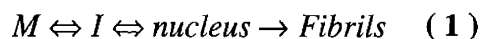
### **Aggregation Kinetics**

Although thioflavin T, Congo red and visible light scattering assays gave similar results, a visible light scattering assay in 96-well plate format was preferentially used to study the aggregation because of its capability for multiple sample handling. Kinetic analysis was performed at 25°C on a Molecular Devices Spectramax 190 plate reader. Peptide solutions were prepared as described previously (CD section) and kinetic studies were initiated by mixing the peptide in water at pH 4 with phosphate buffer at pH 7.5. The 96-well plate was agitated for one second every 20 minutes and absorbance at 425

nm was recorded immediately after agitation. The analyses were performed in duplicate or triplicate and the average and standard deviation values were reported.

### **Evaluation of the Aggregation Kinetics Data**

The model from Nielsen <sup>38</sup> was employed to fit the data and calculate the lag times for the aggregation kinetics (equation 1). Here, M is the peptide monomer and I is an intermediate. In this model, fibril formation is described as a sigmoidal curve defined by an initial lag phase (where no increase in the 425 nm absorbance is observed), followed by a growth phase (when major aggregates start to form) and finally an equilibrium phase when the signal reaches a plateau (when aggregation is complete) <sup>38</sup>. The absorbance at 425 nm was plotted as a function of time and the data was fitted to the model described by equation 2 using Kaleidagraph <sup>38</sup>. Here,  $Y$  is the absorbance at 425 nm,  $x$  is the time,  $x_0$  is the time to reach 50 % of the maximum absorbance and  $1/\tau$  gives the apparent rate constant for fibril growth ( $k_{app}$ ). The lag time is then be calculated from  $x_0 - 2\tau$ . The data analysis showed good agreement with this model (R values of 0.99).



$$Y = y_i + mx + \frac{y_f + mx}{1 + e^{-[(x - x_0)/\tau]}} \quad (2)$$

### **Congo Red Binding**

Aliquots of 40  $\mu\text{L}$  were taken from the aggregation kinetics samples after 24 hours of incubation. Congo red (in 10 mM phosphate buffer at pH 7.5) was added to the aliquots to a final concentration of 10  $\mu\text{M}$  for visual inspection and 5  $\mu\text{M}$  for UV-Vis analysis. The solutions were incubated for 10 minutes and then analyzed in a Beckman DU 7500 spectrophotometer using a 1 cm path length cuvette. A spectrum of the unbound dye was also recorded. Spectra of the peptide without dye were recorded for subtraction from the Congo red-peptide spectra in order to reduce the high baseline caused by the peptide aggregation.

**Electrospray Mass Spectrometry (ESMS).** An Applied Biosystems Mariner ESMS was used to record the mass spectra of the samples. After 5 days of incubation, 10  $\mu\text{l}$  aliquots from the soluble peptide samples were directly injected into the ESMS running in a 50% methanol/water (0.05 % acetic acid) solvent system at 0.25 ml/min. Aggregated samples were first centrifuged and 10  $\mu\text{l}$  from the supernatant were used for analysis.

**NMR Spectroscopy.** Peptides (1mM) were dissolved in a cold (7 °C) solution of 5 mM NaOAc- $\text{d}_3$ , pH 4.5, 10%  $\text{D}_2\text{O}$  in water (0.01 % DMSO was used as internal reference).

All the NMR experiments were performed at pH 4.5 and 7°C in order to prevent

fibrillization. Spin systems for both peptides were assigned using TOCSY, NOESY and COSY experiments<sup>34</sup> with WATERGATE gradient suppression. The  $^3\text{JNH}_\alpha$  coupling constant values were calculated from DQF-COSY experiments at 7°C<sup>34</sup>. NOESY spectra were acquired using 400 ms mixing times. Spectra were recorded on a 600 MHz Bruker DRX 600 Advance spectrometer. The NMR data was processed using Felix 97 software (MSI).



**Table 4.3.** <sup>1</sup>H assignment for PrPUP.

Residue	HN	HC $\alpha$	HC $\beta$	Others
Ac				CH <sub>3</sub> 1.99 NH <sub>2</sub> 7.57,7.18
Phe175	8.36	4.59	3.06,2.96	H2,H6 7.21 H3,H5 7.29
Val176	8.23	4.03	1.96	$\gamma$ CH <sub>3</sub> 0.90,0.86
His177	8.73	4.66	3.26,3.18	H2 8.61 H4 7.30
Asp178	8.64	4.64	2.81,2.72	
Cys179	8.57	4.52	2.91,2.91	
Val180	8.38	4.09	2.08	$\gamma$ CH <sub>3</sub> 0.95,0.93
Asn181	8.63	4.76	2.82,2.73	$\gamma$ NH <sub>2</sub> 7.73, 7.00
Ile182	8.33	4.23	1.80	$\gamma$ CH <sub>2</sub> 1.21,1.18 $\gamma$ CH <sub>3</sub> 0.90 $\delta$ CH <sub>3</sub> 0.86
Thr183	8.41	4.31	4.16	$\gamma$ CH <sub>3</sub> 1.19
Ile184	8.29	4.12	1.83	$\gamma$ CH <sub>2</sub> 1.44,1.18 $\gamma$ CH <sub>3</sub> 0.88 $\delta$ CH <sub>3</sub> 0.85
Lys185	8.53	4.28	1.80,1.73	$\gamma$ CH <sub>2</sub> 1.45 $\delta$ CH <sub>2</sub> 1.69 $\epsilon$ CH <sub>2</sub> 3.00,3.00 $\epsilon$ NH <sub>3</sub> 7.48
Gln186	8.52	4.24	2.04,1.95	$\gamma$ CH <sub>2</sub> 2.36,2.36 $\delta$ NH <sub>2</sub> 7.62,6.98
His187	8.79	4.77	3.28,3.22	H2 8.61 H4 7.31
Thr188	8.41	4.32	4.12	$\gamma$ CH <sub>3</sub> 1.18
Val189	8.56	4.23	2.10	$\gamma$ CH <sub>3</sub> 0.96,0.96
Thr190	8.55	4.45	4.21	$\gamma$ CH <sub>3</sub> 1.20
Thr191	8.43	4.46	4.24	$\gamma$ CH <sub>3</sub> 1.20
Thr192	8.42	4.44	4.25	$\gamma$ CH <sub>3</sub> 1.21
Thr193	8.37	4.34	4.20	$\gamma$ CH <sub>3</sub> 1.21
Lys194	8.63	4.31	1.88,1.86	$\gamma$ CH <sub>2</sub> 1.43 $\delta$ CH <sub>2</sub> 1.67 $\epsilon$ CH <sub>2</sub> 3.01,2.98 $\epsilon$ NH <sub>3</sub> 7.60
Gly195	8.60	3.91,3.91		
CONH <sub>2</sub>				NH <sub>2</sub> 6.92, 6.81

**Table 4.4.**  $^1\text{H}$  assignment for PrPGP.

Residue	HN	HC $\alpha$	HC $\beta$	Others
Ac				CH <sub>3</sub> 1.99 NH <sub>2</sub> 7.57,7.18
Phe175	8.35	4.58	3.06,2.96	H2,H6 7.21 H3,H5 7.29
Val176	8.21	4.02	1.96	$\gamma$ CH <sub>3</sub> 0.90,0.86
His177	8.73	4.65	3.26,3.18	H2 8.61 H4 7.30
Asp178	8.65	4.65	2.81,2.72	
Cys179	8.58	4.52	2.91,2.91	
Val180	8.34	4.07	2.08	$\gamma$ CH <sub>3</sub> 0.95,0.93
Asn181	8.66	4.75	2.85	$\gamma$ NH <sub>2</sub> 7.73, 7.00
Ile182	8.24	4.22	1.80	$\gamma$ CH <sub>2</sub> 1.21,1.18 $\gamma$ CH <sub>3</sub> 0.90 $\delta$ CH <sub>3</sub> 0.86
Thr183	8.43	4.30	4.16	$\gamma$ CH <sub>3</sub> 1.19
Ile184	8.31	4.11	1.83	$\gamma$ CH <sub>2</sub> 1.44,1.18 $\gamma$ CH <sub>3</sub> 0.88 $\delta$ CH <sub>3</sub> 0.85
Lys185	8.52	4.27	1.80,1.73	$\gamma$ CH <sub>2</sub> 1.45 $\delta$ CH <sub>2</sub> 1.69 $\epsilon$ CH <sub>2</sub> 3.00,3.00 $\epsilon$ NH <sub>3</sub> 7.48
Gln186	8.53	4.26	2.04,1.95	$\gamma$ CH <sub>2</sub> 2.36,2.36 $\delta$ NH <sub>2</sub> 7.62,6.98
His187	8.78	4.76	3.28,3.22	H2 8.61 H4 7.31
Thr188	8.42	4.35	4.12	$\gamma$ CH <sub>3</sub> 1.18
Val189	8.55	4.22	2.10	$\gamma$ CH <sub>3</sub> 0.96,0.96
Thr190	8.55	4.45	4.21	$\gamma$ CH <sub>3</sub> 1.20
Thr191	8.43	4.46	4.24	$\gamma$ CH <sub>3</sub> 1.20
Thr192	8.41	4.44	4.25	$\gamma$ CH <sub>3</sub> 1.21
Thr193	8.36	4.34	4.20	$\gamma$ CH <sub>3</sub> 1.21
Lys194	8.62	4.31	1.88,1.86	$\gamma$ CH <sub>2</sub> 1.43 $\delta$ CH <sub>2</sub> 1.67 $\epsilon$ CH <sub>2</sub> 3.01,2.98 $\epsilon$ NH <sub>3</sub> 7.60
Gly195 CONH <sub>2</sub>	8.60	3.91,3.91		NH, 6.92, 6.81

	HN	H1	H2	H3	H4	H5	H6	Ac
GlcNAc	8.34	5.00	3.85	3.74	3.53	3.50	3.80,3.71	1.95
GlcNAc'	8.54	4.58	3.75	3.56	3.48	3.48	3.93,3.91	2.02

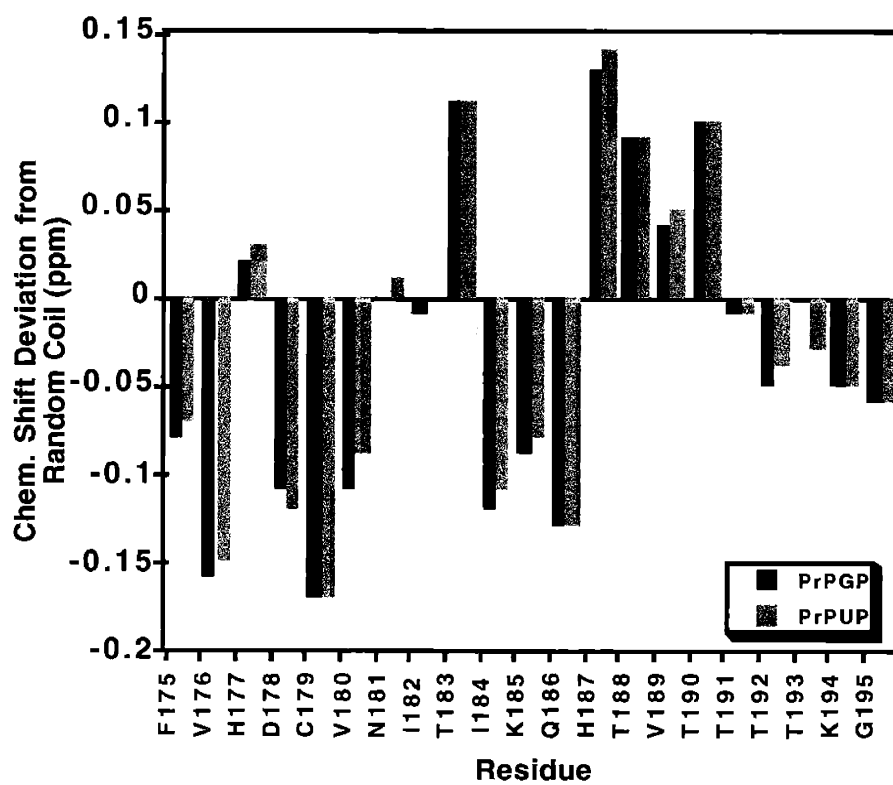


Figure 4.9. Deviations of  $H\alpha$  chemical shift from random coil values.

## References:

- 1) Prusiner, S. B. "Prions" *Proc. Natl. Acad. Sci. USA* **1998**, *95*, 13363-13383.
- 2) Weissmann, C. "Molecular Biology of Prion Disease" *Trends Cell Biol.* **1994**, *4*, 10-14.
- 3) Caughey, B.; Chesebro, B. "Prion Protein and the Transmissible Spongiform Encephalopathies" *Trends Cell Biol.* **1997**, *7*, 56-62.
- 4) Prusiner, S. B. "Novel Proteinaceous Infectious Particles Cause Scrapie" *Science* **1982**, *216*, 136-144.
- 5) Stahl, N.; Borchelt, D. R.; Hsiao, K.; Prusiner, S. B. "Scrapie Prion Protein Contains a Phosphatidylinositol Glycolipid" *Cell* **1987**, *51*, 229-240.
- 6) Jackson, G. S.; Hosszu, L. L. P.; Power, A.; Hill, A. F.; Kenney, J.; Saibil, H.; Craven, C. J.; Waltho, J. P.; Clarke, A. R.; Collinge, J. "Reversible Conversion of Monomeric Human Prion Protein Between Native and Fibrillogenic Conformations" *Science* **1999**, *283*, 1935-1937.
- 7) Zahn, R.; Liu, A.; Lührs, T.; Riek, R.; Schroetter, C. V.; Gracia, F. L.; Billeter, M.; Calzolari, L.; Wider, G.; Wüthrich, K. "NMR Solution Structure of the Human Prion Protein" *Proc. Natl. Acad. Sci. USA* **2000**, *97*, 145-150.

- 8)Pan, K.-M.; Baldwin, M.; Nguyen, J.; Gasset, M.; Serban, A.; Groth, D.; Melhorn, I.; Huang, Z.; Fletterick, R. J.; Cohen, F. E.; Prusiner, S. B. "Conversion of Alpha Helices into Beta-Sheets Features in the Formation of the Scrapie Prion Proteins" *Proc. Natl. Acad. Sci. USA* **1993**, *90*, 10962-10966.
- 9)James, T. L.; Liu, H.; Ulyanov, N. B.; Farr-Jones, S.; Zhang, H.; Donne, D. G.; Kaneko, K.; Groth, D.; Melhorn, I.; Prusiner, S. B.; Cohen, F. E. "Solution Structure of a 142-Residue Recombinant Prion Protein Corresponding to the Infectious Fragment of the Scrapie Isoform" *Proc. Natl. Acad. Sci. USA* **1997**, *94*, 10086-10091.
- 10)Dempski, R. E. Jr.; Imperiali, B. I. "Oligosaccharyl Transferase: Gatekeeper to the Secretory Pathway" *Curr. Opin Chem. Biol.* **2002**, *6*, 844-850.
- 11)Sevier, C. S.; Kaiser, C. A. "Formation and Transfer of Disulphide Bonds in Living Cells" *Nat. Rev. Mol. Cell Biol.* **2002**, *3*, 836-847.
- 12)Kopito, R. R. "ER Quality Control: The Cytoplasmic Connection" *Cell* **1997**, *88*, 427-430.
- 13)Ellgaard, L.; Molinari, M.; Helenius, A. "Setting the Standards: Quality control in the Secretory Pathway" *Science* **1999**, *286*, 1882-1888.
- 14)Ma, J.; Lindquist, S. "Wild-type PrP and a Mutant Associated With Prion Disease are Subject to Retrograde Transport and Proteasome Degradation" *Proc. Natl. Acad. Sci. USA* **2001**, *98*, 14955-14960.

- 15) Yedidia, Y.; Horonchik, L.; Tzaban, S.; Yanai, A.; Taraboulos, A. "Proteasomes and Ubiquitin are Involved in the Turnover of the Wild-type Prion Protein" *EMBO J.* **2001**, *20*, 5383-5391.
- 16) Ma, J.; Lindquist, S. "Conversion of PrP to a Self-Perpetuating PrP<sup>Sc</sup>-like Conformation in the Cytosol" *Science* **2002**, *298*, 1785-1788.
- 17) Ma, J.; Wollmann, R.; Lindquist, S. "Neurotoxicity and Neurodegeneration When PrP Accumulates in the Cytosol" *Science* **2002**, *298*, 1781-1785.
- 18) Ma, J.; Lindquist, S. "De Novo Generation of a PrP<sup>Sc</sup>-like Conformation in Living Cells" *Nat. Cell Biol.* **1999**, *1*, 358-361.
- 19) Wong, B.-S.; Vénien-Bryan, C.; Williamson, R. A.; Burton, D. R.; Gambeti, P.; Sy, M.-S.; Brown, D. R.; Jones, I. M. "Copper Refolding of Prion Protein" *Biochem Biophys Res Com* **2000**, *276*, 1217-1224.
- 20) Stöckel, J.; Safar, J.; Wallace, A. C.; Cohen, F. E.; Prusiner, S. B. "Prion Protein Selectively Binds Copper (II) Ions" *Biochemistry* **1998**, *37*, 7185-7193.
- 21) Taraboulos, A.; Scott, M.; Semenov, A.; Avraham, D.; Laszlo, L.; Prusiner, S. B. "Cholesterol Depletion and Modification of COOH-Terminal Targeting Sequence of the Prion Protein Inhibit Formation of the Scrapie Isoform" *J. Cell Biol* **1995**, *129*, 121-132.

- 22) Priola, S. A.; Caughey, B. "Inhibition of Scrapie-Associated PrP Accumulation. Probing the Role of Glycosaminoglycans in Amyloidogenesis" *Mol. Neurobiol.* **1994**, *8*, 113-120.
- 23) Leteux, C.; Chai, W.; Nagai, K.; Herbert, C.; Lawson, A. M.; Feizi, T. "10E4 antigen of Scrapie Lesions Contains an Unusual Nonsulfated Heparan Motif" *J. Biol. Chem.* **2001**, *276*, 12539-12545.
- 24) Hornemann, S.; Glockshuber, R. "A Scrapie-like Unfolding Intermediate of the Prion Protein Domain PrP(121-231) Induced by Acidic pH" *Proc. Natl. Acad. Sci. USA* **1998**, *95*, 6010-6014.
- 25) Rudd, P. M.; Wormald, M. R.; Wing, D. R.; Prusiner, S. B.; Dwek, R. A. "Prion Glycoprotein: Structure, Dynamics, and Roles for the Sugars" *Biochemistry* **2001**, *40*, 3759-3766.
- 26) Capellari, S.; Zaidi, S. I. A.; Urig, C. B.; Perry, G.; Smith, M. A.; Petersen, R. B. "Prion Protein Glycosylation is Sensitive to Redox Change" *J. Biol. Chem.* **1999**, *274*, 34846-34850.
- 27) Welker, E.; Wedemeyer, W. J.; Sheraga, H. A. "A Role for Intermolecular Disulfide Bonds in Prion Diseases?" *Proc. Natl. Acad. Sci. USA* **2001**, *98*, 4334-4336.
- 28) O'Connor, S. E.; Imperiali, B. "Modulation of Protein Structure and Function by Asparagine-linked Glycosylation" *Chem. Biol.* **1996**, *3*, 803-812.

- 29)Imperiali, B.; O'Connor, S. E. "Effect of N-Linked Glycosylation on Glycopeptide and Glycoprotein Structure" *Curr. Opin. Chem. Biol.* **1999**, *3*, 643-649.
- 30)Live, D. H.; Kumar, R. A.; Beebe, X.; Danishefsky, S. J. "Conformational Influences of Glycosylation of a Peptide: A Possible Model for the Effect of Glycosylation on the Rate of Protein Folding" *Proc. Natl. Acad. Sci. USA* **1996**, *93*, 12759-12761.
- 31)Rickert, K. W.; Imperiali, B. "Analysis of the Conserved Glycosylation Site in the Nicotinic Acetylcholine Receptor: Potential Roles in Complex Assembly" *Chem. Biol.* **1995**, *2*, 751-759.
- 32)Lehmann, S.; Harris, D. A. "Blockade of Glycosylation Promotes Acquisition of Scrapie-Like Properties by the Prion Protein in Cultured Cells" *J. Biol. Chem.* **1997**, *272*, 21479-21487.
- 33)Westermarck, G. T.; Johnson, K. H.; Westermarck, P. "Staining Methods for Identification of Amyloid in Tissue" *Methods in Enzymology* **1999**, *309*, 3-25.
- 34)O'Connor, S. E.; Imperiali, B. "Conformational Switching by Asparagine-linked Glycosylation" *J. Am. Chem. Soc.* **1997**, *119*, 2295-2296.
- 35)Live, D. H.; Wang, Z. G.; Iserloh, U.; Danishefsky, S. J. "A Strategy for Probing the Autonomy of Cross-Domain Stereochemical Communication in Glycoconjugates" *Org. Lett.* **2001**, *3*, 851-854.



36)O'Connor, S. E.; Imperiali, B. "A Molecular Basis for Glycosylation Induced Conformational Switching" *Chem. Biol.* **1998**, *5*, 427-437.

37)Bosques, C. J.; Tai, V. W.-F.; Imperiali, B. "Stereoselective Synthesis of  $\beta$ -linked TBDMS-Protected Chitobiose-Asparagine: a Versatile Building Block for Amyloidogenic Peptides" *Tetrahed. Lett* **2001**, *42*, 7207-7210.

38)Nielsen, L.; Khurana, R.; Coats, A.; Frokjaer, S.; Brange, J.; Vyas, S.; Uversky, V. N.; Fink, A. L. "Effect of Environmental Factors on the Kinetics of Insulin Fibril Formation: Elucidation of the Molecular Mechanism" *Biochem* **2001**, *2001*, 6036-6046.

## **Chapter 5**

### **Photolytic Control of Peptide Self-Assembly**

## Introduction

The self-assembly of proteins and peptides into fibrils is one of the major events which lead to the generation of many neurodegenerative diseases. For example, the formation of  $\beta$ -sheet rich fibrils from the monomeric prion protein is a key event in the development of spongiform encephalopathies such as scrapie, bovine spongiform encephalopathy (BSE), Creutzfeldt-Jakob disease (CJD), Gerstmann-Sträussler-Scheinker syndrom and fatal familial insomnia.<sup>1,2</sup> Similarly, Alzheimer's and Parkinson's diseases are induced by a similar fibrillization of the  $\beta$ -amyloid peptide<sup>3,4</sup> and the  $\alpha$ -Synuclein protein<sup>5,6</sup>. This natural process has served as an inspiration to the field of biomaterials where the independent organization of biomolecules into supramolecular templates provides a novel system for the generation of platforms with many new materials.<sup>7-10</sup> Unfortunately, in most systems, the spontaneous self-assembly process can be very difficult to control. In addition, the uncontrolled polymerization can sometimes represent a significant obstacle to the preparation of the system. For example, the synthesis and purification of most self-assembly systems requires the biomolecules to be in solution for chemical modification and purification. Hence, the temporal control of peptide self-assembly would be desirable. Ideally, a peptide could be synthesized and chemically modified in a soluble and stable form until the fibrillization is triggered without the need for additional steps.

Photolabile linkers have been used in many applications such as solid phase peptide synthesis (for the facile cleavage of peptides from the solid support),<sup>11</sup> as well as the time-controlled release of metal ions<sup>12</sup> and bioactive molecules such as peptides and nucleotides.<sup>13</sup> These compounds can serve as efficient triggers for the exposure of active epitopes. Similarly, photolabile linkers represents very attractive alternative for triggering the exposure of specific amyloidogenic peptide sequences. In this way, the peptide would be in a soluble and stable form until the triggering step.

Small changes to the sequence of amyloidogenic peptides or proteins, introduced either by mutation<sup>14,15</sup> or chemical alterations,<sup>16,17</sup> can have dramatic effects on the fibrillization properties of the polypeptide. Different prosthetic groups have been used to control the fibrillization of amyloidogenic peptides.<sup>16</sup> Among these, *N,N*-dimethylethelenediamine (DMDA) groups have been used to prevent peptide self-assembly in solution at neutral pH. This protective effect is believed to be a result of the positive charge on the tertiary amines at pH values below their  $pK_a$  (10-11).<sup>8</sup> Therefore, DMDA groups can be used to affect the fibrillization characteristics of amyloidogenic peptides that are sensitive to a local electrostatic environment. Extensive studies in our laboratory on the human prion protein fragment that includes residues 175-195<sup>18</sup> have shown that the fibrillization of this peptide is very sensitive to the electrostatic environment near the N-terminus. In fact, the replacement of phenylalanine 175 with *p*-

nitro-phenylalanine results in the rapid transition from random coil to  $\beta$ -sheet in this peptide (Figure 5.1).

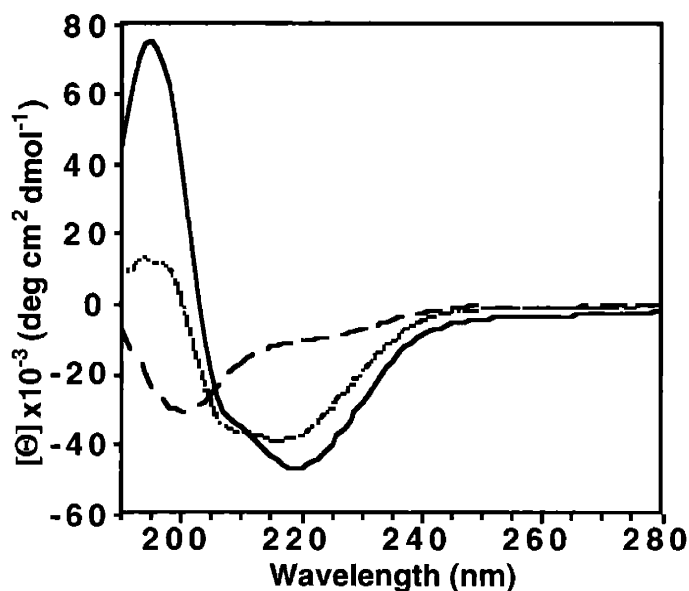
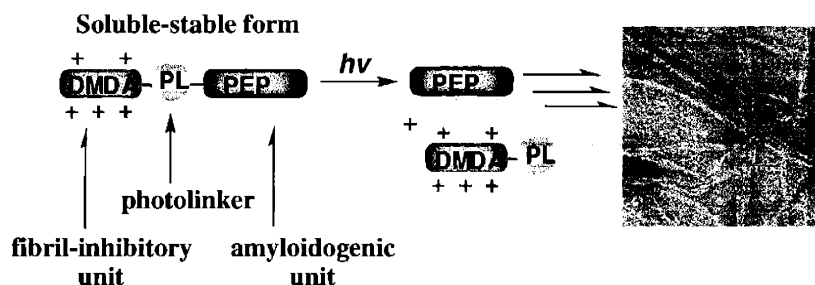


**Figure 5.1.** Effect of the electrostatic environment near the N-terminus of the PrP 175-195 peptide fragment. The addition of a nitro group at the *para* position of phenylalanine 175 induces rapid  $\beta$ -sheet formation in the peptide. WT peptide at 0 (dashed line) and 24 hours (dotted line) incubation in 1mM phosphate buffer pH 7.5 and the *p*-nitro-Phe peptide at 0 hours incubation (solid line).

This chapter describes a novel method for the temporal control of self-assembly into fibrils of an amyloidogenic peptide derived from the human prion protein fragment 174-195.<sup>18,19</sup> The use of a synthetic photolabile linker and a "fibril inhibitory unit" composed of five asparagine-DMDA amino acids, positioned at the N-terminus of the peptide, stabilizes the peptide as a soluble species until photoactivation – the step which triggers peptide self-assembly (Scheme 5.1). Upon photolysis, the fibril-inhibitory unit

and photolinker are released from the amyloidogenic peptide, which is now capable of self-assembly.



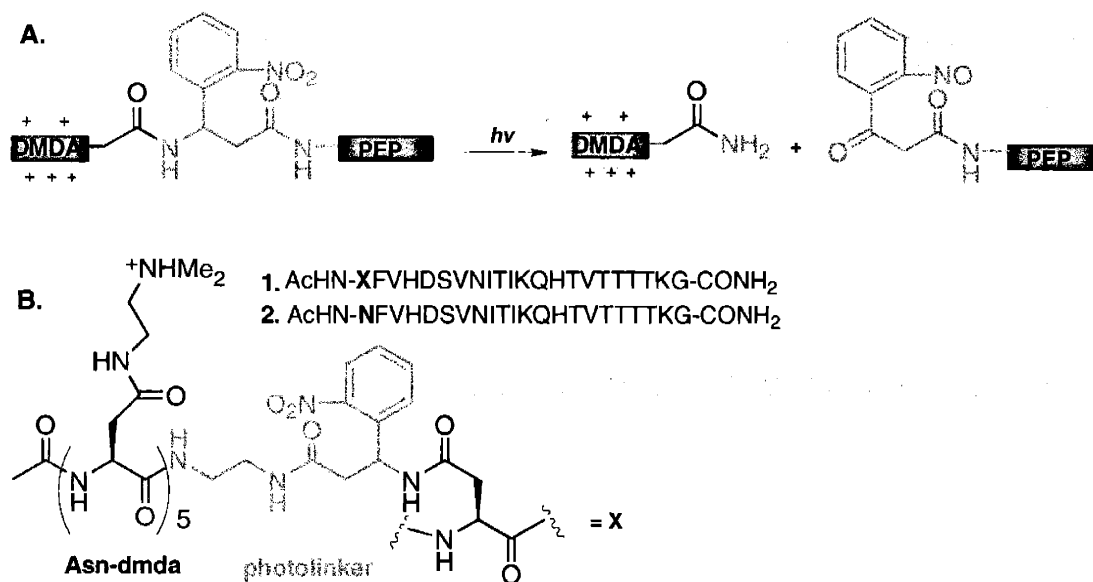
**Scheme 5.1.** General representation of the photolysis-dependent fibrillization of the amyloidogenic peptide. The peptide is stabilized as a soluble form when attached to the fibril inhibitory unit. When the inhibitory unit is photolytically cleaved, the peptide is able to self-assemble into fibrils.

## Results

### Photolinker synthesis

Unfortunately, most commercially available photolinkers for peptide applications are designed to be introduced at the C-terminus of a peptide.<sup>11</sup> If placed at the N-terminus or on the side chain of an amino acid, photo-dissociation results in the photolysis product yielding a nitrosyl moiety to the N-terminus or the side chain of the peptide (Scheme 5.2A). However, due to the effect of the electrostatic environment of the N-terminus of the PrP 174-195 peptide on the tendency to form fibrils, it is very

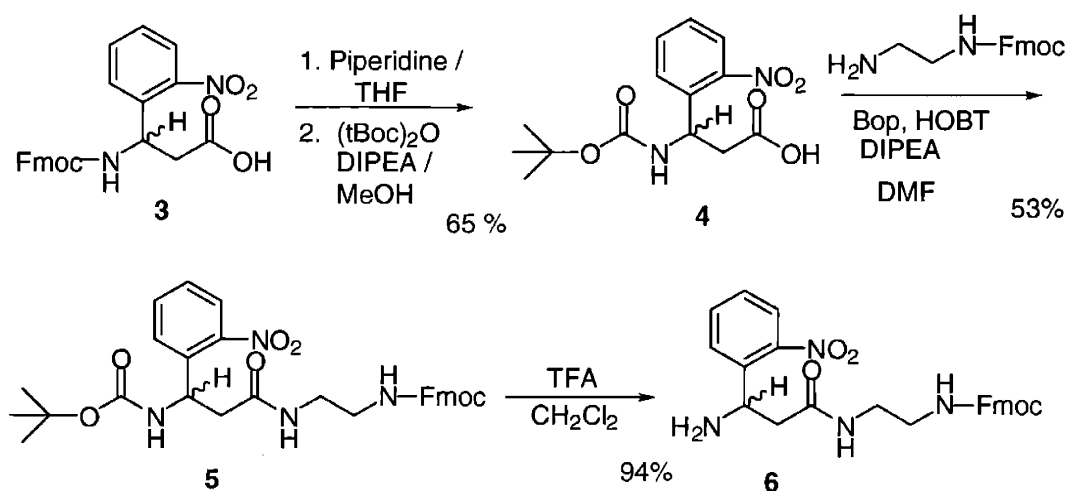
important for this design to place the photolinker and the fibril inhibitory unit near this end.



**Scheme 5.2.** (A) Attachment of photo-adduct to the N-terminus of a peptide using the commercially available ANP linker (Advanced Chemtech). Photolysis results in the photoproduct attached to the N-terminus or side chain. (B) Sequence and structure of peptide 1 (with the modified photolinker – yellow – and inhibitory unit - red) and the resulting peptide 2 (blue) from the photolysis.

To create a photolinker that would liberate the intact amyloidogenic peptide fragment (without adducts attached), we modified the commercially available Fmoc-ANP-linker (Advanced Chemtech) such that it could be attached by an amide linkage to the side chain of the N-terminal residue of our amyloidogenic peptide (Scheme 5.2B). This attachment allows the photolytic release of the intact peptide 2 and leaves an unmodified asparagine residue (Asn 174) at the N-terminus. To prepare the modified

photolinker we first deprotected the commercially available Fmoc-ANP linker (**3**) using 15% piperidine in tetrahydrofuran. The amine was then re-protected as the *tert*-butoxycarbonyl amide using di-*tert*-butyl-dicarbonate (Aldrich) (65% overall yield after the two reactions). Monoprotected Fmoc-ethylenediamine was coupled to the  $\beta$ -carboxylic acid of the Boc-protected photolinker (**4**) in a 53% yield to generate photolinker **5** with orthogonally protected amines. Finally, the *tert*-butoxycarbonyl group was deprotected under acidic conditions to generate the amino-ANP-ethylenediamine-Fmoc (**6**) (94% yield).

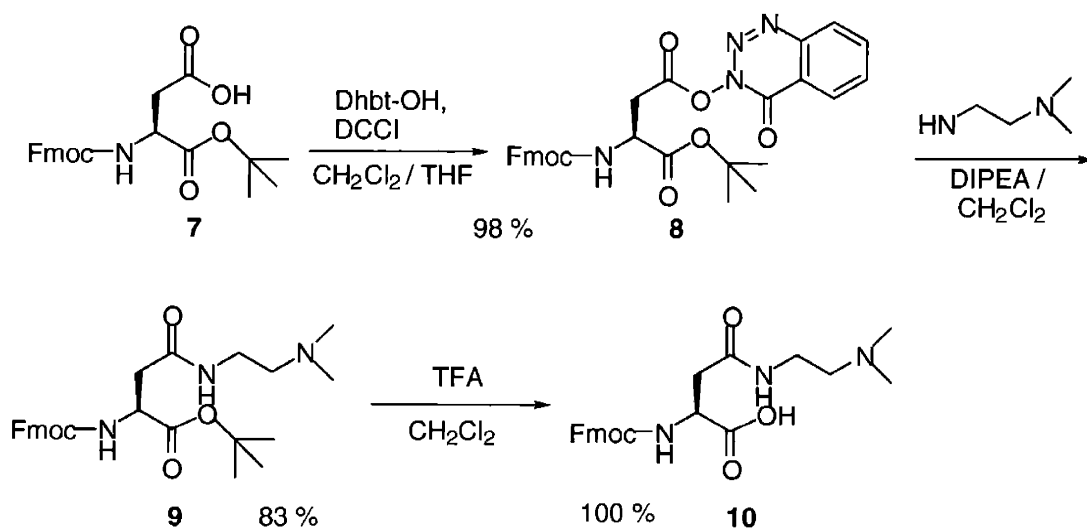


**Scheme 5.3.** Synthetic scheme for the preparation of the amino-ANP-ethylenediamine-Fmoc photolinker.

### Synthesis of fibril-inhibitory unit (Asn-DMDA building block):



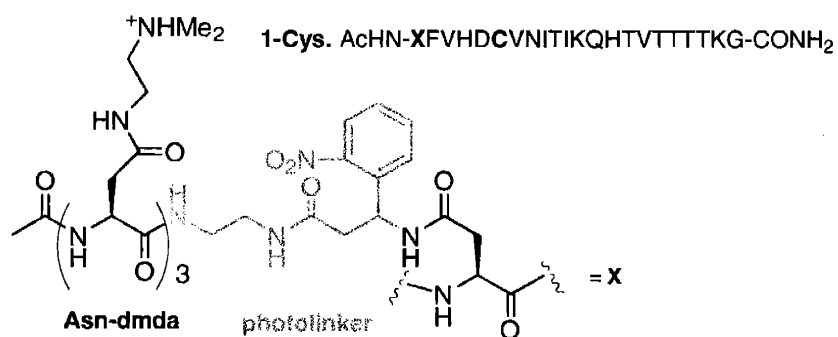
The positive charge and the lower reactivity of tertiary amines, compared to primary amines (an important factor for the photochemistry)<sup>20</sup> makes the *N,N*-dimethylethelenediamine group a good candidate for stabilization of amyloidogenic peptides. To facilitate the introduction of the DMDA groups into the peptide during the SPPS, we synthesized asparagine analogs incorporating the DMDA functionality into the side chain (Scheme 5.4). First, the  $\beta$ -carboxylate of  $N^{\alpha}$ -Fmoc-L-Aspartic acid  $\beta$ -carboxyl *O*-*tert*-butyl ester (**7**) was activated as the 3,4-dihydro-4-oxo-1,2,3-benzotriazin-3-yl (Dhbt) ester (**8**) in 98% yield using the 3-hydroxyl precursor of Dhbt (Dhbt-OH).<sup>21</sup> The activated amino acid was then reacted with *N,N*-dimethylethelenediamine to generate **9** in 83% yield. Finally, the  $\alpha$ -carboxylic acid was deprotected under acidic conditions to yield the  $N^{\alpha}$ -Fmoc-L-Asparagine- $\gamma$ -(*N,N*-dimethylethyleneamide)-OH (**10**) in quantitative yield.



**Scheme 5.4.** Synthetic scheme for the preparation of the asparagine-DMDA amino acid.

## Incompatibility of Cys 179 with the photochemistry of PrP 174-195

In the original attempts to develop this methodology, we used the exact natural sequence of the human prion protein fragment 174-195 that includes a cysteine at position 179 (Scheme 5.5). The photolinker and three Asn-DMDA units were attached to the peptide (as described below for peptide **1**) to generate peptide **1-Cys** (Scheme 5.5). Despite numerous attempts to photolyze the peptide using a wide range of conditions, the photochemistry did not proceed as desired. Ellman's test as well as HPLC and ESMS analysis indicated that Cys 179 seemed to interfere with the photolysis.



**Scheme 5.5.** Sequence and structure of peptide **1-Cys** (with the modified photolinker – yellow - and inhibitory unit - red).

In the Ellman's test, 5,5'-Dithiobis(2-nitrobenzoic acid) (DTNB) reacts with free sulfhydryl groups to produce a species that absorbs at 410 nm. Since this peptide

fragment only contains one cysteine, treating the peptide sample with DTNB at different photolysis times probes the state of the cysteine thiol during UV irradiation. To test whether Cys 179 reacts with the photoproducts, we took samples of peptide 1-Cys at different times during the photolysis and reacted these with DTNB. We then measured the absorbance at 410 nm for each sample and compared it to the absorbance of the mixture before irradiation (Figure 5.2). Before photolysis, similar absorbances were observed for the peptide containing the photolinker and the control peptide (PrP 175-195) without the photolinker. However, an 80% decrease in the 410 nm absorbance was observed upon photolysis only for the peptide containing the photolinker. No reduction in the 410 nm absorbance was observed for the control peptide.

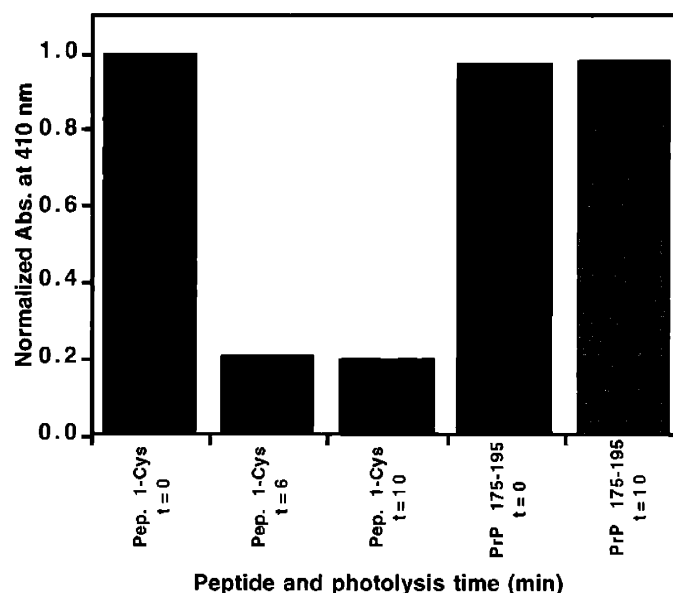


**Figure 5.2.** Reactivity of Cys 179 during photolysis as assessed by Ellman's test. 70  $\mu$ M peptide samples were reacted with DTNB at pH 7.6. Absorbance at 410 nm was normalized by the signal before photolysis.

Analyses of peptide **1-Cys** by HPLC and ESMS during the course of the photolysis also revealed the formation of undesired major products. By 3 minutes of irradiation time, complete disappearance of starting material ( $t_R = 32.9$  min) was observed with no further increase in the yield of photoproduct ( $t_R = 27.7$  min) (**Figure 5.3**). When analyzed by ESMS, this product revealed two major species; one corresponding to the mass of the starting material  $[M+3H^+]/3 = 1111.7$  (obsd.) 1111.6 (calcd);  $[M+4H^+]/4 = 834.3$  (obsd.) 833.9 (calcd) and one corresponding to 32 Da units higher than the expected photoproduct  $[M+2H^+]/2 = 1266.7$  (obsd.) 1266.4 (calcd);  $[M+3H^+]/3 = 844.8$  (obsd.) 844.6 (calcd). Cys 179 is in close proximity to the photolabile linker and may therefore be attacking the reactive nitroso photoproduct as it is liberated (**Figure 5.3**). This attack would result in the generation of a species of the same molecular weight as the starting material that may dissociate during the ESMS analysis to produce the sulfinic acid product that corresponds to the species observed at 32 Da units higher than the expected peptide product.

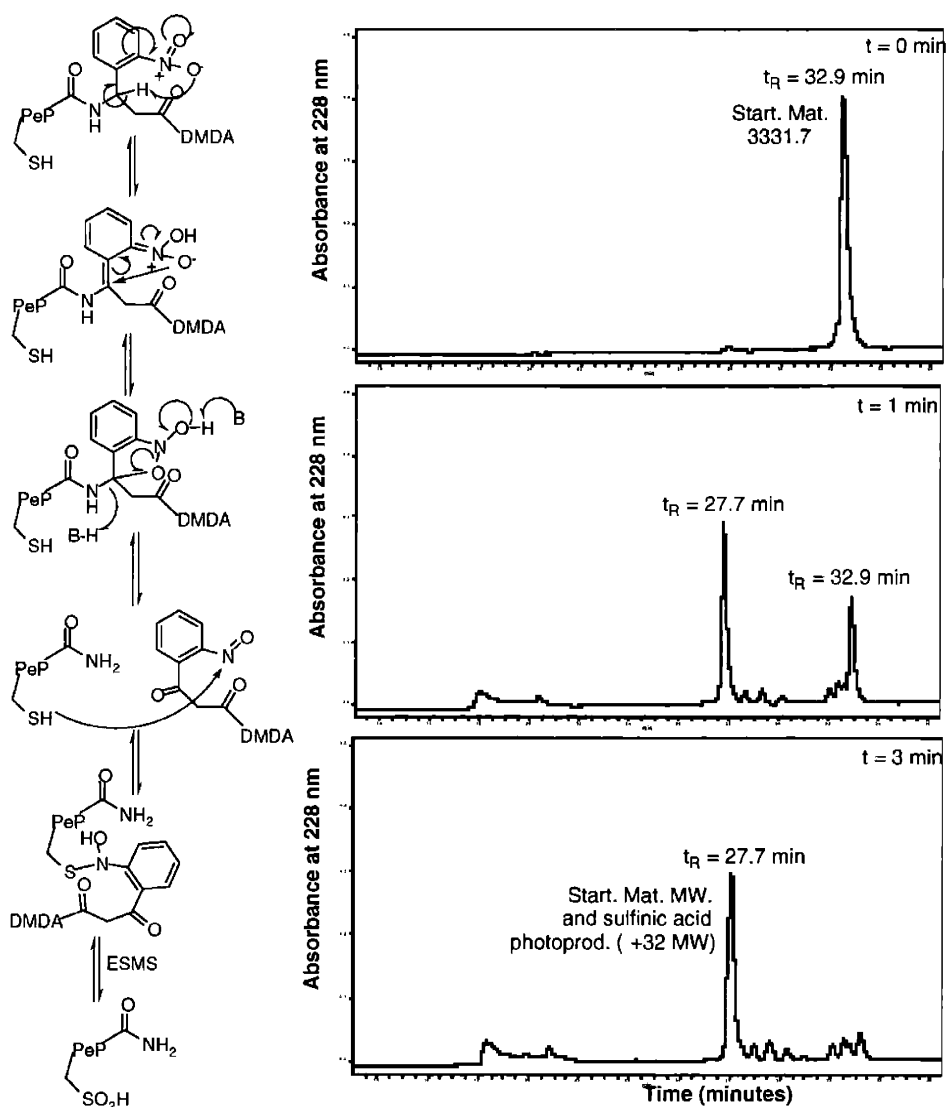


**Figure 5.3.** HPLC traces and a possible mechanism for the formation of the unexpected photoproducts from the photolysis of peptide 1-Cys. Gradient: 10 to 55%  $\text{H}_2\text{O}:\text{CH}_3\text{CN}$ , 0.1% TFA in 35 minutes. Photolysis time is indicated in red and retention times are indicated in black.

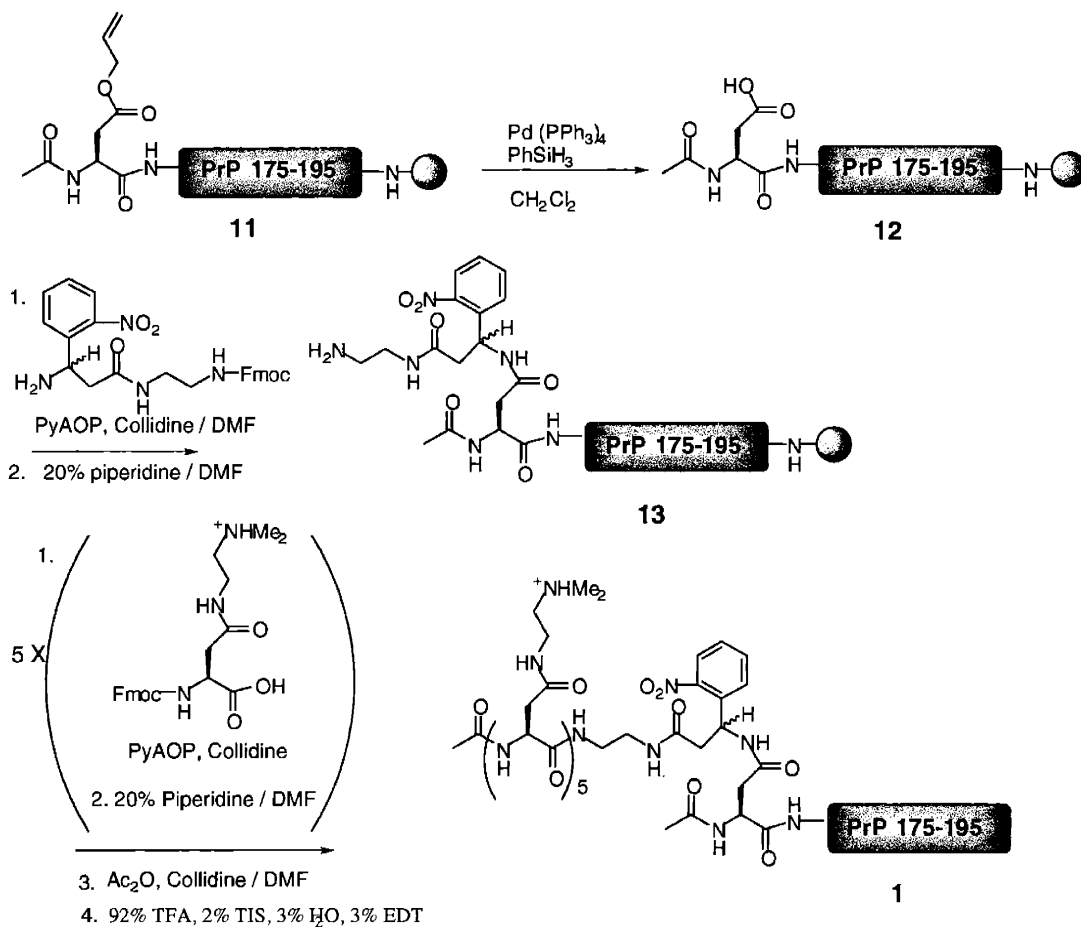
Such side reactions of the nitrobenzyl-based photolabile linkers are fairly common and have been previously observed by other groups.<sup>20</sup> In failed attempts to circumvent this problem, conditions with high concentrations of reducing agents were used and the Cys residue was temporarily capped. Neither of these techniques resulted in

significantly improved photochemistry. Finally, replacement of the cysteine with an unreactive serine was utilized to prevent the formation of the side products.

### **Synthesis of DMDA<sub>5</sub>-PL-PrP 174-195 (peptide 1)**

Photolinker **6** and the Asn-DMDA **10** monomers were attached to the side chain of the N-terminal residue to generate peptide **1** (Scheme 5.6). The peptide was synthesized using standard Fmoc chemistry on a MilliGen/Biosearch 9050 automated peptide synthesizer. To allow for the selective deprotection of the side chain of the N-terminal residue, in order to incorporate the photolinker and fibril-inhibitory unit, the O-allyloxycarbonyl (Alloc) protected Asp was introduced as the last residue. The N-terminal amine was deprotected using 20% piperidine buffered with 2,4-dinitrophenol to prevent aspartimide formation<sup>22</sup> and subsequently acetylated. The side chain of the N-terminal residue was then selectively deprotected by treating the peptide on the resin with Pd(PPh<sub>3</sub>)<sub>4</sub> and PhSiH<sub>3</sub> in dichloromethane to yield **12**. The photolinker was then coupled to the side chain using PyAOP as activator and 2,4,6-collidine as the base. The coupling was verified to be complete by cleaving the peptide from a small portion of resin (2 mg) and analyzing the product by analytical HPLC and ESMS. Treatment of the resin with piperidine yielded **13**. Subsequently, five Asn-DMDA amino acids were coupled to the

free amine and the N-terminus of the fibril-inhibitory unit was acetylated. The peptide was finally cleaved from the resin using 92% TFA, 2% TIS, 3% water and 3% EDT and purified by reverse phase HPLC on a preparative C<sup>18</sup> column. The two peptide epimers resulting from the use of the racemic mixture of the commercial ANP linker were separated at this stage. The major product was used for all analyses.



**Scheme 5.6.** Synthetic scheme for the preparation of peptide **1**.

### Peptide **1** photochemistry

To determine if irradiation of peptide **1** would yield the desired photoproducts and to determine the kinetics of the reaction, the peptide was dissolved in water (120  $\mu\text{M}$  peptide 1mM DTT) and exposed to UV-Vis irradiation from either a nitrogen laser (337 nm, 6mW) or a simple transilluminator (365 nm, 7.3 mW/  $\text{cm}^2$ ). A 2.5 cm diameter



glass container was used for the photolysis with the transilluminator. The large surface area (compared to a 1 cm path length cuvette used with the nitrogen laser) resulted in the best rate of photolysis. The reaction was monitored at different irradiation times by analyzing aliquots from the solution by reverse phase HPLC (Figure 5.4). The expected photoproducts were confirmed by ESMS. After 15 minutes of irradiation, complete disappearance of the starting material was observed with no further increase in peptide 2.

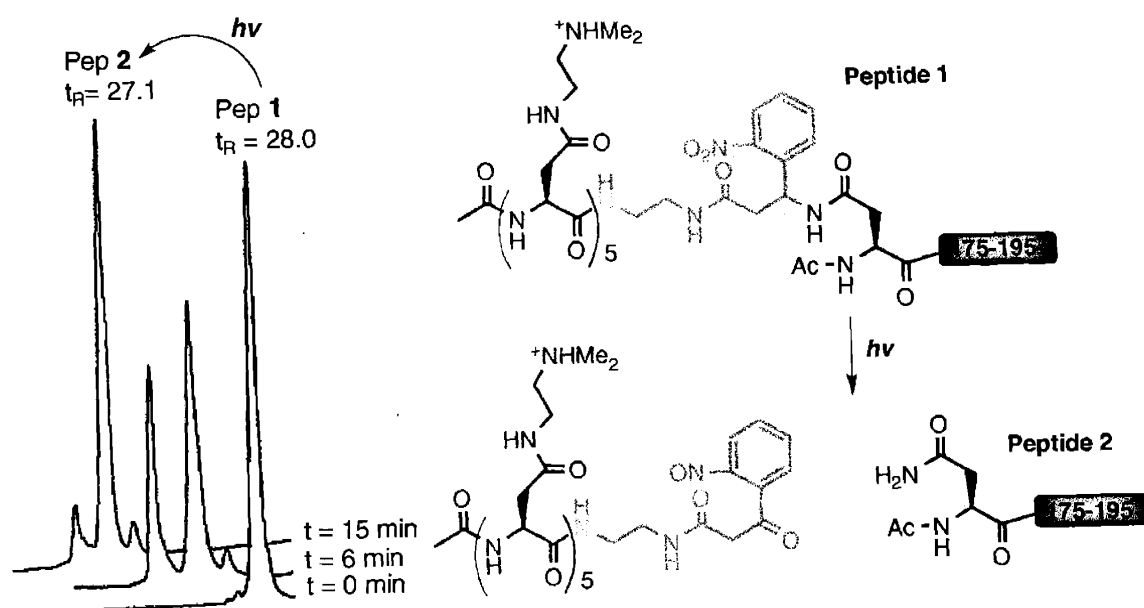


**Figure 5.4.** HPLC traces for the photolysis of 120  $\mu\text{M}$  peptide 1 to release peptide 2. Photolysis time is indicated to the right of each HPLC trace. The peptide structures are also shown. Gradient: 10 to 55%  $\text{H}_2\text{O}:\text{CH}_3\text{CN}$ , 0.1% TFA in 35 minutes. Detection at 228 nm. Peptide 1:  $[\text{M}+3\text{H}^+]/3 = 1229.7$  (obsd.) 1229.7 (calcd);  $[\text{M}+4\text{H}^+]/4 = 922.5$  (obsd.) 922.5 (calcd). Peptide 2:  $[\text{M}+2\text{H}^+]/2 = 1242.6$  (obsd.) 1242.4 (calcd);  $[\text{M}+3\text{H}^+]/3 = 828.4$  (obsd.) 828.6 (calcd);  $[\text{M}+4\text{H}^+]/4 = 621.5$  (obsd.) 621.5 (calcd).

## **Photolysis-dependent fibrillization kinetics for peptide 1**

To test our design and the hypothesis that the fibril-inhibitory unit could provide the desired stabilization of the peptide until photolytic cleavage, we compared the fibrillization kinetics for the photolyzed and unphotolyzed peptide **1** and the independently synthesized peptide **2**. The peptides (120  $\mu\text{M}$ ) were dissolved in water with 1mM DTT. Peptide **1** was either kept in the dark or exposed to UV light from a transilluminator (365 nm, 7.3 mW/  $\text{cm}^2$ ) for 15 minutes. All samples were then rapidly diluted to half the concentration using 5 mM phosphate buffer (pH 7.5) and the aggregation kinetics were monitored using a light scattering assay.<sup>23</sup> As expected from previous studies, peptide **2** forms fibrils and aggregates immediately without a significant lag time (Figure 5.5). On the other hand, peptide **1** is stable in solution for more than 12 hours, indicating that the fibril inhibitory unit is capable of impeding aggregation. However, when the inhibitory unit is photo-dissociated from peptide **1**, the photoproduct (peptide **2**) exhibits rapid aggregation. The lower amount of aggregates in the photolyzed peptide **1** sample (compared to the independently synthesized peptide **2**) could be due to partial inhibition by the detached Asn-DMDA unit.

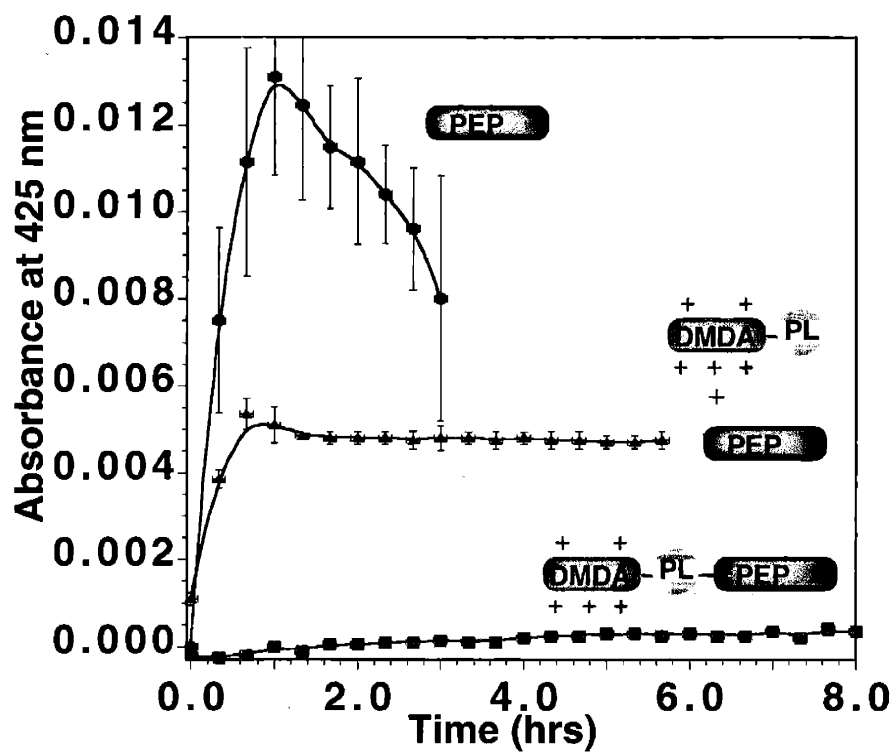


**Figure 5.5.** Aggregation kinetics for 60  $\mu$ M photolyzed (black) and unphotolyzed (red) peptide 1 and peptide 2 (blue) in 5 mM phosphate buffer pH 7.5.

### Time-dependent electron microscopy studies

In order to correlate the aggregation kinetics with the supramolecular arrangement of the peptides, we analyzed the peptide solutions by transmission electron microscopy.

The peptides were placed on EM grids immediately after mixing with phosphate buffer

(and after photolysis of the photodissociated peptide), after 6 hours and after 24 hours of incubation at pH 7.5 (Figure 5.6). The EM results show that peptide **1** is significantly delayed in forming fibrils, while peptide **2** begins to form filaments within the first hour of incubation. By 6 hours peptide **2** has formed extended fibrils, but no fibrils are observed in the peptide **1** sample until 24 hours. However, significant amounts of fibrils were observed in the photolyzed peptide **1** sample by 6 hours. While both, peptide **2** and the photolyzed peptide **1** displayed a high network of entangled fibrils by 24 hours, the unphotolyzed peptide **1** displayed a smaller density of fibrils. These results are consistent with the aggregation kinetics and show the photolysis-dependent fibrillization of this amyloidogenic construct.

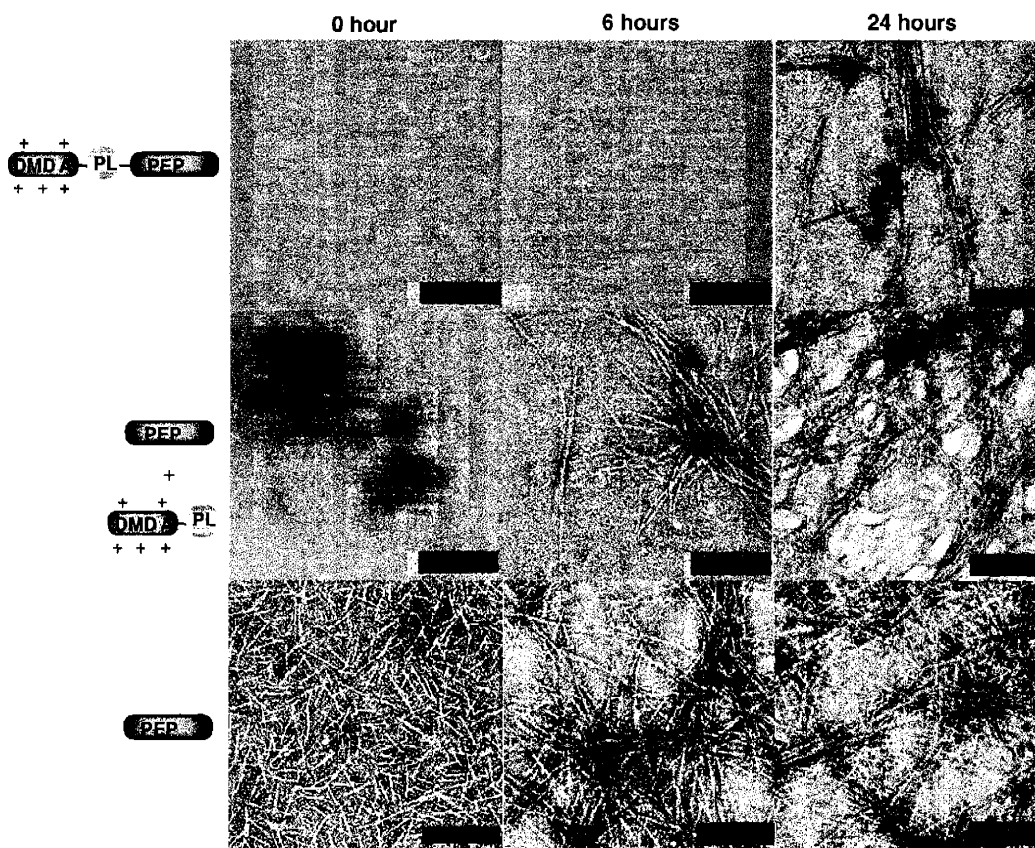


**Figure 5.6.** Time dependent-electron microscopy analysis for 60  $\mu\text{M}$  peptides incubated in 2.5 mM phosphate buffer pH 7.5. Schematic representation of the species present in the solutions are shown. Peptide 1 (top), photolyzed peptide 1 (middle), peptide 2 (bottom). Bar size = 200 nm.

### **Effect of pH on the fibrillization kinetics of peptide 1**

To test the hypothesis that the DMDA groups prevent the self-assembly of peptide 1 by affecting the electrostatic environment near the N-terminus, the fibrillization of peptide 1 near the DMDA  $\text{pK}_a$  was evaluated. As shown in figure 5.7, peptide 1 is stabilized and soluble when incubated at pH values of 7.5 and lower. However, when incubated at pH 10 (near DMDA's  $\text{pK}_a$ ) the stabilizing effect of the fibril inhibitory unit is diminished and the peptide aggregates after a lag time of 2.2 hours. Peptide 2 (without

the inhibitory-unit) aggregates immediately without a significant lag time at pH 7.5 and 10. At pH 10, a significant fraction of the tertiary amines would be neutral, and would have a lessened effect on the electrostatic environment. These results support the hypothesis that the positive charges on the tertiary amines of the DMDA groups can stabilize the amyloidogenic peptide as the soluble species until dissociated from the peptide by photolysis.

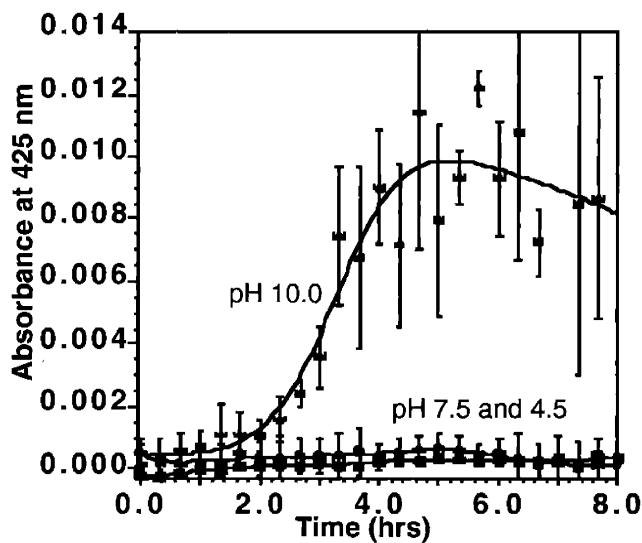


**Figure 5.7.** Effect of pH on the aggregation kinetics for 60  $\mu\text{M}$  peptide 1. The peptide (120  $\mu\text{M}$ ) was dissolved in water and diluted to 60  $\mu\text{M}$  using 5 mM acetate pH 4.5, phosphate pH 7.5 or carbonate pH 10.0 buffer.

## Discussion

In this chapter, a method for the temporal control of peptide-self assembly using an amyloidogenic peptide precursor containing a photolinker and a fibril-inhibitory unit is presented. Due to the sensitivity of the N-terminus of the PrP 174-195 peptide fragment to electrostatic effects, this property was used as the point parameter to affect the self-assembly of this peptide. Our results showed that the electrostatic influence of the positively charged tertiary amines of the *N,N*-dimethylethylenediamine can stabilize the soluble form of the amyloidogenic peptide precursor until dissociated by photolysis of the linker. The use of a synthetic photolabile linker allowed the liberation of the amyloidogenic peptide PrP 174-195 leaving no remnants of the linker attached to the peptide product. One of the major drawbacks of this methodology is the apparent incompatibility of cysteine residues in close proximity to the photolinker. Although the highly reactive nitroso product can typically be quenched by the addition of reducing agents such as DTT, the reactivity of a proximal a cysteine residue appears to successfully compete with the quenching reaction. Therefore, when using this method, careful attention should be paid to the location of cysteine residues in relation to the incorporation site of the photolinker. This methodology should allow for the facile incorporation of any "fibril-inhibitory unit" depending on the properties of the amyloidogenic peptide of interest. For example, sterically demanding organic moieties or

hydrophilic molecules such as carbohydrates could be tethered to the photolinker in order to inhibit the formation of fibrils.<sup>16</sup> When fibrillization is desired, the peptide can be exposed to UV radiation and submitted to conditions that promote self-assembly.

### **Acknowledgements.**

This work was supported by the NIH (GM-39334). Part of this chapter will be submitted to *J. Am. Chem. Soc.* **2003**.



## **Appendix 1**

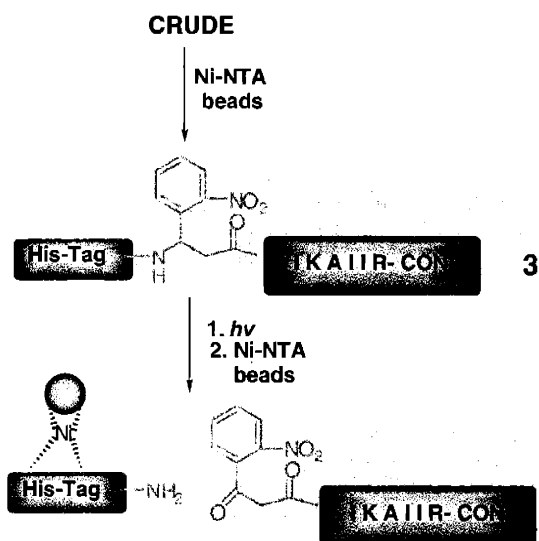
### **Potential use for photolinkers in the purification of synthetic peptides from truncation products**

Solid phase peptide synthesis (SPPS) is sometimes complicated by the presence of difficult sequences.<sup>24</sup> For example, a high content of  $\beta$ -branched amino acids is known to decrease the efficiency of amino acid couplings due to steric hindrance. Some sequences are also more prone to induce the formation of secondary structures (such as  $\beta$ -sheets) while the peptide is on the resin, significantly decreasing the yields.<sup>24</sup>

Amyloidogenic peptides are a good example of such sequences due to the generally high content of  $\beta$ -branched amino acids and the propensity to form secondary structures.<sup>25</sup>

These complications usually result in the generation of multiple truncation products that are difficult to separate from the desired peptide. Although complex solvent systems<sup>26</sup> and pseudoproline building blocks<sup>27</sup> are used to ameliorate this problem, they are either expensive solutions or incompatible with peptide synthesizers. In order to test a methodology to simplify the purification of a desired peptide from truncation products we used a test peptide incorporating six histidines (His-tag) linked through a photolinker to the N-terminus of the peptide. The peptide precursor can be easily purified using standard procedures with nickel-NTA beads (QIAGEN) and separated from the His-tag by

photolysis. Finally the His-tag can be removed from the solution containing the peptide with additional treatments with Ni-NTA beads (Scheme 5.7).



**Scheme 5.7.** Use of His-Tag linked through a photolinker (PL) for purification of PrP peptides.

The commercially available ANP linker and a random peptide sequence were used as a test case. However, this methodology could be applied to more complicated peptide sequences and could utilize other photolinkers (as the one discussed in previous sections) in order to eliminate the undesired photoadduct attached to the peptide fragment. Peptide **3** was synthesized using standard Fmoc chemistry on an Advanced ChemTech  $\Omega$ 396 automated peptide synthesizer. The commercially available Fmoc-ANP linker (Advanced Chemtech) was attached as a standard amino acid. Six histidines were subsequently attached after the photolinker and the N-terminus was acetylated. The best

conditions for the photolytic cleavage of the peptide were determined and the purification of the photolytically-cleaved His-tag was achieved using Ni-NTA beads. Several methods were tested for the photolysis: long wavelength from a simple hand-held UV-lamp (254/365 nm, 115V, 60 Hz, 0.16 AMPS), a nitrogen laser (337 nm, 6 mW) and a transilluminator (365 nm, 7.3 mW / cm<sup>2</sup>). The use of a 2.5 cm diameter glass container for the photolysis on the transilluminator resulted in the best conditions for the photolysis. Low pH values (below 5.5) also showed the most efficient photolysis.<sup>28</sup> The reaction was monitored by analyzing aliquots from the photolysis at different times by reverse phase HPLC. The expected photoproducts were confirmed by ESMS. After 30 minutes of irradiation, complete disappearance of the starting material was observed with no further increase in peptide photoproduct (Figure 5.8).

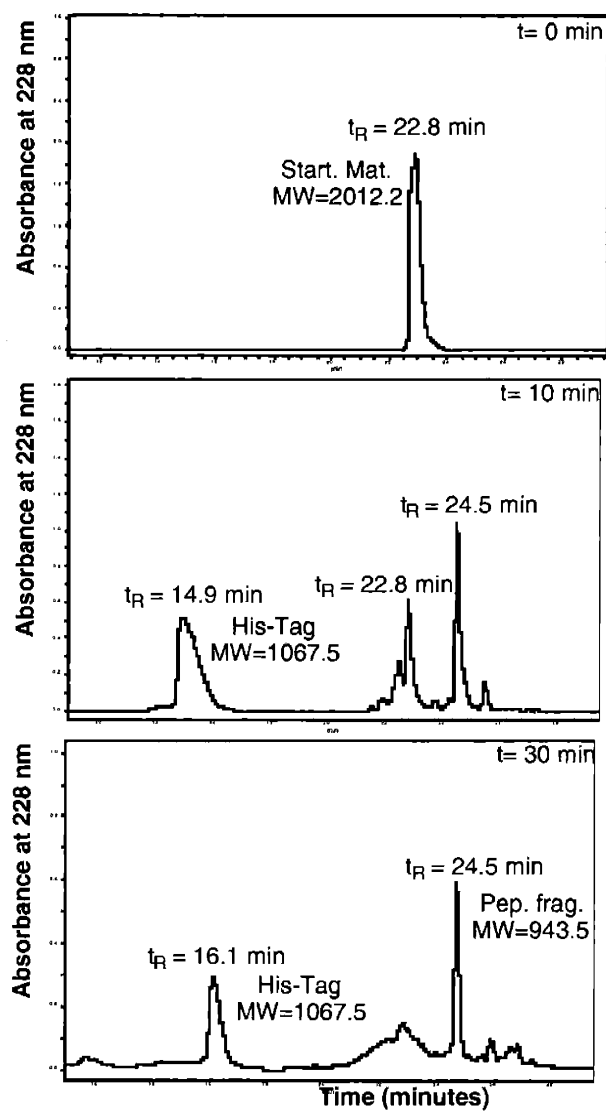


**Figure 5.8.** Photolysis of 1.8 mg/ml peptide 3 in water (pH 4.5) monitored by HPLC. Irradiation time is displayed in red. Masses determined from ESMS results are shown in blue. Chromatography was performed on a C-18 reversed-phase column. Gradient: 10-60% CH<sub>3</sub>CN:H<sub>2</sub>O, 0.1% TFA in 25 minutes.

To purify the peptide from the cleaved His-tag after the photolysis, phosphate buffer pH 7.5 (final concentration 10 mM), NaCl (final concentration 300 mM), imidazole (final concentration 20 mM) and 30  $\mu$ l of Ni-NTA agarose beads (of loading capacity =10 mg peptide/ml of resin) were mixed with the crude peptide solution for 2 minutes. The buffer, imidazole and salt were used to prevent non-specific binding with the Ni-NTA resin. Figure 5.9 shows the efficient recovery of the His-Tag using Ni-NTA.

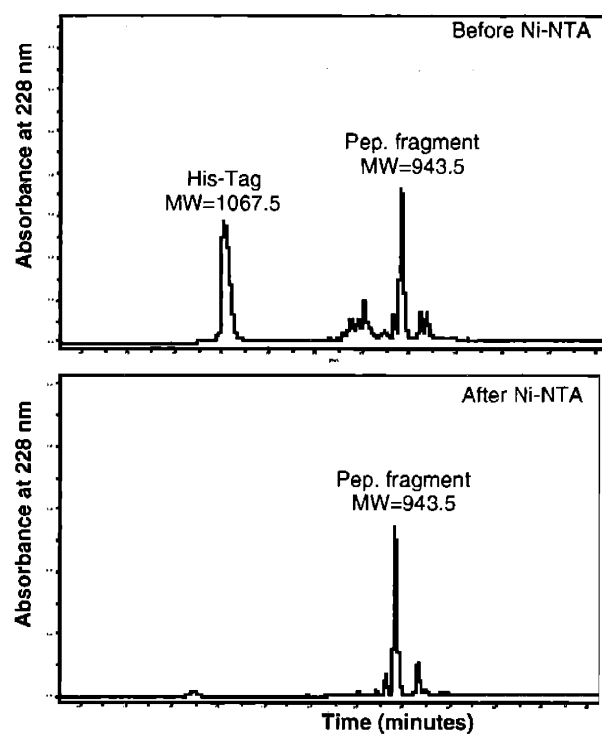
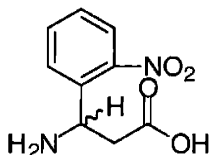


**Figure 5.9.** HPLC traces for the recovery of the His-Tag fragment after photolysis. The HPLC traces before and after incubation with Ni-NTA are displayed. Masses determined from ESMS results are shown in blue. Chromatography was performed on a C-18 reversed-phase column. Gradient: 10-60% CH<sub>3</sub>CN:H<sub>2</sub>O, 0.1% TFA in 25 minutes.

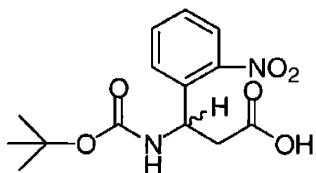
## **Discussion**

This appendix showed that the combination of a His-tag with the photolabile linkers can facilitate purification of a model peptide from truncations products. Our results illustrated that the His-tag can be easily photolyzed from the test peptide and the released His-tag can subsequently be extracted from the peptide solution. This simple purification methodology could prove effective in the synthesis of complex peptide sequences which may result in many truncations products that are otherwise difficult to purify by standard chromatographic methods.

## Experimental section:



*3-Amino-3-(2-nitrophenyl)-propionic acid*: 3-N<sup>α</sup>-Fmoc-Amino-3-(2-nitrophenyl)-propionic acid (Fmoc-ANP-OH from Advanced Chemtech; 562 mg, 1.3 mmol) was dissolved in THF (32.7 ml), piperidine (5.8 ml, 58.4 mmol) was added to the solution and the reaction was stirred at room temperature for 40 minutes. The solution was then diluted with chloroform and the product was extracted into 0.5% HCl. The aqueous layer was lyophilized and the product was then purified by reverse phase HPLC on a C18 preparative column; gradient: 0-70 % CH<sub>3</sub>CN:H<sub>2</sub>O, 0.1 % TFA in 25 minutes; t<sub>R</sub> = 18.5 min, [M+H<sup>+</sup>] 211.10 (obsd); 211.06 (calcd). TLC: (silica, 45:4:1 CHCl<sub>3</sub>:MeOH:AcOH; R<sub>f</sub> = 0.58, UV detection.

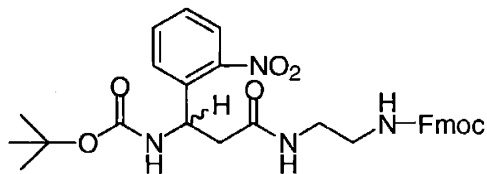


4

*3-N<sup>α</sup>-tBoc-Amino-3-(2-nitrophenyl)-propionic acid*: The unprotected 3-amino-3-(2-nitrophenyl)propionic acid (ANP, 273.1 mg, 1.3 mmol) was dissolved in methanol (13 mL) and DIPEA (1.36 ml, 7.8 mmol). Di-tert-butyl-dicarbonate (2.2 g, 10.4 mmol, Aldrich) was added and the solution was stirred at room temperature for 20 minutes. The solution was concentrated under reduced pressure, diluted with CHCl<sub>3</sub> and washed with 0.1 % HCl twice. The organic layer was dried with sodium sulfate and filtered through Celite. After flash column chromatography (45:3:0.2 CHCl<sub>3</sub>:MeOH:AcOH), the Boc-protected-ANP was obtained in a 65% overall yield over two reactions. TLC:silica, 45:4:1 CHCl<sub>3</sub>:MeOH:AcOH; R<sub>f</sub>= 0.58; UV detection).

<sup>1</sup>H NMR (500 MHz, DMSO-*d*<sub>6</sub>) δ (ppm): 7.91 (d, J = 7.9 Hz, 1H, NO<sub>2</sub>-Phe arom.), 7.75 (m, 2H, NO<sub>2</sub>-Phe arom. and NH-Boc), 7.68 (d, J = 7.6 Hz, 1H, NO<sub>2</sub>-Phe arom.), 7.51 (t, J = 7.6 Hz, 1H, NO<sub>2</sub>-Phe arom.), 5.32 (m, 1H, H<sub>α</sub>), 2.64 (m, 2H, H<sub>β</sub>), 1.30 (s, 9H, tBu).

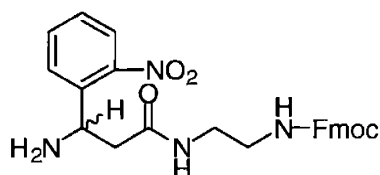




5

*N*<sup>1</sup>-[2-(9-fluorenylmethoxycarbonyl) ethyl]-3-[(*tert*-butoxycarbonyl)amino]-3-(2-nitrophenyl) propanamide: 3-N<sup>α</sup>-Boc-Amino-3-(2-nitrophenyl)propionic acid (Boc-ANP) 217.2 mg, 0.7 mmol) was dissolved in DMF (7 ml). HOBt.H<sub>2</sub>O (117.9 mg, 0.77 mmol, Novabiochem) and BOP (340.7 mg, 0.77 mmol, Novabiochem) was added and the solution stirred for 5 minutes. The monoprotected Fmoc-ethylenediamine•HCl (245.4 mg, 0.77 mmol, Novabiochem) and DIPEA (0.73 ml, 4.2 mmol) were added and the solution stirred at room temperature overnight. The precipitate was filtered and washed with cold chloroform to obtain the Boc-ANP-ethylenediamine-Fmoc in 53% yield. TLC: silica, 45:2:0.2 CHCl<sub>3</sub>:MeOH:AcOH; t<sub>R</sub> = 0.31; UV and CAM stain detection. <sup>1</sup>H NMR (500 MHz, DMSO-*d*<sub>6</sub>) δ (ppm): 7.90-7.83 (m, 5H, Fmoc and NO<sub>2</sub>-Phe arom., CONH(CH<sub>2</sub>)<sub>2</sub>NHCO<sub>2</sub>), 7.72-7.67 (m, 3H, Fmoc arom. and NH-Boc), 7.63 (d, J = 8.0 Hz, 1H, NO<sub>2</sub>-Phe arom.), 7.59 (d, J = 7.6 Hz, 1H, NO<sub>2</sub>-Phe arom.), 7.48 (t, J = 7.7 Hz, 1H, NO<sub>2</sub>-Phe arom.), 7.41 (t, J = 7.3 Hz, 2H, Fmoc arom.), 7.33 (t, J = 7.6 Hz, 2H, Fmoc arom.), 7.27 (m, 1H, NH-Fmoc), 5.32 (m, 1H, H<sup>α</sup>), 4.32 (d, J = 6.7 Hz, 2H, FmocCH<sub>2</sub>),

4.22 (t,  $J = 6.7$  Hz, 1H, FmocCH), 3.03 (m, 4H, CH<sub>2</sub>CH<sub>2</sub>), 2.54 (m, 2H, H<sub>β</sub>), 1.30 (s, 9H, tBu).

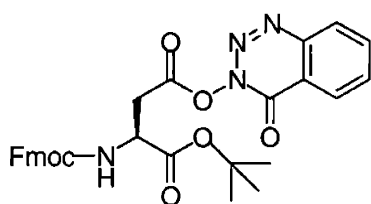


6

*N*<sup>1</sup>-[2-(9-fluorenylmethoxycarbonyl)ethyl]-3-amino-3-(2-nitrophenyl)propanamide:

Boc-ANP-ethylenediamine-Fmoc (165 mg, 0.287 mmol) was dissolved in dichloromethane (10 ml) and the solution was cooled to 0°C. Trifluoroacetic acid (10 ml) was added and the solution was stirred at 0°C for 5 minutes. The reaction was then allowed to warm to room temperature and stirred for an additional 35 minutes. The solvent was concentrated and co-concentrated with toluene. The unprotected ANP-ethylenediamine-Fmoc was obtained in a 94% yield after flash column chromatography (15.7:1:0.1 to 11.5:1:0.1 CHCl<sub>3</sub>:MeOH:DIPEA). TLC: (silica, 15.7:1:0.1 CHCl<sub>3</sub>:MeOH:DIPEA) R<sub>f</sub>=0.27; UV and CAM detection. <sup>1</sup>H NMR (500 MHz, DMSO-*d*<sub>6</sub>) δ (ppm): 8.07 (t,  $J = 5.1$  Hz, 1H, CONH(CH<sub>2</sub>)<sub>2</sub>NHCO<sub>2</sub>), 7.90-7.83 (m, 4H, Fmoc and NO<sub>2</sub>-Phe arom.), 7.73-7.67 (m, 3H, Fmoc and NO<sub>2</sub>-Phe arom.), 7.50 (t,  $J = 8.0$  Hz, 1H, NO<sub>2</sub>-Phe arom.), 7.42 (t,  $J = 7.3$  Hz, 2H, Fmoc arom.), 7.35-7.30 (m, 3H, Fmoc arom.

and NH-Fmoc), 4.65 (m, 1H, H<sup>α</sup>), 4.30 (d, *J* = 6.7 Hz, 2H, FmocCH<sub>2</sub>), 4.22 (t, *J* = 6.7 Hz, 1H, FmocCH), 3.02 (m, 4H, CH<sub>2</sub>CH<sub>2</sub>), 2.57 (t, *J* = 6.2 Hz, 2H, H<sub>β</sub>), 1.22 (d, *J* = 5.9 Hz, 3H, NH<sub>3</sub>).

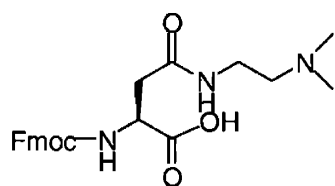


8

*N*<sup>α</sup>-Fmoc-L-Aspartic acid-β-4-(3,4-dihydro-4-oxo-1,2,3-benzotriazin-3-yl) O-tert-butyl

*ester*: The activated N<sup>α</sup>-Fmoc-L-Asp(Dhbt)-OtBu was prepared following published procedures.<sup>21</sup> N<sup>α</sup>-Fmoc-L-Asp-OH (1.93 g, 4.69 mmol) was dissolved in 9 ml of dry THF. The solution was cooled down to -35°C and 977 mg (4.69 mmol) of 1,3-dicyclohexyl carbodiimide (Aldrich) was added and stirred for 10 minutes. The Dhbt-OH (781 mg, 4.69 mmol) was added and the reaction stirred for 2 hours at -35°C then warmed to room temperature. The reaction was filtered through Celite and the flow through concentrated in vacuo to give 98% yield of the activated ester.

TLC: (silica, 1:2 EtOAc/petroleum ether, PMA and UV detection) R<sub>f</sub> = 0.57



**10**

*N*<sup>α</sup>-Fmoc-*N*<sup>β</sup>-(*N*-dimethylethylamine)-*L*-asparagine: The activated *N*<sup>α</sup>-Fmoc-*L*-Asp(Dhbt)-OtBu (768 mg, 1.38 mmol) was dissolved in dichloromethane (10 ml), 192  $\mu$ L (1.66 mmol, Aldrich) of 95% *N,N*-dimethylethylenediamine and DIPEA (2.76 mmol) were added and the solution was stirred at room temperature overnight. The solution was then diluted with dichloromethane and washed with sodium bicarbonate. The organic layer was dried with magnesium sulfate and then dried under vacuum to obtain the product in 83 % yield. The  $\alpha$ -carboxylic acid was finally deprotected in quantitative yield by stirring the protected amino acid (549 mg, 1.14 mmol) in 20 mL 1:1 TFA:CH<sub>2</sub>Cl<sub>2</sub> for 2 hrs. The product was concentrated in vacuo, co-concentrated with toluene and finally dried under high vacuum overnight. The amino acid was redissolved in water with 0.1 % TFA, passed through a 0.45 micron filter, and purified by reverse

phase HPLC on a preparative C<sup>18</sup> column using a 7-70% H<sub>2</sub>O:CH<sub>3</sub>CN, 0.1% TFA gradient in 30 minutes. (R<sub>t</sub> = 29.3 minutes; [M+H<sup>+</sup>] = 426.3 (obsd.) 426.5 (calcd).

<sup>1</sup>H NMR (500 MHz, DMSO-*d*<sub>6</sub>) δ (ppm): 8.20 (t, J = 5.5 Hz, 1H, NHγ), 7.90 (d, J = 7.7 Hz, 2H, Fmoc arom.), 7.70 (d, J = 7.3 Hz, 2H, Fmoc arom.), 7.60 (d, J = 8.5 Hz, 1H, NHα), 7.43 (t, J = 7.3 Hz, 2H, Fmoc arom.), 7.34 (t, J = 7.4 Hz, 2H, Fmoc arom.), 4.39 (m, 1H, Hα), 4.29 (d, J = 6.7 Hz, 2H, FmocCH<sub>2</sub>), 4.22 (t, J = 6.7 Hz, 1H, FmocCH), 3.30-3.20-3.10 (m, 4H, CH<sub>2</sub>CH<sub>2</sub>), 2.77 (s, 6H, N(CH<sub>3</sub>)<sub>2</sub>), 2.65 (dd, J = 5.5 Hz, J = 15.2 Hz, 1H, Hβ), 2.47 (dd, J = 5.6 Hz, J = 15.3 Hz, 1H, Hβ).

#### *DMDA<sub>5</sub>-PL-PrP 174-195*

##### **1**

Fmoc-PrP 174-195 was synthesized on a MilliGen/Biosearch 9050 automated peptide synthesizer using standard N-α-Fmoc chemistry on PAL-PEG-PS resin with a 0.18 mmol/g loading capacity. To selectively deprotect the side chain of the N-terminal aspartic acid and incorporate the photolinker, the allyloxycarbonyl (Alloc) protected aspartic acid was introduced as the last residue. The N-terminal amine was deprotected using 20% piperidine buffered with 0.1M 2,4-dinitrophenol in order to prevent aspartimide formation.<sup>22</sup> The free amine was subsequently acetylated using acetic anhydride and 2,4,6-collidine. Selective deprotection of the allyloxycarbonyl on the Asp

side chain was achieved by treating the peptide on the resin with 0.2 equivalents of  $\text{Pd}(\text{PPh}_3)_4$  and 20 equivalents of  $\text{PhSiH}_3$  in 1.5 ml of dichloromethane (3 times for 20 minutes). The photolinker (1.5 equivalent) was then coupled to the peptide using 2 equivalents of PyAOP as activator and 4 equivalent of collidine and reacting overnight in 1.5 ml of DMF. The coupling efficiency was evaluated by cleaving the peptide from a small portion of resin (2 mg) and analyzing the product by analytical HPLC and ESMS. Subsequently, five Asn-DMDA amino acids were incorporated as standard amino acids. Four equivalents of amino acid, 4 equivalents of PyAOP and 8 equivalent of collidine in 1.5 ml of DMF were used for the coupling. Finally, the N-terminal amine was acetylated with acetic anhydride and collidine. The peptide was cleaved from the resin using 96% TFA, 2% TIS, 3% water and 3% EDT and purified by reverse phase HPLC on a preparative  $\text{C}^{18}$  column. The two epimers resulting from the use of the racemic mixture of photolinker were separated at this stage (approximate ratio of two epimers: 1.2 : 1). The major product was used for all analyses.

HPLC: 15-75%  $\text{H}_2\text{O}:\text{CH}_3\text{CN}$ , 0.1% TFA gradient in 30 minutes. ( $t_{\text{R}} = 19.3$  and 19.9 minutes)  $[\text{M}+3\text{H}^+]/3 = 1229.7$  (obsd.) 1229.7 (calcd);  $[\text{M}+4\text{H}^+]/4 = 922.5$  (obsd.) 922.5 (calcd).

**Ellman's test:**

Aliquots (40  $\mu$ l) of 70  $\mu$ M peptide solutions were mixed with 250  $\mu$ l phosphate buffer pH 7.6 (100 mM) and 10  $\mu$ L of a 4 mg/ml solution of DTNB. After reacting for 15 minutes, the absorbance at 410 nm was measured by UV-Vis spectrophotometry. The reported normalized signal corresponds to the measured absorbance at any specific time of photolysis divided by the absorbance of the peptide-DTNB mixture before photolysis.

## References

- 1) Prusiner, S. B. "Prions" *Proc. Natl. Acad. Sci. USA* **1998**, *95*, 13363-13383.
- 2) Horwich, A. L.; Weissman, J. S. "Deadly Conformations-Protein Misfolding in Prion Disease" *Cell* **1997**, *89*, 499-510.
- 3) Hardy, J.; Allsop, D. "Amyloid Deposition as the Central Event in the Aetiology of Alzheimer's Disease" *Trends Pharmacol. Sci.* **1991**, *12*, 383-388.
- 4) Glenner, G. G. "Alzheimer's Disease: Its Proteins and Genes" *Cell* **1988**, *52*, 307-308.
- 5) Lucking, C. B.; Brice, A. "Alpha-Synuclein and Parkinson's Disease" *Cell Mol. Life Sci.* **2000**, *57*, 1894-1908.
- 6) Trojanowski, J. Q.; Goedert, M.; Iwatsubo, T.; Lee, V. M. "Fatal Attractions: Abnormal Protein Aggregation and Neuron Death in Parkinson's Disease and Lewy Body Dementia" *Cell Death. Differ.* **1998**, *5*, 832-837.
- 7) Aggeli, A.; Bell, M.; Boden, N.; Knowles, P. F.; McLeish, T. C.; Pitkeathly, M.; Radford, S. E. "Responsive Gels Formed by the Spontaneous Self-Assembly of Peptides Into Polymeric Beta-Sheet Tapes" *Nature* **1997**, *386*, 259-262.
- 8) Lashuel, H. A.; LaBrenz, S. R.; Woo, L.; Serpell, L. C.; Kelly, J. W. "Protofilaments, Filaments, Ribbons, and Fibrils from Peptidomimetic Self-Assembly: Implications for



Amyloid Fibril Formation and Material Science" *J. Am. Chem. Soc.* **2000**, *122*, 5262-5277.

9)Brown, C. L.; Aksay, I. A.; Saville, D. A.; Hecht, M. H. "Template-Directed Assembly of a *de Novo* Designed Peptide" *J. Am. Chem. Soc.* **2002**, *124*, 6846-6848.

10)Zhang, S.; Holmes, T. C.; DiPersio, C. M.; Hynes, R. O.; Su, X.; Rich, A. "Self-Complementary Oligopeptide Matrices Support Mammalian Cell Attachment" *Biomaterials* **1995**, *16*, 1385-1393.

11)Brown, B. B.; Wagner, D. S.; Geyesen, H. M. "A Single-Bead Decode Strategy Using Electrospray Ionization Mass Spectrometry and a New Photolabile Linker: 3-Amino-3-(2-Nitrophenyl)Propionic Acid" *Mol. Divers.* **1995**, *1*, 4-12.

12)Kaplan, J. H.; Ellis-Davies, G. C. "Photolabile Chelators for the Rapid Photorelease of Divalent Cations" *Proc. Natl. Acad. Sci. USA* **1988**, *85*, 6571-6575.

13)Corrie, J. E. T.; Trentham, D. R. *Chapter 5*; Morrison, H., Ed.; Wiley & Sons: New York, 1993.

14)Hilbich, C.; Kisters-Woike, B.; Reed, J.; Masters, C. L.; Beyreuther, K. "Substitutions of Hydrophobic Amino Acids Reduce the Amyloidogenicity of Alzheimer's Disease Beta A4 Peptides" *J. Mol. Biol.* **1992**, *228*, 460-473.

15)Lashuel, H. A.; Wurth, C.; Woo, L.; Kelly, J. W. "The Most Pathogenic Transthyretin Variant, L55P, Forms Amyloid Fibrils Under Acidic Conditions and Protofilaments under Physiological Conditions" *Biochemistry* **1999**, *38*, 13560-13573.

16)Findeis, M. A.; Musso, G. M.; Arico-Muendel, C. C.; Benjamin, H. W.; Hundal, A. M.; Lee, J.-J.; Chin, J.; Kelley, M.; Wakefield, J.; Hayward, N. J.; Molineaux, S. M. "Modified-Peptide Inhibitors of Amyloid  $\beta$ -Peptide Polymerization" *Biochemistry* **1999**, *38*, 6791-6800.

17)Hammarström, P.; Wiseman, R. L.; Powers, E. T.; Kelly, J. W. "Prevention of Transthyretin Amyloid Disease by Changing Protein Misfolding Energetics" *Science* **2003**, *299*, 713-716.

18)Zahn, R.; Liu, A.; Lührs, T.; Riek, R.; Schroetter, C. V.; Gracia, F. L.; Billeter, M.; Calzolari, L.; Wider, G.; Wüthrich, K. "NMR Solution Structure of the Human Prion Protein" *Proc. Natl. Acad. Sci. USA* **2000**, *97*, 145-150.

19)In this study we use serine at position 179 in order to eliminate the reactivity of the cysteine thiol with the nitroso product.

20)Rinnova, M.; Novakova, M.; Kasicka, V.; Jiracek, J. "Side Reactions During Photochemical Cleavage of an Alpha-Methyl-6-Nitroveratryl-Based Photolabile Linker" *J. Pept. Sci.* **2000**, *6*, 355-365.

- 21)Meinjohanns, E.; Meldal, M.; Paulsen, H.; Dwek, R. A.; Bock, K. "Novel Sequential Solid-Phase Synthesis of N-Linked Glycopeptides from Natural Sources" *J. Chem. Soc., Perkin Trans.* **1998**, *1*, 549-560.
- 22)Martinez, J.; Bodanszky, M. "Side Reactions in Peptide Synhtesis. IX. Suppression of the Formation of Aminosuccinyl Peptides With Additives" *Int. J. Pep. Prot. Res.* **1978**, *12*, 277-283.
- 23)Findeis, M. A.; Molineaux, S. M. "Design and Testing of Inhibitors of Fibril Formation" *Methods in Enzymology* **1999**, *309*, 476-488.
- 24)Kent, S. B. H. *Peptides, Structure and Function; Proceedings of the 9th American Peptide Symposium*; Pierce Chemical Co.: Rockford, Il, 1985.
- 25)Ball, H. L.; King, D. S.; Cohen, F. E.; B., P. S.; Baldwin, M. A. "Engineering the Prion Protein Using Chemical Synthesis" *J. Pept. Res.* **2001**, *58*, 357-374.
- 26)Zhang, L.; et. al. *Innovation and Perspectives in Solid Phase Peptide Synthesis, 3rd International Symposium*; Mayflower Scientific Ltd., Brimingham, 1994.
- 27)Mutter, M.; Nefzi, A.; Sato, T.; Sun, X.; Wahlf, F.; Wohr, T. "Pseudo-Prolines (PSI-PRO) For Accessing Inaccessible Peptides" *Pept. Res.* **1995**, *8*, 145-153.

28) Walker, J. W.; Reid, G. P.; McCray, J. A.; Trentham, D. R. "Photolabile 1-(2-Nitrophenyl)ethyl Phosphate Esters of Adenine Nucleotide Analogues. Synthesis and Mechanism of Photolysis" *J. Am. Chem. Soc.* **1987**, *110*, 7170-7177.

**Curriculum Vitae**  
**Carlos J. Bosques**

---

**Personal Data**

Date of Birth: December 18, 1974  
Place of Birth: Aguadilla, Puerto Rico

**Education**

**Graduate**

1999 - 2003      **Massachusetts Institute of Technology**      **Cambridge, MA**  
Doctoral Program in Biological Chemistry

1997 - 1999      **California Institute of Technology**      **Pasadena, CA**  
Doctoral Program in Chemistry

1997      **Undergraduate**  
**University of Puerto Rico**      **Río Piedras, P.R.**  
B.S. in Chemistry received on May, 1997

**Honors and Awards**

- 1999 - 2001      - NIH Biotechnology Training Grant: M.I.T.
- 1997 - 1999      - James Irvine Fellowship: California Institute of Technology
- 1995 - 1997      - NIH - Minority Access for Research Careers (MARC):U.P.R.
- 1994 - 1995      - NSF - Research Careers for Minority Scholars:U.P.R.
- 1997      - Magna cum Laude
- Best Chemistry Student of Puerto Rico Award - Chemistry Board of Puerto Rico
- Faculty of Natural Sciences Award
- Chemistry Department Award
- 1996 - 1997      - Dean's list

**Societies**

- 1999 - 2001      - BPEC/BTG Student Leadership Council - member
- 1996 - 1997      - American Chemical Society - Student Chapter President
- 1994 - 1997      - Golden Key National Honor Society - member

**Publications**

- *Bosques, C. J., Tai, V. -F., Imperiali, B.* "Stereoselective synthesis of  $\beta$ -linked TBDMS-protected chitobiose-asparagine: a versatile building block for amyloidogenic glycopeptides" *Tetrahedron Lett.* **2001**, *42*, 7207-7210.
- *Ilin, S. Bosques, C. J., Turner, C. Scwalbe, H.* "*T*-HMBC: An experiment for the conformational analysis of the O-glycosidic linkage in glycopeptides" *Angew. Chem.* **2003**, *115*, *12*, 1432-1435.
- *Carrasquillo, K. G., Stanley, A. M., Aponte-Carro, J. C., De Jesús, P., Costantino, H. R., Bosques, C. J., Gribenow, K.* "Non-aqueous encapsulation of excipient-stabilized spray-freeze dried BSA into poly(lactide-co-glycolide) microspheres results in release of native protein" *J. Control Release* **2001**, *76*, 199-208.
- *Bosques, C. J., Imperiali, B.,* "The interplay of glycosylation and disulfide formation influences fibrillization in a prion protein fragment" **2003**, *submitted*.
- *Bosques, C. J., Imperiali, B.* "Photolytic control of peptide self-assembly" **2003**, *submitted*.
- *Bosques, C. J., Imperiali, B.* "Effects of carbohydrate stereochemistry on glycopeptide structure" **2003**, *in preparation*.